Pathological studies on the rabid dogs and mice experimentally infected with rabies virus

Hassadin Boonsriroj

2015

狂犬病発病犬および狂犬病ウイルスに感染したマウスに

関する病理学的研究

ハッサデン・ブンシロー

平成 27 年度

Table of contents

Chapter 1 A pathological study of the salivary glands of rabid dogs in the Philippines

Introduction

Rabies virus is a highly neurotropic virus that affects the nervous system in humans and animals [14]. Rabies is as endemic disease in many the developing and developed countries worldwide and causes approximately 37,000-86,000 human deaths each year [36]. In endemic countries, domestic dogs remain principal reservoir and vector for rabies virus infection and play an important role in transmission of rabies virus to human [2, 24]. In addition, more than 98% of human rabies deaths in the Philippines are associated with dog bites [8]. Viral transmission is achieved through contact with the virus contained in the saliva of an infected animal, often through biting. After deep biting by an infected animal, the rabies virus binds to the nicotinic acetylcholine receptors at the neuromuscular junction in the muscle fibers [21]. The virus enters through the peripheral nerve and reaches the central nervous system (CNS) by centripetal spread. The rabies virus then spreads to peripheral non-nervous tissues, including salivary glands, adrenal glands, gastrointestinal tract, pancreas and heart [7, 12, 16, 32].

The salivary glands are an important site of viral replication and portals of exit for the rabies virus into saliva [14]. A previous study found that dogs have the ability to excrete virus particles into the saliva for up to 14 days before any clinical symptoms of rabies are apparent [10]. Moreover, saliva samples can be used as alternatives to brain [18] and cerebrospinal fluid [28] samples for ante-mortem diagnosis of canine rabies. The acinar epithelium of salivary gland has been shown contain abundant rabies virus antigens in infected animals [3, 6, 10]. However, detailed pathological findings in salivary glands and analysis of the excretion mechanism have not been reported.

Therefore, in this chapter, I investigated the histopathological and immunohistological finding of the salivary glands of rabid dogs and evaluated the excretion mechanism of the virus into the oral cavity, following a careful initial examination of the normal histological structure of dog salivary glands.

Materials and methods

Animals and direct fluorescence antibody test (dFAT)

Mandibular and parotid glands samples were obtained from 22 rabid dogs, which had been submitted to the Research Institute of Tropical Medicine (RITM), Philippines for postmortem diagnosis of rabies. Small transverse sections (2-3 mm in thickness) of ammon's horn and medulla were cut and slide was touched against the surface of the section and then placed on cold acetone overnight for fixing. After fixation, slides were air dried at room temperature. Then 450 µl of fluorescence isothiocyanate conjugate anti-rabies monoclonal antibody (Fujirebio®, Malvern, Pennsylvania) was added. The slides were incubated for 30 minutes at 37°C in a high humidity chamber. Slides were then dipped rinsed for 20 to 25 times in PBS twice followed by distilled water for further washing. Small amounts of the mounting, 20% glycerol-Tris buffered saline pH 9.0, was placed on the slides before covering with coverslips for examination. The slides were examined under the fluorescent microscope (Nikon eclipse 80i).

Histopathological examination

Mandibular and parotid salivary glands of rabid (n=22) and control (n=3) dogs were fixed in 10% neutral buffered formalin at room temperature for more than 72 hour, embedded in paraffin, sectioned (3 µm thickness), and mounted. Three rabies-vaccinated domestic Japanese mixed dogs (8 to 10 years old) were used as a control group. The sections were then subjected to hematoxylin and eosin, special straining (Alcian blue stain, reticulin silver impregnation) and immunohistochemistry, and terminal deoxynucleotidyl transferase-mediated deoxyuridine triphosphate (dUTP) nick end labeling (TUNEL) assay as described below.

Staining with hematoxylin and eosin (HE)

The sections were stained with hematoxylin and eosin for general histopathological examination.

Protocol

Paraffin was removed from the sections by a series of xylene and ethanol rinses. Tissue sections were rinsed in distilled water for 5 minutes and stained with hematoxylin solution (Certistain®, Darmstadt, Germany) for 3 minutes, rinsed in running tap water for 5 minutes and stained with eosin solution (Sakura Finetek Japan Co.,Ltd., Tokyo, Japan) for 5 minutes, rinsed in distilled water for three times and dehydrated through a series of ethanol and xylene. The sections were then mounted in microscopy mounting medium.

Staining with Alcian blue (pH 2.5)

Alcian blue stain used for the demonstration of acid mucosubstances of mucous acinar epithelial cells.

Protocol

Paraffin was removed from the sections by a series of xylene and ethanol rinses. Sections were rinsed in distilled water for 5 minutes, and then sections were immersed in 3% acetic acid solution for 5 minutes, followed by immerse with Alcian blue solution (pH 2.5; Certistain®, Darmstadt, Germany) for 30 minutes at room temperature, washed in 3% acetic acid solution for 5 times once again, and rinsed in distilled water for 5 minutes. Sections were counterstained with Nuclear-fast red solution (TCI Co., Ltd., Tokyo Kasei, Japan) for 1 minute at room temperature, rinsed in distilled water for 1 minute and dehydrated through a series of ethanol and xylene. Sections were mounted in microscopy mounting medium.

Staining with reticulin silver impregnation

Reticulin silver impregnation stain used for the demonstration of specific basement membrane of the cell.

Protocol

Paraffin was removed from the sections by a series of xylene and ethanol rinses. Sections were rinsed in distilled water for 5 minutes, and then sections were immersed in 0.25% potassium permanganate for 5 minutes, washed in running tab water for 5 minutes, followed by immerse with 2% oxalic acid dihydrate solution for 2 minutes, washed in distilled water for 5 minutes, then sections were immersed in 2% ferric ammonium sulfate solution for 1 minute, washed in distilled water for 5 minutes, then sections were immerse in ammonium silver solution for 10 minute, rinsed in 100% ethanol for 1 time, followed by immerse with 1% formalin solution for 1 minute, washed in distilled water for 5 minutes, then sections were immerse in 0.2% silver chloride solution for 10 minutes, washed in distilled water for 5 minutes, then sections were immersed in 2% oxalic acid dihydrate solution for 2 minutes once again, washed in distilled water for 5 minutes, and then sections were immersed in 5% sodium thiosulfate solution for 2 minutes, followed by washed in distilled water for 5 minutes, and dehydrated through a series of ethanol and xylene. Sections were mounted in microscopy mounting medium.

Immunohistochemistry

1. *For detection of the rabies virus antigens in tissues*

The sections were stained using the streptavidin-biotin-peroxidase complex method with rabbit anti-phosphoprotein (P) antibodies.

Protocol

The sections were deparaffinized by a series of xylene and ethanol rinses, rehydrated, and washed twice with distilled water. The sections were treated for the activation of antigen with 0.25% trypsin at room temperature for 30 minutes. After this treatment, sections were washed

three times for 5 minutes in distilled water. After washing, to removed endogenous peroxidase activity the sections were immersed with 0.3% H_2O_2 in methanol for 60 minutes; then they were washed three times for 5 minutes in distilled water once again. The sections were treated with 10% normal goat serum (Nichirei Biosciences, Tokyo, Japan) for 60 minutes to block non-specific reaction. Sections were then incubated with primary antibody for overnight at 4°C in a humidified chamber. Primary antibody was diluted 1:1200. After incubation with primary antibody, sections were washed three times for 5 minutes in phosphate buffer saline (PBS, pH 7.4) and incubated for 30 minutes at room temperature with the biotinylated anti-rabbit IgG (Nichirei Biosciences) as a secondary antibody. Sections were again washed three times for 5 minutes in PBS; then incubated for 30 minutes in room temperature with peroxidase-streptavidin enzyme (Nichirei Biosciences) for 30 minutes, washed in PBS three times for 5 minutes. Finally, sections were visualized using 3-3'-diaminobenzidine tetrachloride substrate (DAB substrate; DAKO, Kyoto, Japan), followed by rinsing in distilled water. The sections were counterstained with hematoxylin, and rinsing in running tap water again for 5 minutes. The sections were then dehydrated and mounted in microscopy mounting medium. Negative control was processed with rabbit serum instead of primary antibody.

2. *For detection of T lymphocytes*

The sections were stained using the polymer-based immunohistochemical method with polyclonal rabbit anti-CD3 antibodies (DAKO, Kyoto, Japan) for detection of T lymphocytes.

Protocol

The sections were deparaffinized by a series of xylene and ethanol rinses, rehydrated, and washed twice with distilled water. The sections were treated with Histofine® pH 9.0 (Nichirei Biosciences, Japan) for activation of antigens by microwaving at 750W for 5 minutes; then were washed in distilled water with three changes of 5 minutes each. After washing, incubation for 10

minutes in 3% H_2O_2 in methanol to removed endogenous peroxidase activity, and the sections were rinsed in distilled water (three changes, 5 minutes each). To block non-specific reaction, the sections were treated with 10% normal goat serum (Nichirei Biosciences) for 60 minutes, followed by incubation with the primary antibody for overnight at 4°C in a humidified chamber. Primary antibody was diluted 1:50. After incubation with the primary antibody, sections were rinsed in PBS (three changes, 5 minutes each), then incubated for 30 minutes at room temperature with the Envision + System Labelled Polymer-HRP anti-rabbit (DAKO), rinsed in PBS (three changes, 5 minutes each) once again. Finally, sections were visualized using DAB substrate, followed by rinsing in distilled water. The sections were counterstained with hematoxylin, and rinsing in running tap water again for 5 minutes. The sections were then dehydrated and mounted in microscopy mounting medium.

3. For detection of B lymphocytes and plasma cells

The sections were stained using the polymer-based immunohistochemical method with polyclonal rabbit anti-CD20 antibodies (Spring Bioscience, Fremont, USA) for detection of B lymphocytes, and anti-CD79α antibodies (DAKO, Kyoto, Japan) for detection of plasma cells.

Protocol

The sections were deparaffinized by a series of xylene and ethanol rinses, rehydrated, and washed twice with distilled water. The sections were treated with Histofine® pH 9.0 (Nichirei Biosciences) for activation of antigens by microwaving at 750W for 5 minutes; then were washed in distilled water with three changes of 5 minutes each. After washing, incubation for 10 minutes in 3% H_2O_2 in methanol to removed endogenous peroxidase activity, and the sections were rinsed in distilled water (three changes, 5 minutes each). To block non-specific reaction, the sections were treated with 10% normal goat serum (Nichirei Biosciences) for 30 minutes, followed by incubation with the primary antibody for overnight at 4°C in a humidified chamber.

After incubation with the primary antibody, sections were rinsed in PBS (three changes, 5 minutes each), then incubated for 30 minutes at room temperature with the Envision + System Labelled Polymer-HRP anti-rabbit (DAKO), rinsed in PBS (three changes, 5 minutes each) once again. Finally, sections were visualized using DAB substrate, followed by rinsing in distilled water. The sections were counterstained with hematoxylin, and rinsing in running tap water again for 5 minutes. The sections were then dehydrated and mounted in microscopy mounting medium.

4. For detection of myoepithelial cells

The sections were stained using the polymer-based immunohistochemical method with the monoclonal mouse anti-alpha-smooth muscle actin antibodies (α-SMA, DAKO, Kyoto, Japan) for detection of myoepithelial cells.

Protocol

The sections were deparaffinized by a series of xylene and ethanol rinses, rehydrated, and washed twice with distilled water. The sections were treated with Histofine® pH 9.0 (Nichirei Biosciences) for activation of antigens by autoclaving at 121°C for 15 minutes; then were washed in distilled water with three changes of 5 minutes each. After washing, incubation for 15 minutes in 3% H_2O_2 in methanol to removed endogenous peroxidase activity, and the sections were rinsed in distilled water (three changes, 5 minutes each). To block non-specific reaction, the sections were treated with 10% normal goat serum (Nichirei Biosciences) for 30 minutes, followed by incubation with the primary antibody for overnight at 4°C in a humidified chamber. Primary antibody was diluted 1:1000). After incubation with the primary antibody, sections were rinsed in PBS (three changes, 5 minutes each), then incubated for 30 minutes at room temperature with the Histofine® Simple Stain MAX-PO (Mouse) (Nichirei Biosciences), rinsed in PBS (three changes, 5 minutes each) once again. Finally, sections were visualized using DAB

substrate, followed by rinsing in distilled water. The sections were counterstained with hematoxylin, and rinsing in running tap water again for 5 minutes. The sections were then dehydrated and mounted in microscopy mounting medium.

5. For detection of basement membranes

The sections were stained using the polymer-based immunohistochemical method with polyclonal rabbit anti-laminin antibodies (Thermo Scientific, USA) for detection of basement membranes.

Protocol

The sections were deparaffinized by a series of xylene and ethanol rinses, rehydrated, and washed twice with distilled water. After washing, the sections were treated for the activation of antigens with proteolytic enzyme solution diluted in 0.05 mol/L Tris-HCL, 0.015 mol/L sodium azide, pH 7.5 (Proteinase-K, DAKO, Kyoto, Japan) at room temperature for 15 minutes; then they were rinsed in distilled water with three changes of 5 minutes each. Incubation for 15 minutes in 3% H_2O_2 in methanol to removed endogenous peroxidase activity, and the sections were rinsed in distilled water (three changes, 5 minutes each). To block non-specific reaction, the sections were treated with 10% normal goat serum (Nichirei Biosciences) for 30 minutes, followed by incubation with the primary antibody for overnight at 4°C in a humidified chamber. Primary antibody was diluted 1:100. After incubation with the primary antibody, sections were rinsed in PBS (three changes, 5 minutes each), then incubated for 30 minutes at room temperature with the Envision + System Labelled Polymer-HRP anti-rabbit (DAKO), rinsed in PBS (three changes, 5 minutes each) once again. Finally, sections were visualized using DAB substrate, followed by rinsing in distilled water. The sections were counterstained with hematoxylin, and rinsing in running tap water again for 5 minutes. The sections were then dehydrated and mounted in microscopy mounting medium.

6. For detection of nerve fibers

The sections were stained using the polymer-based immunohistochemical method with monoclonal mouse anti-neurofilament protein antibodies (NF, DAKO, Kyoto, Japan) for detection of nerve fibers.

Protocol

The sections were deparaffinized by a series of xylene and ethanol rinses, rehydrated, and washed twice with distilled water. After washing, the sections were treated for the activation of antigens with Proteinase-K at room temperature for 30 minutes; then they were rinsed in distilled water with three changes of 5 minutes each. Incubation for 10 minutes in 3% H_2O_2 in methanol to removed endogenous peroxidase activity, and the sections were rinsed in distilled water (three changes, 5 minutes each), followed by incubation with the primary antibody for overnight at 4°C in a humidified chamber. Primary antibody was diluted 1:100. After incubation with the primary antibody, sections were rinsed in PBS (three changes, 5 minutes each), then incubated for 30 minutes at room temperature with the Histofine® Simple Stain MAX-PO (Mouse) (Nichirei Biosciences) rinsed in PBS (three changes, 5 minutes each) once again. Finally, sections were visualized using DAB substrate, followed by rinsing in distilled water. The sections were counterstained with hematoxylin, and rinsing in running tap water again for 5 minutes. The sections were then dehydrated and mounted in microscopy mounting medium.

7. For detection of nerve cells

The sections were stained using the polymer-based immunohistochemical method with monoclonal mouse anti-neuron specific enolase antibodies (NSE, DAKO, Kyoto, Japan) for detection of nerve cells.

Protocol

The sections were deparaffinized by a series of xylene and ethanol rinses, rehydrated, and washed twice with distilled water. The sections were treated with Histofine® pH 9.0 (Nichirei Biosciences) for activation of antigens by autoclaving at 121°C for 15 minutes; then were washed in distilled water with three changes of 5 minutes each. After washing, incubation for 10 minutes in 3% H_2O_2 in methanol to removed endogenous peroxidase activity, and the sections were rinsed in distilled water (three changes, 5 minutes each). To block non-specific reaction, the sections were treated with 10% normal goat serum (Nichirei Biosciences) for 10 minutes, followed by incubation with the primary antibody for 60 minutes at room temperature. Primary antibody was diluted 1:100. After incubation with the primary antibody, sections were rinsed in PBS (three changes, 5 minutes each), then incubated for 30 minutes at room temperature with the Envision + System Labelled Polymer-HRP anti-rabbit (DAKO), rinsed in PBS (three changes, 5 minutes each) once again. Finally, sections were visualized using DAB substrate, followed by rinsing in distilled water. The sections were counterstained with hematoxylin, and rinsing in running tap water again for 5 minutes. The sections were then dehydrated and mounted in microscopy mounting medium.

8. For detection of apoptotic cells

The sections were stained using the polymer-based immunohistochemical method with anti-activated cysteine aspartic acid specific protease (cleaved caspase-3) antibodies for detection of apoptotic cells (Cell Signaling Technology, Inc., Beverley, MA, USA).

Protocol

The sections were deparaffinized by a series of xylene and ethanol rinses, rehydrated, and washed twice with distilled water. The sections were treated with Histofine® pH 9.0 (Nichirei Biosciences) for activation of antigens by heating in a water bath at 95°C for 15 minutes; then were washed in distilled water with three changes of 5 minutes each. After

washing, incubation for 15 minutes in 3% H_2O_2 in methanol to removed endogenous peroxidase activity, and the sections were rinsed in distilled water (three changes, 5 minutes each). To block non-specific reaction, the sections were treated with 10% normal goat serum (Nichirei Biosciences) for 60 minutes, followed by incubation with the primary antibody for overnight at 4°C in a humidified chamber. Primary antibody was diluted 1:50. After incubation with the primary antibody, sections were rinsed in PBS (three changes, 5 minutes each), then incubated for 30 minutes at room temperature with the Envision + System Labelled Polymer-HRP anti-rabbit (DAKO), rinsed in PBS (three changes, 5 minutes each); followed by incubated for 30 minutes at room temperature with peroxidase-streptavidin enzyme, washed in PBS three times for 5 minutes once again. Finally, sections were visualized using DAB substrate, followed by rinsing in distilled water. The sections were counterstained with hematoxylin, and rinsing in running tap water again for 5 minutes. The sections were then dehydrated and mounted in microscopy mounting medium.

9. Double immunostaining and immunostaining with a special stain

Double staining of a single tissue section was used for identification of cell type and co-expression of antigens.

Protocol

Staining for α-SMA was performed as described above, and slides were incubated with DAB until color developed. The reaction was then stopped by washing in distilled water, and anti-P antibodies were added. Histofine Simple stain AP (Nichirei Biosciences) was used as a secondary antibody. A color reaction was developed with Histofine New Fuchsin (Nichirei Biosciences). The slides were counterstained with hematoxylin. For immunostaining combination with special stain, anti-P antibody staining was performed as described above, and slides were incubated with DAB substrate until color developed. The reaction was stopped by

washing the slides in distilled water, and the slides were then incubated in 3% acetic acid for 5 minutes, followed by staining with Alcian blue solution for 30 minutes. Slides were then washed in distilled water for 5 minutes, stained with Nuclear-fast red for 1 minute, washed in distilled water for 5 minutes, and mounted for light microscopy.

Terminal deoxynucleotidyl transferase-mediated deoxyuridine triphosphate (dUTP) nick end labeling (TUNEL) assay

The sections were evaluated using TUNEL assay kit (ApopTag® Plug peroxidase In Situ Apoptosis Detection Kit, Millipore Corporation, Billerica, MA, USA) for detection of fragmented DNA of apoptotic cells.

Protocol

The sections were deparaffinized by a series of xylene and ethanol rinses, rehydrated, and washed twice with distilled water. After washing, sections were treated with Proteinase-K (DAKO) for 15 minutes at room temperature to activated antigens, rinsed in PBS (three changes, 5 minutes each). Then, endogenous peroxidase activity was removed with 0.3% H_2O_2 in methanol for 15 minutes at room temperature, rinsed in PBS (three changes, 5 minutes each). After washing in PBS, sections were covered with 50 µl of the TUNEL reaction mixture, which containing terminal deoxynucleotidyl transferase (TdT) and fluorescein-dUTP, and incubated under a coverslip in a humidified chamber for 60 minutes at 37°C. The reaction was stopped by washing sections in PBS. Sections were then incubated with anti-digoxigenin peroxidase for 30 minutes at room temperature. Then, washed in PBS (three changes, 5 minutes each) once again. Finally, sections were visualized using DAB substrate, followed by rinsing in distilled water. The sections were counterstained with hematoxylin, and rinsing in running tap water again for 5 minutes. The sections were then dehydrated and mounted in microscopy mounting medium.

Results

Clinical characteristics of the dogs

Eighteen dogs were discovered after having died, while four dogs were subjected to euthanasia. The 22 dogs (11 male, 8 female, and 3 of unknown sex) ranged in age from 1 to more than 24 months, with six dogs having unknown ages. Sixteen of the 22 dogs had no history of rabies vaccination, one dog had a history of rabies vaccination, and no information on rabies vaccination status was available for five dogs. Sixteen dogs were free-roaming dogs with owners, three were strays, two were confined with household contact, and one had unknown living conditions. The primary clinical symptoms of canine rabies infection, such as unprovoked aggressiveness, mad biting of inanimate objects, aimless running, and excessive salivation, were observed in 18 of the 22 dogs. All brain specimens were diagnosed as positive for rabies virus antigen through the direct immunofluorescence antibody test (dFAT). The clinical information and results of dFAT are summarized in the Table 1.

Gross and histological findings of salivary glands in control dogs

No gross findings were observed in the parotid glands, mandibular glands, and mandibular lymph nodes in control dogs (Fig. 1). The mandibular glands were divided into several lobules by dense connective tissue septa and were composed of serous and mucous acinar epithelium. Many ganglion cells and peripheral nerve fibers were observed in the interlobular septa (Fig. 2). The parotid gland was composed exclusively of serous acinar epithelium in association with striated ducts and interlobular excretory ducts, but interlobular ganglion cells were not found (Fig 3).

Histopathological findings of salivary glands of rabid dogs

In the mandibular glands, 19 out of 22 rabid dogs exhibited mild to moderate non-suppurative sialadenitis characterized by fragmentation and cytolysis of the acinar epithelium with infiltration of moderate to marked lymphocytes and plasma cells (Figs. 4-7). These cells consistently surrounded fragmented acini, interstitial connective tissue, and striated ducts. Infiltration of inflammatory cells was not found in three of the four euthanized dogs, but small foci of necrotic acinar cells were scattered throughout the samples (Fig. 8). In all cases, no histological changes in striated and interlobular ductal epithelial cells and interlobular ganglion cells were found. In the parotid glands, no morphological evidence of acinar, duct units, and interlobular stroma was observed (Fig. 9).

Immunohistochemical examination of the mandibular glands and parotid glands

Detection of rabies virus antigen by anti-P antibodies

No viral antigen was detected in control dogs (data not shown). In all rabid dogs, viral antigens were detected in the cytoplasm of the mucous acinar epithelium and interlobular ganglion cells in the mandibular glands (Figs. 10-12). Some viral antigens were observed in the myoepithelium and peripheral nerves, but viral antigens were not found in the striated and interlobular ductal epithelia. In parotid gland, rabies virus antigens were only detected in the interlobular peripheral nerves (Figs. 13, 14). These immunohistochemistry results are summarized in Table 2.

Detection of lymphocytes by anti-CD3, anti-CD20, and anti-CD79α antibodies

In mandibular glands of rabid dogs, there are moderate numbers of anti-CD3 positive cells appeared in the interstitial connective tissue and around fragmented acinar epithelium (Fig. 15), while anti-CD20 (Figs. 16, 17) and anti-CD79α (Fig. 18) positive cells were mainly

detected in the interstitial connective tissue and periductal areas. No positive cells were detected in the parotid glands.

Detection of basement membranes by anti-laminin antibodies and reticulin silver impregnation staining

In control dogs, laminin immunoreactivity and reticulin silver impregnation staining appeared as linear, continuous staining around individual acini and ducts of the parotid and mandibular glands (Fig. 19). In the mandibular glands of rabid dogs, staining was irregular and weak because acinar epithelium and basement membranes were disrupted (Figs. 20, 21).

Detection of myoepithelial cells by anti-α-SMA antibodies

In control dogs, anti-α-SMA antibody was positive in the myoepithelial cells surrounding acinar epithelium (Fig. 22) and intercalated duct epithelium of the mandibular and parotid glands. However, in rabid dogs, the intensity of immunostaining of anti-α-SMA-positive cells was decreased in glands that showed severe inflammation (Fig. 23).

Detection of apoptotic cells by TUNEL assays and anti-cleaved caspase-3 antibodies

In mandibular glands of rabid dogs, the acinar epithelium and lymphocytes exhibited apoptotic features, such as nuclear fragmentation and cytolysis, were positive in TUNEL assays (Figs. 24, 25). The numbers of TUNEL-positive cells were higher in the glands that showed severe inflammation. However, TUNEL-positive signals were not detected in the ductal epithelium, interlobular ganglion cells, and serous demilune. In parotid glands, the acinar epithelium and the ductal epithelium were negative for TUNEL staining (Fig. 26). The patterns of anti-cleaved caspase-3 immunostaning were similar to those of TUNEL staining in the mandibular glands, but with fewer positive cells (Fig. 27).

Detection of nervous tissues by anti-NF and anti-NSE antibodies

Interlobular ganglion cells and peripheral nerve fibers were positive for anti-NSE antibodies in the mandibular glands (Figs. 28, 29). Interlobular ganglion cells were not found in the parotid glands (Fig. 30). Anti-NF immunoreactivity was observed as a fine network in the fibers distributed throughout the stroma and around acini in the mandibular glands (Fig. 31). The staining patterns were same between control and rabid dogs.

Identification of the virus infected cells by combination of anti-P antibody and either anti-α-SMA or Alcian blue staining

In the mandibular gland of rabid dogs, anti-α-SMA-positive myoepithelial cells showed co-expression with anti-P antibody reactivity (Fig. 32). In addition, the mucous acinar epithelium showed co-stained with anti-P antibody reactivity and Alcian blue staining (Fig. 33). In contrast, anti-α-SMA-positive myoepithelial cells of the parotid glands were negative for anti-P antibody reactivity.

Discussion

Centrifugal spread from the CNS to peripheral sites along neuronal routes is essential for transmission of rabies virus to its natural hosts. Salivary gland infection is necessary for the transfer of infections oral fluids by rabid vectors. In this study, non-suppurative sialadenitis, characterized by fragmentation, cytolysis of acinar epithelium, basement membrane disruption, and lymphoplasmacytic infiltration, was observed in the mandibular glands of most rabid dogs. No inflammatory cells were found in three of four euthanized dogs; however, small foci of necrotic acinar cells were scattered throughout the samples, and these cells were positive for anti-caspase-3 and TUNEL staining. These pathological findings suggested that early sialadenitis was induced by direct disruption of the acinar epithelium by rabies virus infection.

In this chapter, the viral antigen was mainly detected in the mucous acinar epithelium and myoepithelium in the mandibular glands. These findings are consistent with previous reports of skunks and foxes infected with the street rabies virus [1]. In addition, the viral antigen was present in the myoepithelium between the basal lamina and acinar epithelial cells. Thus, the rabies virus may propagate in the myoepithelium and affect nerve terminal innervation. Previous studies have described the morphological structure of neuro-effector that innervates the acinar epithelium and myoepithelium of the salivary glands of carnivores [11, 20, 27]. These neuro-effectors may be the hypolemmal type (i.e., non-myelinated axons that penetrate below the acinar basement membrane and adjacent to the myoepithelium) or the epilemmal type (i.e., non-myelinated axons found outside the acinar epithelium and myoepithelium). Furthermore, the intra-acinar nerve endings in the mandibular glands are restrictively localized only in the intercellular space between myoepithelial cells and mucous acinar cells, whereas no intra-acinar nerve endings occur among the serous cells [17]. Therefore, it was suggested the rabies virus may directly enter mucous acinar epithelial cells and myoepithelial cells via both innervation. However, several mammalian species lack apparent hypolemmal innervation in the striated

ducts and interlobular excretory ducts [31, 32]. In the present study, I did not observe degeneration, inflammation, or viral antigen in the duct unit of striated and interlobular ducts in the mandibular gland, suggesting that hypolemmal and epilemmal innervation were not present in the duct system of dogs. Thus, viral proliferation and cytotoxicity could not occur there, ensuring that secretions containing the virus were efficiently excreted into the oral cavity.

Interlobular ganglions were observed in the interlobular septa of the mandibular glands, similar to findings in humans [34] and rats [24]. These ganglions included a number of cholinergic neurons that received motor impulses form pre- and postganglionic parasympathetic fibers carried by the facial nerve [9]. Ganglion neurons are responsible for innervation of the salivary parenchyma and for regulation of saliva secretion [24, 26]. In the present study, viral antigens were detected in the ganglion neurons and their fibers. Thus, centrifugal viral propagation progresses to the mandibular glands via motor innervations. After the rabies virus replicates within the facial nerve nuclei, located in the ventral part of the rostral medulla oblongata, the virus then descends along the facial nerve to reach the submandibular ganglion and the interlobular ganglions [3, 30, 35]. In this study, I did not observe interlobular ganglia in the parotid gland and also no viral antigens detected here. Therefore, it was suggested that these ganglia are important for viral replication and serve as a main source of virus to acinar epithelium of the mandibular glands.

In the present study, virus-infected ganglion neurons were negative for TUNEL staining and cleaved caspase-3, indicating that virus-infected neurons did not undergo apoptosis, similar to results reported in natural infection of dogs and humans by a street rabies virus strain [15, 30]. Therefore, I concluded that lack of neuronal apoptosis in rabies in dogs infected by street rabies virus may promote prolonged infection within ganglion neurons and continually supply virus to the saliva acinar epithelium. On the other hand, virus-infected mucous acinar epithelial cells exhibited fragmentation and cytolysis, and migrating T lymphocytes were positive for TUNEL

and cleaved caspase-3, suggesting that rabies virus may trigger apoptotic cascades through the Fas/Fas ligand and caspase-dependent apoptotic pathway [29].

In the present study, the inflammatory cells were composed mainly CD3, CD20, and CD79α-positive lymphocytes and were present in the virus-infected mandibular glands. These findings suggested that a combination of cell-mediated and humoral immune responses was important for the clearance of rabies virus from the salivary gland and that the inflammatory cytokines released by T lymphocytes activated plasma cell infiltration. CD79α is a surface marker of B lymphocytes and plasma cells. B lymphocytes play an important role in producing virus-neutralizing antibodies and are critical for control of rabies virus replication and essential in the clearance rabies virus from the CNS [13]. In addition, high titers of tissue-neutralizing antibody suppress viral spread to salivary epithelial cells [4]. The plasma cells in the salivary tissue are the source of locally produced antibodies, such as immunoglobulin A (IgA), which provides mucosal surface immunity against various antigens and neutralizes viruses [5, 22]. Furthermore, IgA-producing plasma cells infiltrate the salivary gland via regulation of T lymphocytes and various inflammatory cytokines, such as interleukin (IL)-5 and interferon (IFN)-α [23]. In the present study, however, the direct roles of lymphocytes in the salivary gland of rabid dogs remains unresolved because most of present cases were discovered after died, therefore, further studies are required.

In summary, our results confirmed the path through which the rabies virus descends along the facial nerve after proliferation in the brain to reach the ganglion neurons of the mandibular gland, subsequently traveling to the acinar epithelium and salivary gland myoepithelium. Furthermore, viral proliferation and cytotoxicity did not occur in the duct system, ensuring that secretions containing the virus were efficiently excreted into the oral cavity.

References

1. Balachandran, A. and Charlton, K. 1994. Experimental rabies infection of non-nervous tissues in skunks (*Mephitis mephitis*) and foxes (*Vulpes vulpes*). *Vet. Pathol.* **31**: 93-102.
2. Banyard, A. C., Horton, D. L., Freuling, C., Müller, T. and Fooks, A. R. 2013. Control and prevention of canine rabies: the need for building laboratory-based surveillance capacity. *Antiviral Res.* **98**: 357-364.
3. Charlton, K. M., Casey, G. A. and Campbell, J. B. 1983. Experimental rabies in skunks: mechanism of infection of the salivary glands. *Can. J. Comp. Med.* **47**: 363-369.
4. Charlton, K. M., Casey, G. A. and Campbell, J. B. 1987. Experimental rabies in skunks: immune response and salivary gland infection. *Comp. Immune. Microbiol. Infect.* **10**: 227-235.
5. Corthesy, B. 2010. Role of secretory immunoglobulin A and secretory component in the protection of mucosal surface. *Future Micro.* **5**: 817-829.
6. Dierks, R. E., Murphy, F. A. and Harrison, A. K. 1969. Extraneural rabies virus infection: virus development in fox salivary gland. *Am. J. Pathol.* **54**: 251-273.
7. Dietzschold, B., Li, J., Faber, M. and Schnell, M. 2008. Concepts in the pathogenesis of rabies. *Future Virol.* **3**: 481-490.
8. Dimaano, E. M., Scholand, S. J., Alera, M. P. and Belandres, D. B. 2011. Clinical and epidemiological features of human rabies cases in the Philippines: a review from 1987 to 2006. *Int. J. Infect. Dis.* **15**: 495-499.
9. Evans, H. E. 1993. pp: 953-986. *In*: Miller's Anatomy of the Dog, 3rd ed., W. B. Saunders Company, St. Louis.
10. Fekadu, M. and Shaddock, J. H. 1984. Peripheral distribution of virus in dogs inoculated with two strains of rabies virus. *Am. J. Vet. Res.* **45**: 724-729.

11. Garrett, J. R. and Kidd, A. 1993. The innervation of salivary glands as revealed by morphological methods. *Microsc. Res. Tech.* **26**: 75-91.

12. Hemachudha, T., Laothamatas, J. and Rupprecht, C. E. 2002. Human rabies: a disease of complex neuropathogenic mechanisms and diagnostic challenge. *Lancet Neurol.* **1**: 101-109.

13. Hooper, D. C., Phares, T. W., Fabris, M. J. and Roy, A. 2009. The production of antibody by invading B cells is required for the clearance of rabies virus from the central nervous system. *PLoS Negl. Trop. Dis.* **3**: e535.

14. Jackson, A. C. and Wunner, W. H. 2007. pp: 341-372. *In*: Rabies, 2nd ed., Elsevier Saunders, Amsterdam.

15. Jackson, A. C., Randle, E., Lawrance, G. and Rossiter, J. P. 2008. Neuronal apoptosis does not play and important role in human rabies encephalitis. *J. Neurovirol.* **14**: 368-375.

16. Jogai, S., Radotra, B. D. and Banerjee, A. K. 2002. Rabies viral antigen in extracranial organs: a post-mortem study. *Neuropathol. Appl. Neurobiol.* **28**: 334-338.

17. Kagayama, M. 1971. The fine structure of the monkey submandibular gland with a special reference to intra-acinar nerve ending. *Am. J. Anat.* **131**: 185-195.

18. Kasempimolporn, S., Saengseesom, W., Lumlertdacha, B. and Sitprija, V. 2000. Detection of rabies virus antigen in dog saliva using a latex agglutination test. *J. Clin. Microbiol.* **38**: 3098-3099.

19. Kojima, D., Park, C. H., Satoh, Y., Inoue, S., Noguchi, A. and Oyamada, T. 2009. Pathology of the spinal cord of C57BL/6J mice infected with rabies virus (CVS-11). *J. Vet. Med. Sci.* **71**: 319-324.

20. König Jr B. and Masuko, T. S. 1998. Ultrastructure of the parotid and submandibular glands of the Old World Marten. *Ann. Anat.* **180**: 31-36.

21. Lewis, P., Fu, Y. and Lentz, T. L. 2000. Rabies virus entry at the neuromuscular junction in nerve-muscle cocultures. *Muscle Nerve* **23**: 720-730.

22. Mestecky, J. 1993. Saliva as a manifestation of the common mucosal immune system. *Ann. N. Y. Acad. Sci.* **694**: 184-194.

23. Mega, J., McGhee, J. R. and Kiyono, H. 1992. Cytokine- and Ig-producing T cells in mucosal effector tissues: analysis of IL-5- and IFN-gamma-producing T cells, T cell receptor expression, IgA plasma cells from mouse salivary gland-associated tissue. *J. Immuno.* **148**: 2030-2039.

24. Ng, Y. K., Wong, W. C. and Ling, E. A. 1992. The intraglandular submandibular ganglion of postnatal and adult rats I. A light and electron microscopic study. *J. Anat.* **180**: 305-314.

25. Prager, K. C., Mazet J. A., Dubovi, E. J., Frank, L. G., Munson, L., Wagner, A. P. and Woodroffe, R. 2012. Rabies virus and canine distemper virus in wild and domestic canivores in northen Kenya: are domestic dogs the reservoir? *Ecohealth* **9**: 483-498.

26. Proctor, G. B. and Carpenter, G. H. 2007. Regulation of salivary gland function by autonomic nerves. *Auton. Neurosci*. **133**: 3-18.

27. Redman, R. S. 1994. Myoepithelium of salivary glands. *Microsc. Res. Tech.* **27**: 25-45.

28. Saengseesom, W., Mitmoonpitak, C., Kasempimolporn, S. and Sitprija, V. 2007. Real-Time PCR analysis of dog cerebrospinal fluid and saliva samples for ante-mortem diagnosis of rabies. *Southeast Asian J. Trop. Med. Public Health* **38**: 53-57.

29. Sarmento, L., Tseggai, T. Dhingra, V. and Fu, Z. F. 2006. Rabies virus-induced apoptosis involves caspase-dependent and casepase-independent pathways. *Virus Res.* **121**: 144-151.

30. Suja, M. S., Mahadevan, A., Madhusudana, S. N., Vijayasarathi, S. K. and Shankar, S. K. 2009. Neuroanatomical mapping of rabies nucleocapsid viral antigen distribution and

apoptosis in pathogenesis in street dog rabies: an immunohistochemical study. *Clin. Neuropathol.* **28**: 113-124.

31. Tandler, B., Gresik, E. W., Nagato, T. and Phillips, C. J. 2001. Secretion by striated ducts of mammalian major salivary glands: review from an ultrastructural, functional, and evolutionary perspective. *Anat. Rec.* **264**: 121-145.

32. Tandler, B., Pinkstaff, C. A. and Phillips, C. J. 2006. Interlobular excretory ducts of mammalian salivary glands: structural and histochemical review. *Anat. Rec. A. Discov. Mol. Cell Evol. Biol*. **288**: 498-526.

33. Tobuime, M., Sato, Y., Katano, H., Nakajima, N., Tanaka, K., Noguchi, A., Inoue, S., Hasegawa, H., Iwasa, Y., Tanaka, J., Hayashi, H., Yoshida, S., Kurane, I. and Sata, T. 2009. Rabies virus dissemination in neural tissues of autopsy cases due to rabies imported into Japan from the Philippines: Immunohistochemistry. *Pathol. Int*. **59**: 555-566.

34. Tosios, K. I., Nikolakis, M., Prigkos, A. C., Diamanti, S. and Sklavouvou, A. 2010. Nerve cell bodies and small ganglia in the connective tissue stroma of human submandibular glands. *Neurosci. Lett.* **475**: 53-55.

35. Umoh, J. U. and Blenden, D. C. 1982. The dissemination of rabies virus into cranial nerves and other tissues of experimentally infected goats and dogs and naturally infected skunks. *Int. J. Zoonoses.* **9**: 1-11.

36. WHO, Expert consultation on rabies. Second report. 2013. *WHO Tech. Rep. Ser.* **982**: 1-139.

Table 1. Clinical information and laboratory findings of rabid dogs (samples obtained postmortem)

No.	Age (months)	Sex	Owned	Manner of death	Vaccination	Animal conditions	Neurological symptoms	dFAT
1	48	Male	Yes	Found dead	No	Free-roaming and owned	Unprovoked aggressiveness, excessive salivation	+
2	Unknown	Male	Yes	Euthanasia	Unknown	Stray	Unprovoked aggressiveness, mad biting of inanimate objects	+
3	24	Female	Yes	Found dead	Yes	Free-roaming and owned	Excessive salivation, mad biting of inanimate objects, watchful look, paralysis	+
4	1	Male	Yes	Found dead	No	Free-roaming and owned	Unknown	+
5	6	Male	Yes	Found dead	No	Free-roaming and owned	Unprovoked aggressiveness, mad biting of inanimate objects	+
6	6	Male	Yes	Found dead	No	Free-roaming and owned	Unknown	+
7	1	Male	Yes	Found dead	No	Free-roaming and owned	Unprovoked aggressiveness	+
8	60	Male	Yes	Found dead	No	Confined with household contact	Unprovoked aggressiveness, excessive salivation, apprehension, watchful look, mad biting of inanimate objects	+
9	2	Female	Yes	Found dead	No	Free-roaming and owned	Unprovoked aggressiveness, mad biting of inanimate objects, aimless running	+
10	12	Female	Yes	Found dead	No	Free-roaming and owned	Unknown	+
11	1	Female	Yes	Found dead	No	Unknown	Unknown	+
12	36	Male	Yes	Found dead	No	Free-roaming and owned	Unprovoked aggressiveness, mad biting of inanimate objects, paralysis of jaw and tongue	+
13	16	Female	Unknown	Found dead	No	Free-roaming and owned	Unprovoked aggressiveness	+
14	Unknown	Unknown	Unknown	Euthanasia	Unknown	Stray	Unprovoked aggressiveness	+
15	2	Male	Unknown	Found dead	Unknown	Free-roaming and owned	Apprehensive, watchful look, paralysis	+
16	Unknown	Unknown	Unknown	Found dead	No	Free-roaming and owned	Unprovoked aggressiveness	+
17	2	Female	Unknown	Found dead	No	Free-roaming and owned	Unprovoked aggressiveness	+
18	8	Female	Unknown	Found dead	No	Free-roaming and owned	Unprovoked aggressiveness, mad biting of inanimate objects	+
19	Unknown	Male	Unknown	Euthanasia	Unknown	Free-roaming and owned	Unprovoked aggressiveness	+
20	Unknown	Male	Unknown	Found dead	No	Free-roaming and owned	Unprovoked aggressiveness, aimless running	+
21	Unknown	Unknown	Unknown	Euthanasia	Unknown	Stray	Unprovoked aggressiveness	+
22	3	Female	Unknown	Found dead	No	Confined with household contact	Unprovoked aggressiveness, mad biting of inanimate objects, aimless running	+

+: positive, dFAT: direct fluorescent antibody test

Table 2. Summary of inflammatory cells infiltration and distribution of viral antigen in the mandibular glands of 22 rabid dogs

No	Inflammatory cells	Virus antigen distribution			
		Mucous epithelium	Serous epithelium	Ductal units (striated and interlobular duct)	Interlobular ganglion
1	Moderate	+	-	-	+
2	Mild	+	-	-	+
3	Mild	+	-	-	+
4	Moderate	+	-	-	+
5	Mild	+	-	-	+
6	Mild	+	-	-	+
7	Moderate	+	-	-	+
8	Moderate	+	-	-	+
9	Moderate	+	-	-	+
10	Mild	+	-	-	+
11	None	+	+	-	+
12	Mild	+	-	-	+
13	Moderate	+	-	-	+
14	None	+	-	-	+
15	Mild	+	-	-	+
16	Moderate	+	-	-	+
17	Mild	+	-	-	+
18	Moderate	+	-	-	+
19	Moderate	+	-	-	+
20	Mild	+	-	-	+
21	None	+	-	-	+
22	Moderate	+	-	-	+

+: positive, -: negative

Figure legends

Fig. 1. Cutting position of the right external ear (E), parotid gland (PG), mandibular gland (MG), and mandibular lymph node (LN) after formalin fixation in a control dog.

Fig. 2. Mandibular gland. The mandibular gland is composed of mixed components of mucous and serous acinar cells (A). The positions of the interlobular duct (D), ganglion cells (arrows), and vessels (V) are indicated in the stroma.

Fig. 3. Parotid gland. The parotid gland is composed of the serous acinar gland (A) and interlobular stroma. The positions of the interlobular duct (D), peripheral nerve bundles (arrow), and vessels are indicated in the interlobular stroma.

Figs. 4-6. Mandibular gland. In rabid dogs, non-suppurative sialadenitis characterized by cytolysis of acinar epithelium and infiltration of lymphoplasmacytic cells (asterisks). The striated ducts are intact (arrows).

Fig. 7. Mandibular gland. No histological changes were observed in the interlobular ganglia (arrows), vessel (V) and interlobular duct (D).

Fig. 8. Mandibular gland. Necrotic foci of the acinar epithelium (arrow heads) without inflammatory cells were observed in the euthanasia case.

Fig. 9. Parotid gland. No pathological findings were observed in the serous acinar epithelium or striated ducts (D).

Fig. 10. Mandibular gland. Viral antigens were detected by immunohistochemistry with anti-P antibody in the acinar epithelium (A) and ganglion cells (arrow), but the interlobular duct (D) and blood vessels (V) were negative.

Fig. 11. Mandibular gland. High magnification of Fig. 10. Viral antigens were detected by immunohistochemistry with anti-P antibodies in the cytoplasm of mucous acinar cells (asterisk). In contrast, serous cells of the demilume (arrows) and striated duct (D) were negative.

Fig. 12. Mandibular gland. Higher magnification of Fig. 10. Viral antigens were detected by immunohistochemistry with anti-P antibodies in the ganglion cells and peripheral nerves.

Figs. 13-14. Parotid gland. Viral antigens were detected only in the interlobular nerve fibers (13), but acinar epithelium (A) and ductal units (D) were negative (14).

Fig. 15. Mandibular gland. Many of anti-CD3 positive cells were observed in the interstitial connective tissue and surrounding acinar epithelium (asterisks).

Figs. 16-17. Mandibular glands. Many of anti-CD20 positive cells were observed surrounding ductal epithelium (D).

Fig. 18. Mandibular gland. Many of anti-CD79α positive cells were observed in the interstitial connective tissue.

Figs. 19-20. Mandibular gland. In control dog, anti-laminin immunostaining appeared as linear, continuous staining around individual acini and ducts (19), whereas the intensity of immunostaining decreased and irregular because acinar epithelium and basement membranes were disrupted in rabid dogs (20).

Fig. 21. Mandibular gland. Reticulin silver impregnation staining revealed irregular positive reactions, with disruption of acinar epithelium (asterisk) and basement membranes. Special staining.

Figs. 22-23. Mandibular gland. In control dog, myoepithelial cells surrounding acinar epithelium showed strong reactivity for anti-α-SMA (22), whereas the intensity of immunostaining decreased in rabid dogs (asterisk, 23).

Figs. 24-25. Mandibular gland. Necrotic foci (asterisks) in the acinar epithelium were TUNEL staining positive (arrows).

Fig. 26. Parotid gland. The acinar epithelium and ductal units were negative for TUNEL staining.

Fig. 27. Mandibular gland. Necrotic foci (asterisk) in the acinar epithelium were anti-caspase-3 antibodies positive (arrow).

Figs 28-29. Mandibular gland. In control dog, Interlobular ganglion cells and peripheral nerve fibers (29) were positive for anti-NSE antibodies. Interlobular ducts (D) and acinar epithelium (A).

Fig. 30. Parotid gland. In control dog, anti-NSE immunoreactivity was detected only the interlobular nerve fibers (arrows), whereas interlobular ganglion cells were not found. Interlobular ducts (D) and acinar epithelium (A).

Fig. 31. Mandibular gland. In control dog, anti-NF immunoreactivity was observed as a fine network in the fibers distributed throughout the stroma and around acini.

Fig. 32. Mandibular gland. Myoepithelial cells (arrow) were double positive immunostaining for anti-α-SMA (brown) and anti-P antibodies (red).

Fig. 33. Mandibular gland. The mucous acinar epithelium showed co-strained with anti-P antibody reactivity (arrows) and Alcian blue staining.

Figs.1-3: Gross and histological findings

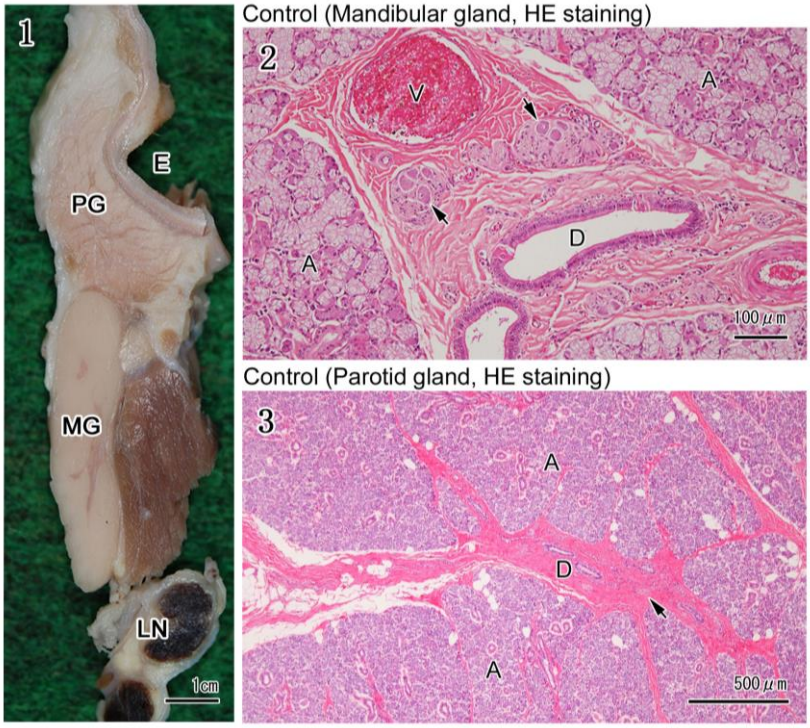

Figs.4-9: Histopathological findings (HE)

No.9 (Mandibular gland)

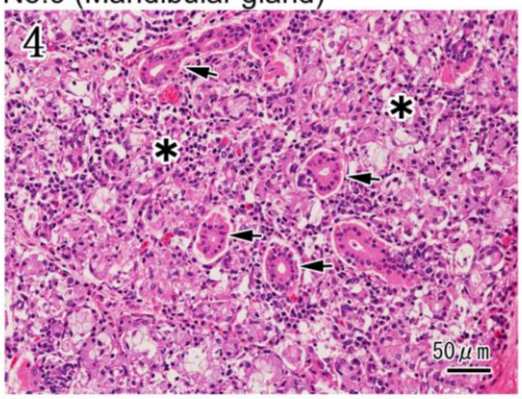

No.4 (Mandibular gland)

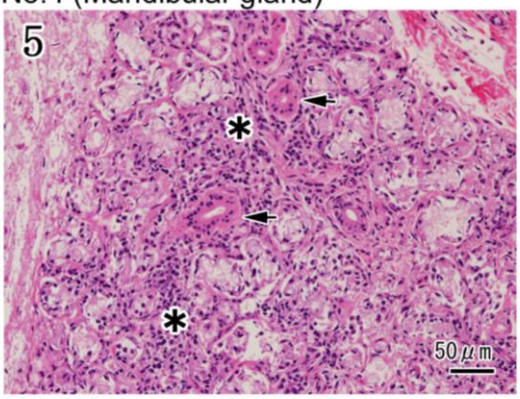

No.3 (Mandibular gland)

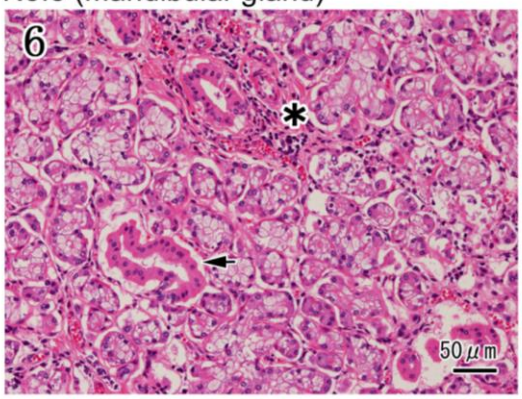

No.3 (Mandibular gland)

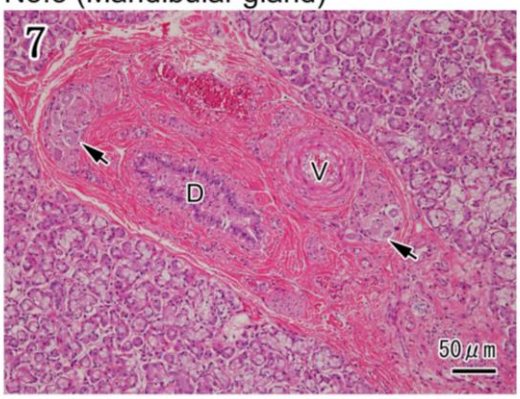

No.14 (Mandibular gland)

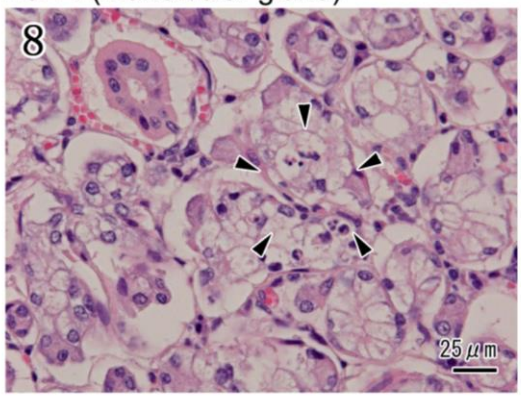

No.3 (Parotid gland)

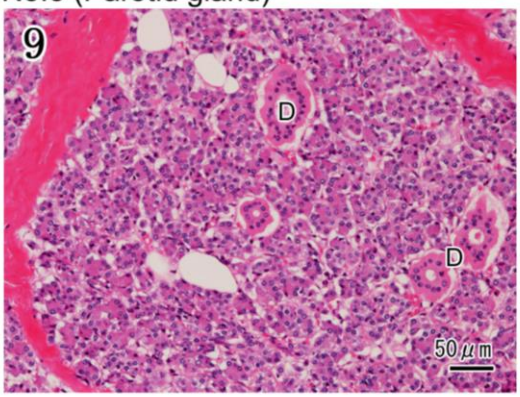

Figs.10-14: Immunohistochemistry (anti-P)

No.3 (Mandibular gland)

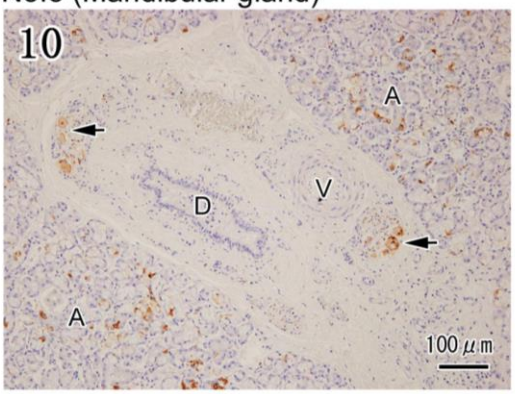

No.9 (Mandibular gland)

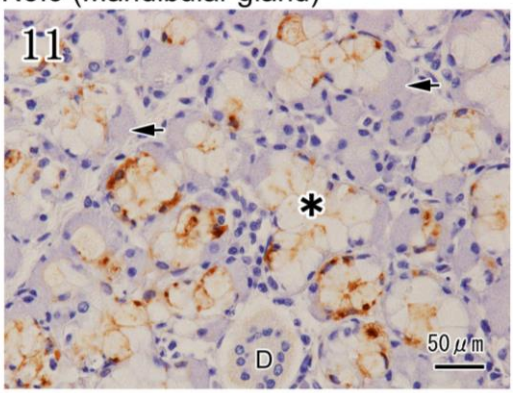

No.3 (Mandibular gland)

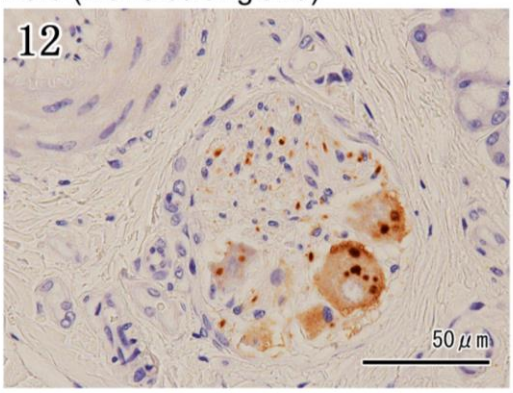

No.3 (Parotid gland)

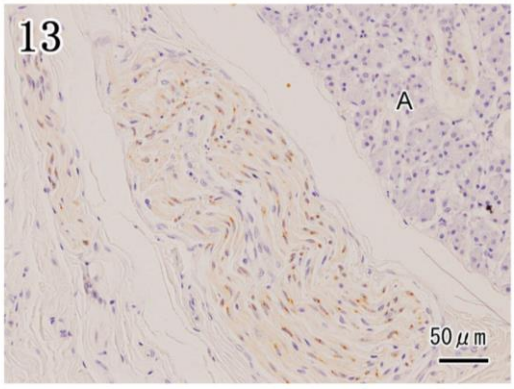

No.9 (Parotid gland)

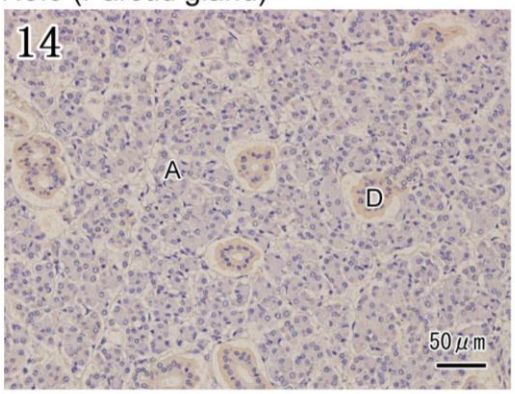

Figs.15-18: Immunohistochemistry (CD3, CD20, CD79 α)

No.9 (Mandibular gland, CD3)

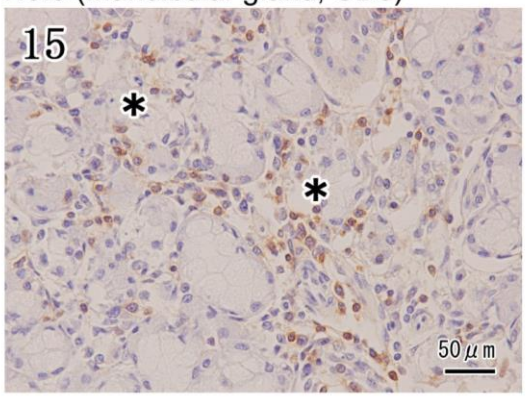

No.13 (Mandibular gland, CD20)

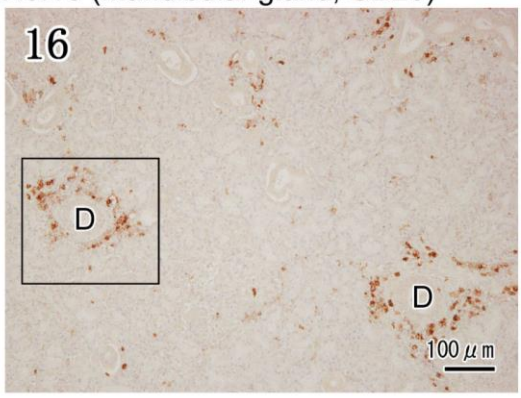

No.13 (Mandibular gland, CD20)

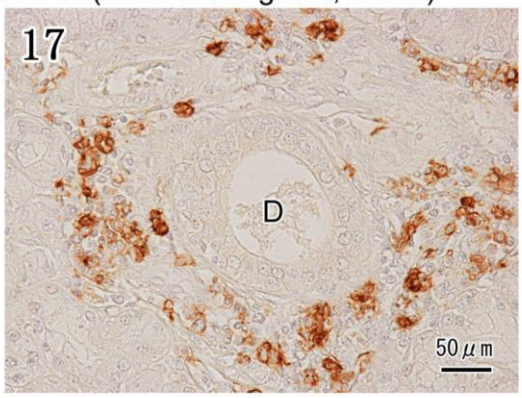

No.9 (Mandibular gland, CD79 α)

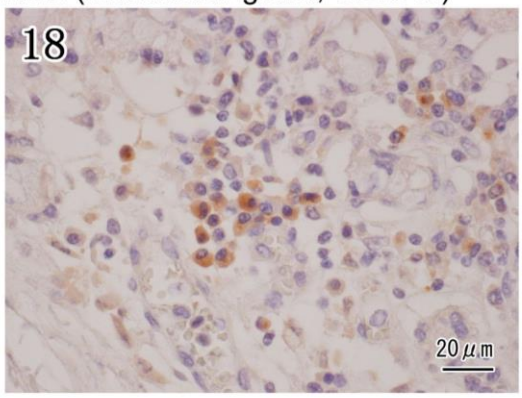

Figs.19-23: Immunohistochemistry (laminin, α-SMA), reticulin silver staining

Control (Mandibular gland, laminin)

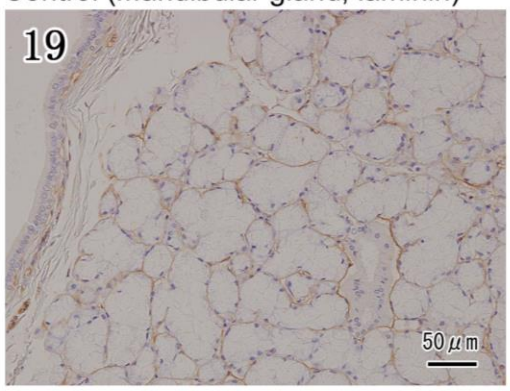

No.2 (Mandibular gland, laminin)

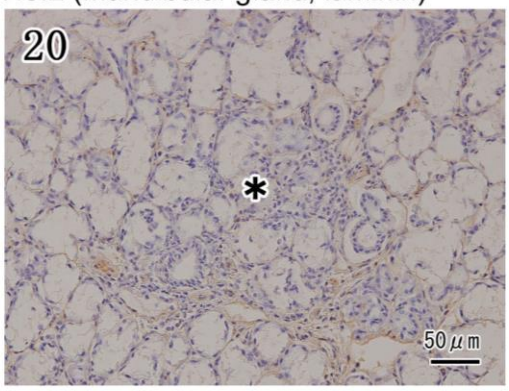

No.19 (Mandibular gland, silver staining)

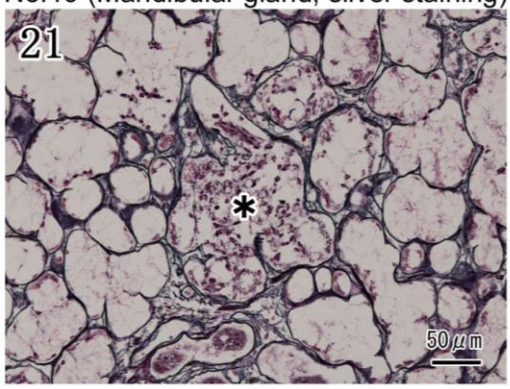

Control (Mandibular gland, α-SMA)

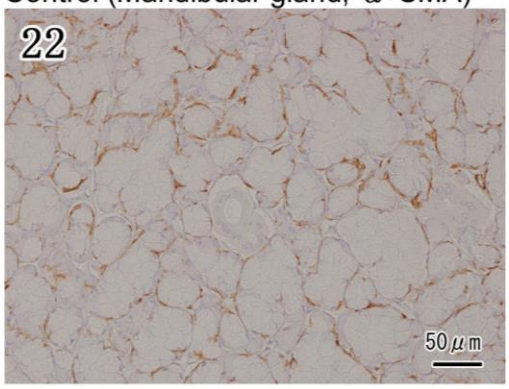

No.19 (Mandibular gland, α-SMA)

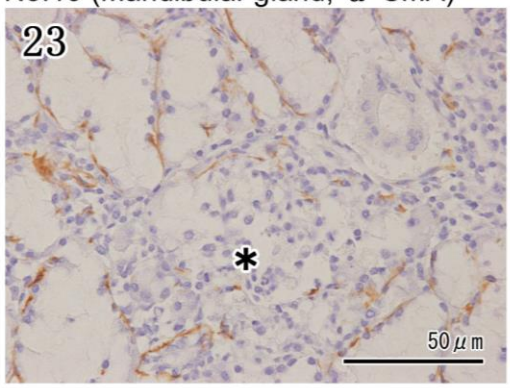

Figs.24-27: Immunohistochemistry (caspase-3), TUNEL assays

No.19 (Mandibular gland, TUNEL)

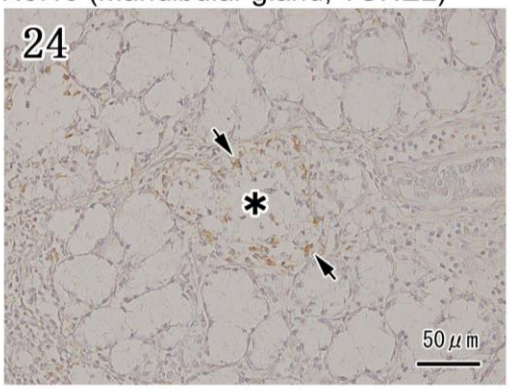

No.9 (Mandibular gland, TUNEL)

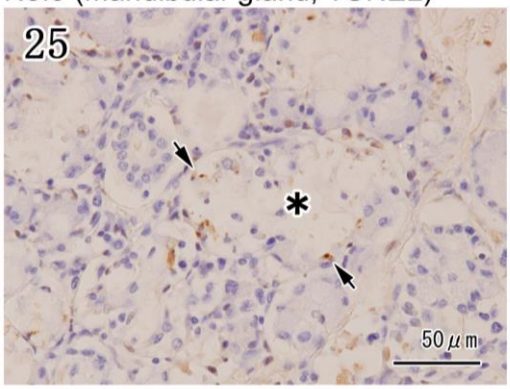

No.19 (Parotid gland, TUNEL)

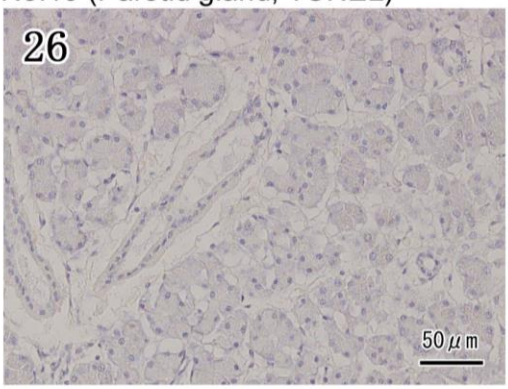

No.9 (Mandibular gland, caspase-3)

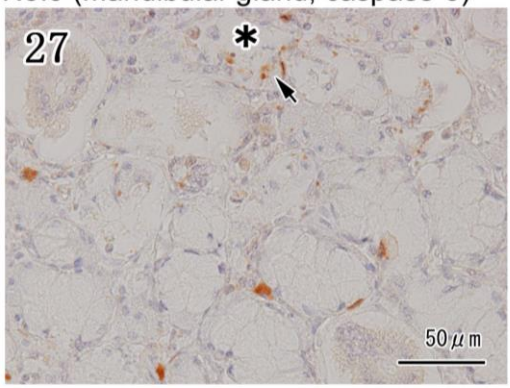

Figs.28-31: Immunohistochemistry (NSE, NF)

Control (Mandibular gland, NSE)

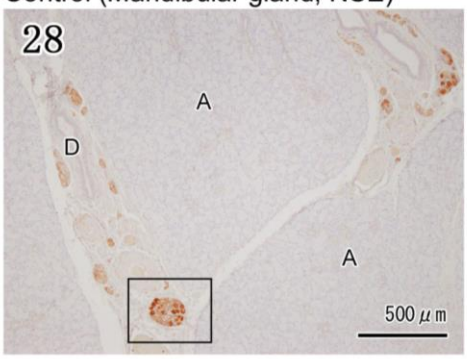

Control (Mandibular gland, NSE)

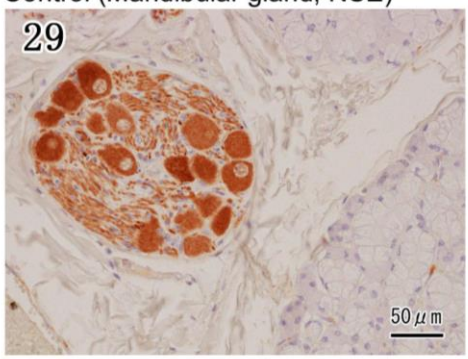

Control (Parotid gland, NSE)

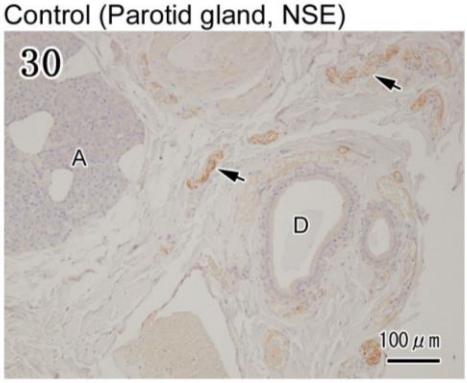

Control (Mandibular gland, NF)

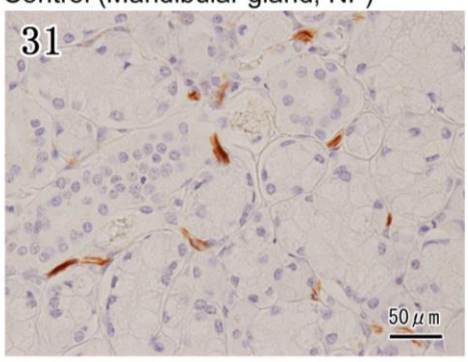

Figs.32-33: Double staining

No.3 (Mandibular gland, α-SMA+anti-P)

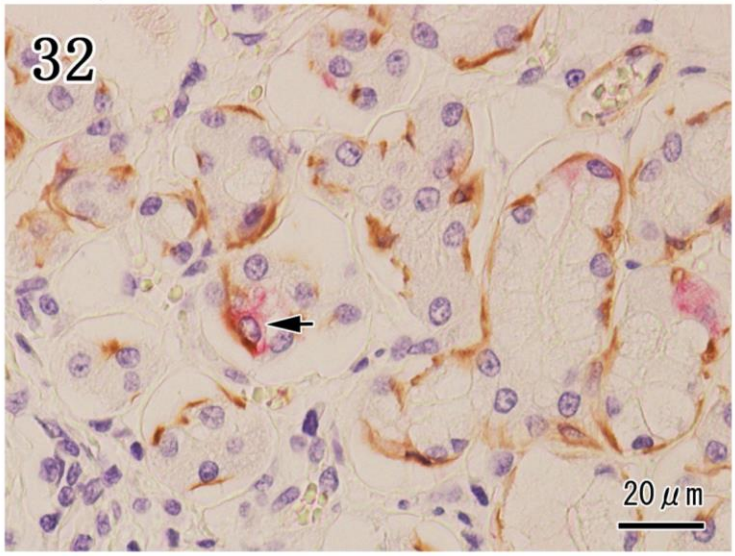

No.3 (Mandibular gland, AB+anti-P)

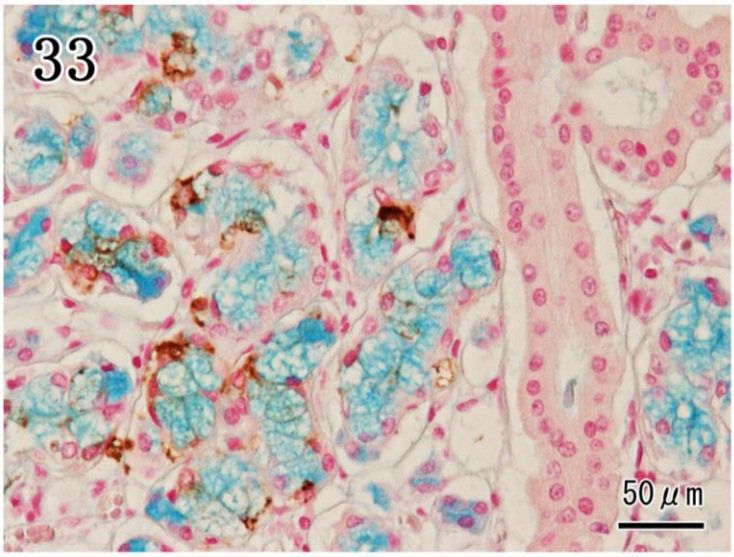

Chapter 2 Localization of the rabies virus antigens and diagnostic utility of the muzzle skins of rabid dogs

Introduction

Rabies is a highly fatal zoonotic disease caused by the rabies virus that can be transmitted through infected saliva of mammals [20]. More than 150 countries and territories are currently infected with rabies. It is occurring worldwide and more than 55,000 people die of rabies every year and approximately 34,500 of these deaths come from Asia [33]. In addition, domestic dogs are the major vector of rabies and cause more than 98% of all human rabies deaths in the Philippines [11]. In dogs, rabies diagnosis based on clinical symptoms alone is difficult and unreliable due to this disease can manifest in various forms [22]; besides, rabies should be strongly considered in the differential diagnosis of any animals presenting with similar neurological symptoms from other diseases such as canine distemper virus infection [16, 18]. According to the World Health Organization recommendation, the most commonly method used for postmortem diagnosis of rabies is the direct fluorescent antibody test [33]. This method utilizes fresh brain sample such as hippocampus, brain stem or cerebellum. However, using brain samples is laborious, time-consuming and there is a high risk of exposure to the rabies virus. In addition, decomposed brain sample can yield to reduce the sensitivity of the test and may even result in false negative [25]. Thus, alternative methods for rabies diagnosis are needed based on a simple collection of non-nervous specimens. Delays in diagnosis of rabies vectors greatly increase the number of contacts that require post-exposure prophylaxis [17]. Therefore, the early diagnosis of rabies is essential to eliminate the expense and discomfort of unnecessary diagnostic tests and inappropriate therapy, help to reduce the spread of the disease and for initiation of specific therapy if an aggressive approach is considered [15, 32].

Recently, in humans, ante-mortem detection of rabies by molecular techniques based on detecting virus or viral RNA can be established from skin biopsy of hair follicle at the nape of the neck [8, 9, 26]. Likewise, in dogs, a molecular technique by using the TaqMan RT-PCR from whisker follicles and hair follicles collected from dead animals has been applied for postmortem diagnosis of rabies [31]. However, the limitation of molecular techniques is the need for an expensive equipment, required standardization and also very stringent quality control in order to avoid false positive results [25]. Also, a major limitation of the immunofluorescence test is required the use of expensive fluorescent microscope and this method may not be practical and also need a cryostat in order to prepare frozen section, and limits its use in many developing countries [25]. Using the formalin-fixed samples in immunohistochemistry, the rabies virus is rapidly inactivated by formaldehyde, and making the transport and laboratory processing of samples much safer; besides, this method is important when the diagnosis must be made overseas and requiring international transportation of sample with zoonotic diseases [28]. Previously, immunohistochemistry method by using skin samples is available for ante-mortem diagnosis of rabies in humans [2, 29]. To my knowledge, however, using this method for the localization of rabies viral antigen in the muzzle skin of rabid dogs with detailed the route of virus propagation has not been investigated. Therefore, the aims of the present study were to evaluate the diagnostic utility of the muzzle skins containing follicle-sinus complexes and localization of the viral antigen in the follicle-sinus complexes (FSCs) by using immunohistochemistry and immunofluorescent antibody test of rabid dogs in the Philippines.

Materials and methods

Animals and direct fluorescence antibody test (dFAT)

The samples were obtained from 9 rabid dogs, which had been submitted to the Research Institute of Tropical Medicine (RITM), Philippines for postmortem diagnosis of rabies. The skin samples containing approximately 15-20 tactile hair follicles were collected from area around lips and muzzle. Small transverse sections (2-3 mm in thickness) of ammon's horn and medulla were cut and slide was touched against the surface of the section and then placed on cold acetone overnight for fixing. After fixation, slides were air dried at room temperature. Then 450 µl of fluorescence isothiocyanate conjugate anti-rabies monoclonal antibody (Fujirebio®, Malvern, Pennsylvania) was added. The slides were incubated for 30 minutes at 37°C in a high humidity chamber. Slides were then dipped rinsed for 20 to 25 times in PBS twice followed by distilled water for further washing. Small amounts of the mounting, 20% glycerol-Tris buffered saline pH 9.0, was placed on the slides before covering with coverslips for examination. The slides were examined under the fluorescent microscope (Nikon eclipse 80i, Japan).

Histopathological examination

The muzzle skin containing FSCs of rabid (n=9) and control (n=3) dogs were fixed in 10% neutral buffered formalin at room temperature for more than 48 hour, trimmed at the level of the ring sinus, embedded in paraffin, sectioned (3 µm thickness), and mounted. Three rabies-vaccinated domestic Japanese mixed dogs (8 to 10 years old) were used as a control group. The sections were then subjected to hematoxylin and eosin, immunohistochemistry and indirect immunofluorescence test as described below.

Staining with hematoxylin and eosin (HE)

The sections were stained with hematoxylin and eosin for general histopathological examination.

Protocol

Paraffin was removed from the sections by a series of xylene and ethanol rinses. Tissue sections were rinsed in distilled water for 5 minutes and stained with hematoxylin solution (Certistain®, Darmstadt, Germany) for 3 minutes, rinsed in running tap water for 5 minutes and stained with eosin solution (Sakura Finetek Japan Co.,Ltd., Tokyo, Japan) for 5 minutes, rinsed in distilled water for three times and dehydrated through a series of ethanol and xylene. The sections were then mounted in microscopy mounting medium.

Immunohistochemistry

1. *For detection of the rabies virus antigens in tissues*

The sections were stained using the streptavidin-biotin-peroxidase complex method with rabbit anti-phosphoprotein (P) antibodies.

Protocol

The sections were deparaffinized by a series of xylene and ethanol rinses, rehydrated, and washed twice with distilled water. The sections were treated for the activation of antigen with 0.25% trypsin at room temperature for 30 minutes. After this treatment, sections were washed three times for 5 minutes in distilled water. After washing, to removed endogenous peroxidase activity the sections were immersed with 0.3% H_2O_2 in methanol for 60 minutes; then they were washed three times for 5 minutes in distilled water once again. The sections were treated with 10% normal goat serum (Nichirei Biosciences, Tokyo, Japan) for 60 minutes to block non-specific reaction. Sections were then incubated with primary antibody for overnight at 4°C in a

humidified chamber. Primary antibody was diluted 1:1200. After incubation with primary antibody, sections were washed three times for 5 minutes in phosphate buffer saline (PBS, pH 7.4) and incubated for 30 minutes at room temperature with the biotinylated anti-rabbit IgG (Nichirei Biosciences) as a secondary antibody. Sections were again washed three times for 5 minutes in PBS; then incubated for 30 minutes in room temperature with peroxidase-streptavidin enzyme (Nichirei Biosciences) for 30 minutes, washed in PBS three times for 5 minutes. Finally, sections were visualized using 3-3'-diaminobenzidine tetrachloride substrate (DAB substrate; DAKO, Kyoto, Japan), followed by rinsing in distilled water. The sections were counterstained with hematoxylin, and rinsing in running tap water again for 5 minutes. The sections were then dehydrated and mounted in microscopy mounting medium. Negative control was processed with rabbit serum instead of primary antibody.

2. For detection of the Merkel cells

The sections were stained using the polymer-based immunohistochemical method with rabbit anti-cytokeratin 20 antibodies (CK20, Spring Bioscience, Fremont, USA.) for detection of the Merkel cells.

Protocol

The sections were deparaffinized by a series of xylene and ethanol rinses, rehydrated, and washed twice with distilled water. The sections were treated with 10mM Sodium citrate buffer (pH 6.0) for activation of antigens by microwaving at 170W for 10 minutes; then were washed in distilled water with three changes of 5 minutes each. After washing, incubation for 10 minutes in 3% H_2O_2 in methanol to removed endogenous peroxidase activity, and the sections were rinsed in distilled water (three changes, 5 minutes each). The slides were treated with the primary antibody for overnight at 4°C in a humidified chamber. Primary antibody was diluted 1:200. After incubation with the primary antibody, sections were rinsed in PBS (three

changes, 5 minutes each), then incubated for 30 minutes at room temperature with Envision + System Labelled Polymer-HRP anti-rabbit (DAKO, Tokyo, Japan) was used as a secondary antibody, rinsed in PBS (three changes, 5 minutes each) once again. Finally, sections were visualized using DAB substrate, followed by rinsing in distilled water. The sections were counterstained with hematoxylin, and rinsing in running tap water again for 5 minutes. The sections were then dehydrated and mounted in microscopy mounting medium.

3. For detection of the Merkel cells

The sections were stained using the polymer-based immunohistochemical method with mouse anti-cytokeratin (CAM 5.2) antibodies (Bection Dickinson, San Jose, USA.) for detection of the Merkel cells.

Protocol

The sections were deparaffinized by a series of xylene and ethanol rinses, rehydrated, and washed twice with distilled water. After washing, incubation for 10 minutes in 3% H_2O_2 in methanol to removed endogenous peroxidase activity, and the sections were rinsed in distilled water (three changes, 5 minutes each). The sections were treated for the activation of antigens with Proteinase-K at room temperature for 30 minutes; then they were rinsed in distilled water with three changes of 5 minutes each. The sections were incubated with the primary antibody for 60 minutes in room temperature. After incubation with the primary antibody, sections were rinsed in PBS (three changes, 5 minutes each), then incubated for 30 minutes at room temperature with Envision + System Labelled Polymer-HRP anti-mouse (DAKO, Tokyo, Japan) was used as a secondary antibody, rinsed in PBS (three changes, 5 minutes each) once again. Finally, sections were visualized using DAB substrate, followed by rinsing in distilled water. The sections were counterstained with hematoxylin, and rinsing in running tap water

again for 5 minutes. The sections were then dehydrated and mounted in microscopy mounting medium.

4. For detection of nerve fibers

The sections were stained using the polymer-based immunohistochemical method with monoclonal mouse anti-neurofilament protein antibodies (NF, DAKO, Kyoto, Japan) for detection of nerve fibers.

Protocol

The sections were deparaffinized by a series of xylene and ethanol rinses, rehydrated, and washed twice with distilled water. After washing, the sections were treated for the activation of antigens with Proteinase-K at room temperature for 30 minutes; then they were rinsed in distilled water with three changes of 5 minutes each. Incubation for 10 minutes in 3% H_2O_2 in methanol to removed endogenous peroxidase activity, and the sections were rinsed in distilled water (three changes, 5 minutes each), followed by incubation with the primary antibody for overnight at 4°C in a humidified chamber. Primary antibody was diluted 1:100. After incubation with the primary antibody, sections were rinsed in PBS (three changes, 5 minutes each), then incubated for 30 minutes at room temperature with the Histofine® Simple Stain MAX-PO (Mouse) (Nichirei Biosciences) rinsed in PBS (three changes, 5 minutes each) once again. Finally, sections were visualized using DAB substrate, followed by rinsing in distilled water. The sections were counterstained with hematoxylin, and rinsing in running tap water again for 5 minutes. The sections were then dehydrated and mounted in microscopy mounting medium.

Double immunofluorescence staining

Double staining of a single tissue section was used for identification of cell type and the co-expression of antigens. Primary antibodies used were rabbit anti-P for detection of rabies

viral antigen in tissue. For detection of the Merkel cell, the sections were stained using mouse anti-CK20 or anti-CAM 5.2. The FITC-conjugated goat anti-rabbit IgG (H+L) (Southern Biotech, Birmingham, USA) was used as a secondary antibody for immunostaining for against rabbit anti-P, and Alexa Fluor® 546 goat anti-mouse IgG (H+L) (Molecular Probes, Eugene, OR, USA) was used for against anti-CK20 or anti-CAM 5.2.

Protocol

After fixed the muzzle skin samples within 10% buffer formalin, the tissues were washing in running tap water, and these samples were trimmed in 5 mm thick contained tactile hair follicles, then embedded samples in medium for tissue freezing (Tissue-Tek® OCT™ Compound); frozen tissue blocks are transferred to the cryo-chamber for sectioning or are stored in firmly closed vials at -80°C until use. The sections of 10 μm thickness are cut with the cryo-microtome at -25°C and collected on glass slides. Prior to immunostaining, sections are warmed at room temperature and air-dried. Thereafter, washing slides by PBS or distilled water

, followed by sections are incubated with diluted primary antibody for anti-P (1:1000) for 30 minutes at 37°C in an incubator, then washing in PBS (three changes, 5 minutes each). After washing, sections are incubated with diluted secondary antibody, the FITC-conjugated goat anti-rabbit IgG (H+L) (1:200) for 30 minutes at 37°C in an incubator, then washing in PBS (three changes, 5 minutes each). After washing, sections are incubated with diluted primary antibody for anti-CK20 or anti-CAM 5.2 (1:200) for 30 minutes at 37°C in an incubator, then washing in PBS (three changes, 5 minutes each), followed by incubated with diluted secondary antibody, the Alexa Fluor® 546 goat anti-mouse IgG (H+L) (1:200) for 30 minutes at 37°C in an incubator. Finally, sections are mounted under cover glass with a drop of glycerol. The slides are examined under the fluorescence microscope (Nikon, Japan).

Results

Clinical characteristics of the dogs

Six dogs were discovered after having died, while three dogs were subjected to euthanasia. The 9 dogs (3 male, 3 female, and 3 of unknown sex) ranged in age from 1 to 16 months, with five dogs having unknown ages. Five of the 9 dogs had no history of rabies vaccination, and no information on rabies vaccination status was available for four dogs. Six dogs were free-roaming dogs with owners, two were strays, and one was confined with household contact. The primary clinical symptoms of canine rabies infection, such as unprovoked aggressiveness, mad biting of inanimate objects, aimless running, and excessive salivation, were documented in all dogs. All brain specimens were diagnosed as positive for rabies virus antigen through the direct immunofluorescence antibody test (dFAT). The clinical information and results of dFAT are summarized in the Table 1.

Gross and histological findings of the muzzle skin in control dogs

No gross findings were observed in muzzle skin in rabid dogs (Fig. 1). The muzzle skin was included many of tactile hairs (also called follicle-sinus complexes, FSCs) (Fig. 2). Each FSC was comprised of a blood filled sinus called ring sinus and cavernous sinus that locate between the outer and the inner layers of the dermal sheath (Fig. 3). A relatively sizable ring-wulst was present in the ring sinus. Histologically, in control dogs, the upper portion of the FSC is a simple cavity filled with blood and does not contain connective tissue referred to as the ring sinus, and the lower half portion contains numerous trabeculae is referred to as the cavernous sinus, which are strands of connective tissue that bridge the cavity to constitute part of its framework. A cross section of the FSCs at the level of ring sinus demonstrates slightly thickened of the outer root sheath, the basal layer of the outer root sheath consists of the keratinocytes admixed with melanocytes and Merkel cells (Figs. 4, 5). The Merkel cells are

characterized by slightly larger than the associated keratinocytes and melanocytes, and the cells had distinctive clear cytoplasm.

Histopathological examination of the muzzle skin of rabid dogs

In all rabid dogs, there was no histological evidence of inflammation or necrosis observed in the FSCs, primary hair follicle, perifollicular nerves, and any of accessory glands **(**Figs. 6-9**)**. Furthermore, Negri bodies were not observed in all samples examined

Immunohistochemical examination of the muzzle skin

Detection of rabies virus antigen by anti-P antibodies

No viral antigen was detected in control dogs (data not shown). In all rabid dogs, viral antigens were detected in the basal layer of the outer root sheath and peripheral nerves surrounding the base of FSCs (Figs. 10, 11). Similar findings were observed in longitudinal sections (Figs. 12-14). Viral antigens were also detected in the outer root sheath and perifollicular nerves of the primary hair follicle (Fig. 15).

Detection of nervous tissues by anti-NF antibodies

In control dogs, anti-NF immunoreactivity was demonstrated numerous peripheral nerves surrounding FSCs. In addition, anti-NF positive cells were detected in the basal layer of the outer root sheath at the level of ring sinus. Similar findings were also observed in rabid dogs (Figs. 16, 17).

Detection of the Merkel cells by anti-CK20 antibodies

In control dogs, anti CK20-positive Merkel cells were observed in the basal layer of the outer root sheath at the level of ring sinus. In addition, a few anti-CK20-positive Merkel cells

were also detected scattered in the ring-bulge structure of ring sinus. Similar findings were observed in rabid dogs (Figs. 18, 19).

Detection and localization of the Merkel cells by anti-CAM 5.2 antibodies

In rabid dogs, anti-CAM 5.2 positive Merkel cells were observed in the basal layer of the outer root sheath at the level of ring sinus (Figs. 20, 21). Similar findings were observed in control dogs.

Identification of virus-infected cells by combination of anti-P and anti-CK20 or anti-CAM 5.2 double immunofluorescence staining

In rabid dogs, viral antigens were detected in the basal cell layer of the outer root sheath at the level of ring sinus of FSCs, as indicated by the greenish staining (Figs. 22, 26, 31). Similar findings were observed in longitudinal sections (Fig. 25). The Markel cells were demonstrated by anti-CK20 (Fig. 23) and anti-CAM 5.2 (Figs. 27, 28, 32) antibodies in the basal cell layer of the outer root sheath at the level of ring sinus, as indicated by the reddish staining. The most of anti-CK20 positive Markel cells showed co-expression with anti-P antibody reactivity, as indicated by the yellowish-orange staining (Figs. 24). Likewise, viral antigens were detected in cells showing anti-CAM 5.2 staining (Figs. 29, 30, 33).

Discussion

Human rabies cases in developing countries have continued to increase in recent years. In a national epidemiological survey, 97.1% of patients had bitten by dogs, and only 2.9% had been infected by cats [11]. Therefore, it is important to control and prevent rabies in dogs in order to eliminate human rabies in the Philippines and other developing countries. The most widely used method for postmortem diagnoses of rabies are the direct fluorescent antibody test (dFAT) and reverse transcription polymerase chain reaction (RT-PCR). The dFAT is laborious, time-consuming and there is a high risk of exposure to the rabies virus. Molecular detection of the rabies viral RNA by RT-PCR technique has the highest sensitivity, but it requires standardization and very stringent quality control in order to avoid false results. The neck skin biopsy samples are the most widely studied specimens for attempting antemortem and postmortem diagnosis [8, 29]. The aim of the present study was to evaluate the diagnostic utility of the muzzle skin containing FSCs of rabid dogs and was to localization of the rabies viral antigen in the FSCs with detailed viral propagation were discussed.

In all canines with rabies analyzed in this study, no histological evidence of inflammation or necrosis was observed in the FSCs, primary hair follicle, perifollicular nerves, and any of accessory glands, as well as Negri body was not found in all samples examined though the viral antigen was detected here. These findings are consistent with human cases were infected with a canine-variant of rabies [29]. Therefore, it was suggested that viral proliferation in the follicle-sinus complexes and perifollicular nerves dose not induced inflammation and cytolysis in the skin and its adnexa.

In animals, the FSCs of the muzzle skin included numerous mechanoreceptors and free nerve endings received sensory innervation from a deep vibrissal nerve, a branch of the infraorbital branch of the trigeminal nerve [12, 13, 24]. In addition, the FSCs play an important

role in the tactile sensitivity and assist to explore their environment in some mammals [24]. In this study, the viral antigens were detected in the basal layer of the outer root sheath at the level of ring sinus and perifollicular nerves of the FSCs, similar to results reported in skunks and foxes infected with the street rabies virus [3]. Thus, centrifugal viral propagation spreads to the FSCs via sensory innervations. After rabies virus proliferates in the trigeminal nuclei, located in the pons region of the brainstem, and the virus then descends to the trigeminal ganglion and move along the trigeminal nerve and their branches to reach the FSCs [1, 21, 27].

In the present study, virus-infected cells in the FSCs were identified as the Merkel cells. Thus, the rabies virus may propagate in Merkel cells and affect nerve innervation. Previous studies have described the morphological structures and sensory innervation of the Merkel cells [6, 23]. These Merkel cells are considered to be neuroendocrine cells because of their ability to produce numerous neurotransmitters and hormones, and make synaptic-like contacts with sensory afferent terminals. In addition, studies of transneuronal propagation of rabies virus have revealed it propagates exclusively between connected neurons at chemical synapses [30]. Therefore, it was suggested that the rabies virus may directly enter Merkel cells via the synaptic junctions, and also infection of rabies virus in the Merkel cells and trigeminal tract might be responsible for reduction or loss of skin sensation [10].

The detection of rabies viral antigen in the muzzle skin after the onset of clinical symptoms until the terminal stages of the disease is usually occurred, while an early confirmed diagnosis 2-4 days before the onset of symptoms was possible in experimental infection of mice infected by a street rabies virus strain, and decreasing amounts to lack of the viral antigen present in the muzzle skin occurred in recovered mice [5]. By contrast, these observations differ from dogs infected with the street rabies virus that the viral antigen was not detected in the muzzle skin taken before rabies symptoms appear [14], suggesting that animals with a negative skin result at the time before symptoms appear may not free from the risk of rabies, it was may

be likely reflects the presence of a limited amount of viral antigen rather than none. Furthermore, the lack of the rabies viral antigen present in the skin tissues of recovered animals, it was probably due to CNS-produced neutralizing antibody formed in response to the infection, while the percentage of positive skin results increased as the infection progressed [4, 5]. In the present study, viral antigen was detected in the muzzle skin of all rabid dogs, which were discovered after died or euthanized after rabies symptoms developed, and they were confirmed rabies by FAT on brain tissue samples. These findings are consistent with those of previous studies, therefore, it was suggested that the presence of viral antigen in the FSCs was strongly associated with viral antigen appears in the brain tissue.

The anatomical placement and the localization of rabies viral antigen in muzzle skin is an important consideration. In this study, in the case of dogs, the author recommended sampling area is the muzzle skin contains tactile hairs and thought to be optimal for examination. This is because the tactile hair, being very large and have abundant nerve supply which increasing the possibilities that rabies virus will be present in quantity adequate to be detected [5, 31]. Furthermore, the cutting level of the hair follicle is also should be considered. Previously, in routine laboratory testing use the immunofluorescence method for intravitam diagnosis of rabies in humans using skin biopsy from the nape of the neck, Crepin *et al.* [7] noticed that a minimum of 20 sections were needed to ensure the observation of hair follicles, and also the technique of skin biopsy, the sample should be containing at least 10 hair follicles [19]. In the present study, the viral antigen was mainly detected in the level of ring sinus of the FSCs because of this area had the highest concentration of Merkel cells and numerous perifollicular nerves. Thus, cutting area in the level of ring sinus was recommended.

Dogs with rabies can manifest in either the furious or paralytic forms [22]. Previous studies have described the distribution of the rabies viral antigen in CNS of furious and paralytic rabid dogs [27]. In furious dogs, the viral antigen was wildly distributed in all part of the brain,

and midbrain particularly the trigeminal nucleus were also heavily infected regions, while in paralytic dogs, the viral antigen was confined mainly to the cerebellum and medulla oblongata. Wacharapluesadee *et al*. [31] have demonstrated that paralytic rabid dogs had higher rate of false-negative results of the RT-PCR for detection of rabies viral RNA when using whisker hairs and saliva, suggesting that much lower amounts of rabies viral RNA are found in the brains of paralytic rabid dogs than their furious counterparts [22]. In the present study, the initial clinical symptoms of furious rabies such as unprovoked aggression, mad biting of inanimate object and aimless running were noted in all rabid dogs. The viral antigen was also detected in all brain samples. Therefore, these findings suggested that higher amount of viral load in the brain of furious rabid dogs may affect the amount of virus progresses to FSCs. In this study, however, the presence of viral antigen in the FSCs of paralytic rabid dogs remains uninvestigated, therefore, further studies are required.

In summary, in this study confirmed the presence of viral antigen was localized in the Merkel cells, which were an important mechanosensory receptor cell of the tactile hair, and also the path through which the rabies virus descends along the trigeminal nerve after proliferation in the brain to reach the Merkel cells of the tactile hair. Although, the positive rate when using muzzle skin samples was 100% (9/9), in spite of, the numbers of rabid dogs studied is not sufficient for used these muzzle skin samples for ante-mortem diagnosis of rabies in dogs because of the present study is lack of serial sampling and correlation with stage of infection and most of the present cases were discovered after died. It was, however, suggested that muzzle skin are very useful as alternative source of postmortem diagnosis of rabies, especially in rabies-endemic developing countries.

References

1. Abreu, C. C., Nakayama, P. A., Nogueira, C. I., Mesquita, L. P., Lopes, P. F., Wouters, F., Varaschin, M. S. and Bezerra P. S. Jr. 2014. Histopathology and immunohistochemistry of tissues outside central nervous system in bovine rabies. *J. Neuroviral.* **20**: 388-397.
2. Bagó, Z., Revilla-Fernández, S., Allerberger, F. and Krause, R. 2005. Value of immunohistochemistry for rapid ante mortem rabies diagnosis. *Int. J. Infect. Dis.* **9**: 351-352.
3. Balachandran, A. and Charlton, K. 1994. Experimental rabies infection of non-nervous tissues in skunks (*Mephitis mephitis*) and foxes (*Vulpes vulpes*). *Vet. Pathol*. **31**: 93-102.
4. Blenden, D. C., 1981. Rabies in a litter of skunks predicted and diagnosed by skin biopsy. *J. Am. Vet. Med. Assoc.* **179**: 789-791.
5. Blenden, D. C., Bell, J. F., Tsao, A. T. and Umoh, J. U. 1983. Immunofluorescent examination of the skin of rabies-infected animals as a means of early detection of rabies virus antigen. *J. Clin. Microbiol.* **18**: 631-636.
6. Boulais, N. and Misery, L. 2007. Merkel cells. *J. Am. Acad. Dermatol.* **57**: 147-165.
7. Crepin, P., Audry, L., Rotivel, Y., Gacoin, A., Caroff, C. and Bourhy, H. 1998. Intravitam diagnosis of human rabies by PCR using saliva and cerebrospinal fluid. *J. Clin. Microbiol.* **36**: 1117-1121.
8. Dacheux, L., Reynes, J. M., Buchy, P., Sivuth, O., Diop, B. M., Rousset, D., Rathat, C., Jolly, N., Dufourcq, J. B., Nareth, C., Diop, S., Iehlé, C., Rajerison, R., Sadorge, C. and Bourhy, H. 2008. A reliable diagnosis of human rabies based on analysis of skin biopsy specimens. *Clin. Infect. Dis.* **47**: 1410-1417.
9. Dacheux, L., Wacharapluesadee, S., Hemachudha, T., Meslin, F. X., Buchy, P., Reynes, J. M. and Bourhy, H. 2010. More accurate insight into the incidence of human rabies in

developing countries through validated laboratory techniques. *PLoS Negl. Trop. Dis.* **4**: e765.

10. De Lahunta, A. and Glass, E. 2009. *In*: Veterinary Neuroanatomy and Clinical Neurology. Elsevier, St. Louis.

11. Dimaano, E. M., Scholand, S. J., Alera, M. P. and Belandres, D. B. 2011. Clinical and epidemiological features of human rabies cases in the Philippines: a review from 1987 to 2006. *Int. J. Infect. Dis.* **15**: 495-499.

12. Erzurumlu, R. S., Murakami, Y. and Rijli, F. M. 2010. Mapping the face in the somatosensory brainstem. *Nat. Rev. Neurosci.* **11**: 252-263.

13. Esteves, A., Ribeiro, C. F., Dâmaso, C. S., Moreira, F. L., Fernandes, G. J. M., Carvalho, F. J. and Rossi Jr W. C. 2009. Anatomical description of the trigerminal nerve [V] and its branching in mongrel dogs. *Braz. J. Morphol. Sci.* **26**: 187-192.

14. Fekadu, M. and Shaddock, J. H. 1984. Peripheral distribution of virus in dogs inoculated with two strains of rabies virus. *Am. J. Vet. Res.* **45**: 724-729.

15. Gadre, G., Satishchandra, P., Mahadevan, A., Suja, M. S., Madhusudana, S. N., Sundaram, C. and Shankar, S. K. 2010. Rabies viral encephalitis: clinical determinants in diagnosis with special reference to paralytic form. *J. Neurol. Neurosurg. Psychiatry* **81**: 812-820.

16. Hamir, A. N., Summers, B. A. and Rupprecht, C. E. 1998. Concurrent rabies and canine distemper encephalitis in a raccoon (*Procyon lotor*). *J. Vet. Diag. Invest.* **10**: 194-196.

17. Haupt, W. 1999. Rabies – risk of exposure and current trends in prevention of human cases. *Vaccine* **17**: 1742-1749.

18. Jackson, A. C. and Wunner, W. H. 2007. pp: 210-246. *In*: Rabies, 2nd ed., Elsevier Saunders, Philadelphia.

19. Jackson, A. C. 2011. Update on rabies. *Res. Rep. Trop. Med.* **2011**: 31-43.

20. Jackson, A. C. 2014. Rabies. *Handbook of Clinical Neurology*. **123** (3rd series). Elsevier Saunders, Philadelphia.

21. Jenson, A. B., Rabin, E. R., Bentinck, D. C. and Melnick, J. L. 1969. Rabiesvirus neuronitis. *J. Virol.* **3**: 265-270.

22. Laothamatas, J., Wacharapluesadee, S., Lumlertdacha, B., Ampawong, S., Tepsumethanon, V., Shuangshoti, S., Phumesin, P., Asavaphatiboon, S., Worapruekjaru, L., Avihingsanon, Y., Israsena, N., Lafon, M., Wilde, H. and Hemachudha, T. 2008. Furious and paralytic rabies of canine origin: neuroimaging with virological and cytokine studies. *J. Neurovirol.* **14**: 119-129.

23. Maksimovic, S., Baba, Y. and Lumkin, E. A. 2013. Neurotransmitters and synaptic components in the Merkel cells-neurite ceomplex, a gentle-touch receptor. *Ann. N. Y. Acad. Sci.* **1279**: 13-21.

24. Marshall, C. D., Rozas, K., Kot, B. and Gill, V. A. 2014. Innervation patterns of sea otter (*Enhydra lutris*) mystacial follicle-sinus complexes. *Front. Neuroanat.* **8**: 121.

25. Mani, R. S. and Madhusudana, S. N. 2013. Laboratory diagnosis of human rabies: recent advances. *Scientific World Journal* **2013**: 569712.

26. Mani, R. S., Madhusudana, S. N., Mahadevan, A., Reddy, V., Belludi, A. Y. and Shankar, S. K. 2014. Utility of real-time Taqman PCR for antemortem and postmortem diagnosis of human rabies. *J. Med. Virol.* **86**: 1804-1812.

27. Suja, M. S., Mahadevan, A., Madhusudhana, S. N., Vijayasarathi, S. K. and Shankar, S. K. 2009. Neuroanatomical mapping of rabies nucleocapsid viral antigen distribution and apoptosis in pathogenesis in street dog rabies – an immunohistochemistry study. *Clin. Neuropathol.* **28**: 113-124.

28. Stein, L. T., Rech, R. R., Harrison, L. and Brown, C. C. 2010. Immunohistochemical study of rabies virus within the central nervous system of domestic and wildlife species. *Vet. Pathol.* **47**: 630-636.

29. Tobiume, M., Sato, Y., Katano, H., Nakajima, N., Tanaka, K., Noguchi, A., Inoue, S., Hasegawa, H., Iwasa, Y., Tanaka, J., Hayashi, H., Yoshida, S., Kurane, I. and Sata, T. 2009. Rabies virus dissemination in neural tissues of autopsy cases due to rabies imported into Japan from the Philippines: immunohistochemistry. *Pathol. Int.* **59**: 555-566.

30. Ugolini, G. 2011. Rabies virus as a transneuronal tracer of neuronal connections. *Adv. Virus Res.* **79**: 165-202.

31. Wacharapluesadee, S., Tepsumethanon, V., Supavonwong, P., Kaewpom, T., Intarut, N. and Hamachudha, T. 2012. Detection of rabies viral RNA by TaqMan real-time RT-PCR using non-neural specimens from dogs infected with rabies virus. *J. Virol. Methods* **184**. 109-112.

32. Warrell, M. J. and Warrell, D. A. 2015. Rabies: the clinical features, management and prevention of the classic zoonosis. *Clin. Med.* **15**: 78-81.

33. WHO, Expert consultation on rabies. Second report. 2013. *WHO Tech. Rep. Ser.* **982**: 1-139.

Table 1. Clinical information and laboratory findings of rabid dogs (samples obtained postmortem)

No.	Age (months)	Sex	Owned	Manner of death	Vaccination	Animal conditions	Neurological symptoms	dFAT
1	16	Female	Unknown	Found dead	No	Free-roaming and owned	Unprovoked aggressiveness	+
2	Unknown	Unknown	Unknown	Found dead	Unknown	Stray	Unprovoked aggressiveness	+
3	Unknown	Unknown	Unknown	Euthanasia	No	Free-roaming and owned	Unprovoked aggressiveness	+
4	2	Male	Unknown	Found dead	Unknown	Free-roaming and owned	Apprehensive, watchful look, paralysis	+
5	Unknown	Unknown	Unknown	Found dead	No	Free-roaming and owned	Unprovoked aggressiveness	+
6	8	Female	Unknown	Found dead	No	Free-roaming and owned	Unprovoked aggressiveness, mad biting of inanimate objects	+
7	Unknown	Male	Unknown	Euthanasia	Unknown	Free-roaming and owned	Unprovoked aggressiveness	+
8	Unknown	Male	Unknown	Found dead	Unknown	Stray	Unprovoked aggressiveness	+
9	3	Female	Unknown	Euthanasia	No	Confined with household contact	Unprovoked aggressiveness, mad biting of inanimate objects, aimless running	+

+: positive, dFAT: direct fluorescent antibody test

Figure legends

Fig. 1. The muzzle skin. In control dog, the muzzle skin included many of tactile hairs or follicle-sinus complexes of varying size.

Fig. 2. The muzzle skin. In rabid dogs, no gross findings were observed in the FSCs (arrows).

Fig. 3. High magnification of the muzzle skin after formalin fixation in a control dog. FSCs were composed of hair shaft (H), ring sinus (RS) and ring-wulst (arrow).

Figs. 4-5. Histological findings of FSCs in control dogs. Hair shaft (1) surrounded by multi-layer epithelial cells (2), outer root sheath (3), ring-wulst (RW) and ring sinus (RS) (Fig. 4). The Merkel cells were scattered in the basal layer of outer root sheath (Fig. 5, arrows).

Fig. 6. Cross-section of the FSCs of rabid dogs. No histological evidence of inflammation or necrosis was observed in the hair shaft (1), epithelial cells (2), outer root sheath (3), peripheral nerves (4) and ring sinus (RS).

Fig. 7. FSCs. High magnification of Fig. 6. Cross-section at the level of ring sinus showing slightly thickened of the outer root sheath (asterisk), the basal layers of outer root sheath consist of the keratinocytes admixed with melanocytes and Merkel cells (arrows).

Fig. 8. Longitudinal section of the FSCs of rabid dogs. FSCs were composed of hair shaft (1), multi-layer epithelial cells (2), outer root sheath (3), peripheral nerves (4) and ring sinus (RS).

Fig. 9. FSCs. High magnification of Fig. 8. The Merkel cells are slightly larger than the associated keratinocytes and melanocytes, and cells had distinctive clear cytoplasm (arrows).

Figs. 10-11. FSCs. In rabid dogs, viral antigens were detected in the basal layer of the outer root sheath (arrows) and perifollicular nerves (Fig. 11, arrow heads). Immunohistochemistry.

Figs. 12-14. FSCs. In rabid dogs, longitudinal section showing viral antigens was detected in the basal layer of the outer root sheath at level of ring sinus (Figs. 12-13, arrows) and perifollicular nerves (Fig. 14, arrow heads). Immunohistochemistry.

Fig. 15. Primary hair follicle. Viral antigens were also detected in the perifollicular nerves (arrow). Immunohistochemistry.

Figs. 16-17. FSCs. In rabid dogs, anti-NF immunoreactivity demonstrated numerous peripheral nerves surrounding FSCs (Fig. 16, arrow heads) and anti-NF positive cells were observed in the basal layer of the outer root sheath (Fig. 17, arrows). Immunohistochemistry.

Figs. 18-19. FSCs. In rabid dogs, anti-CK20 antibodies demonstrated Merkel cells in the basal layer of outer root sheath. Immunohistochemistry.

Figs. 20-21. FSCs. In rabid dogs, anti-CAM 5.2 antibodies demonstrated Merkel cells in the basal layer of the outer root sheath. Immunohistochemistry.

Fig. 22. FSCs. In rabid dogs, anti-P positive cells were mainly observed in the basal layer of the outer root sheath (green). Immunofluorescence staining.

Fig. 23. FSCs. In rabid dogs, Merkel cells were positive for anti-CK20 antibodies (red). Immunofluorescence staining.

Fig. 24. FSCs. The most of anti-CK20 positive cells were merged to anti-P positive cells (yellow, arrows). Immunofluorescence staining.

Figs. 25-26. FSCs. In rabid dogs, anti-P positive cells were mainly observed in the basal layer of the outer root sheath (green, arrows). Immunofluorescence staining.

Figs. 27-28. FSCs. In rabid dogs, Merkel cells were positive for anti-CAM5.2 antibodies (red). Immunofluorescence staining.

Figs. 29-30. FSCs. The most of anti-CAM5.2 positive cells were merged to anti-P positive cells (yellow, arrows). Immunofluorescence staining.

Fig. 31. FSCs. High magnification of Fig. 26. Anti-P positive cells were mainly observed in the basal layer of the outer root sheath (green). Immunofluorescence staining.

Fig. 32. FSCs. High magnification of Fig. 28. Anti-CAM5.2 positive Merkel cells were observed in the basal layer of outer root sheath (red). Immunofluorescence staining.

Fig. 33. FSCs. High magnification of Fig. 30. The most of anti-CAM 5.2 positive cells were merged to anti-P positive cells (yellow, arrows). Immunofluorescence staining.

Figs.1-3: Gross findings

Control (Muzzle skin, formalin-fixed)

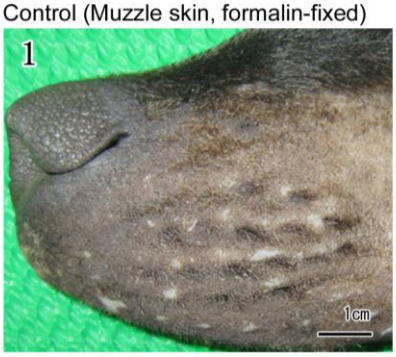

No.3 (FSCs, formalin-fixed)

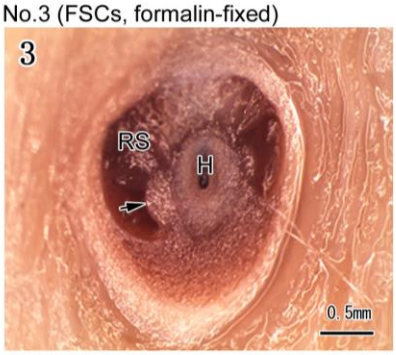

No.3 (Muzzle skin, formalin-fixed)

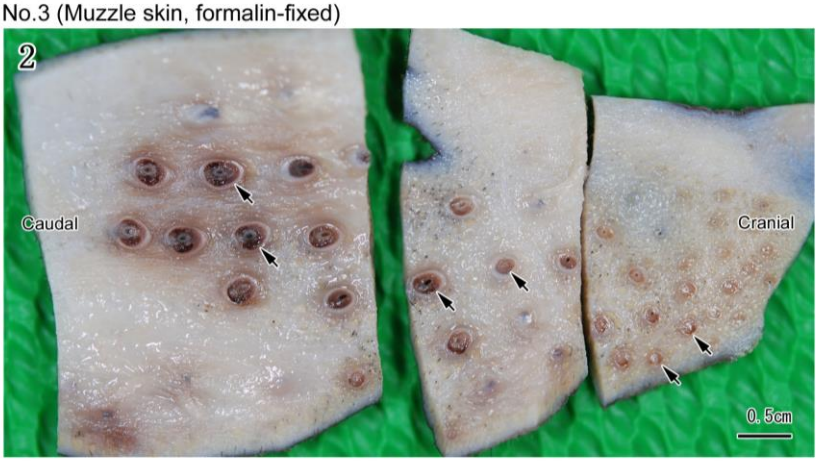

Figs.4-9: Histological findings (HE)

Control (FSCs, cross section)

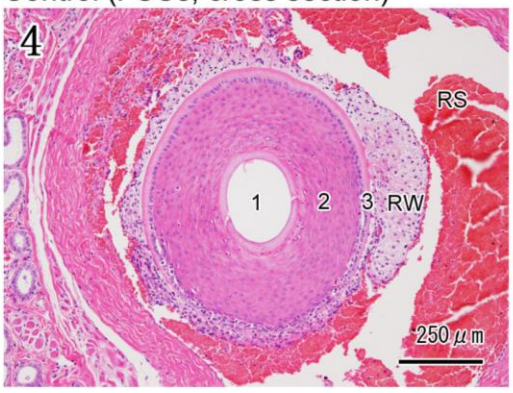

Control (FSCs, cross section)

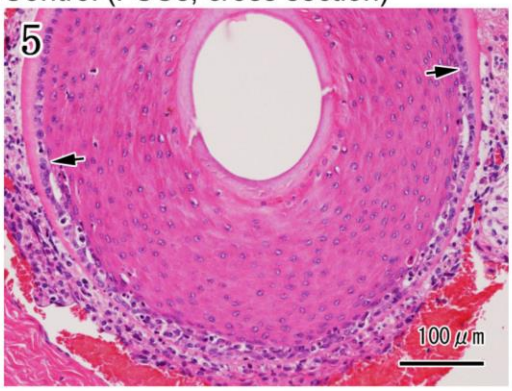

No.3 (FSCs, cross section)

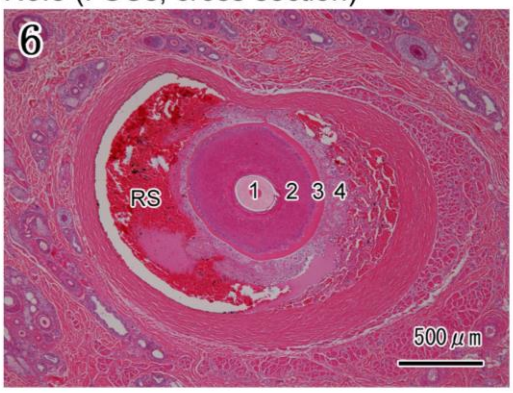

No.3 (FSCs, cross section)

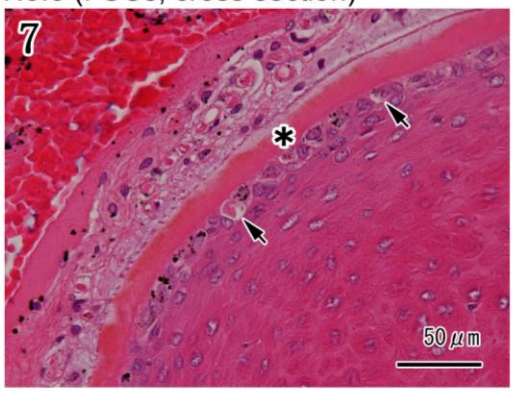

No.3 (FSCs, longitudinal section)

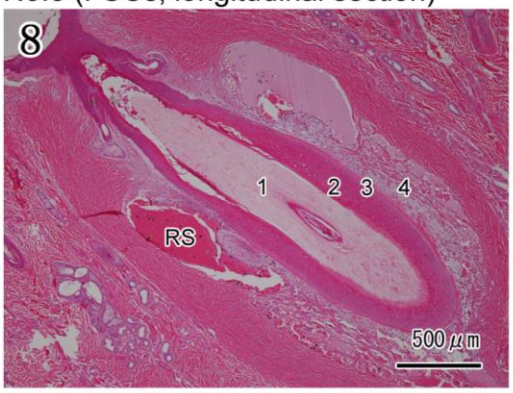

No.3 (FSCs, longitudinal section)

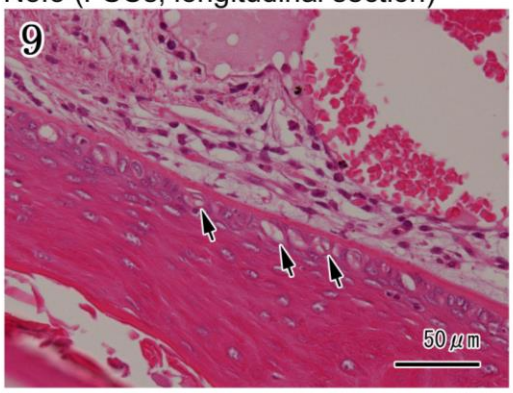

Figs.10-15: Immunohistochemistry (anti-P)

No.4 (FSCs, cross section)

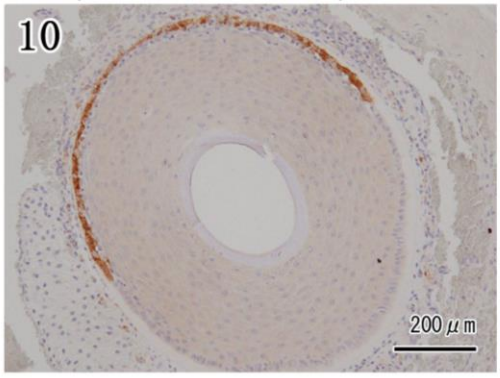

No.4 (FSCs, cross section)

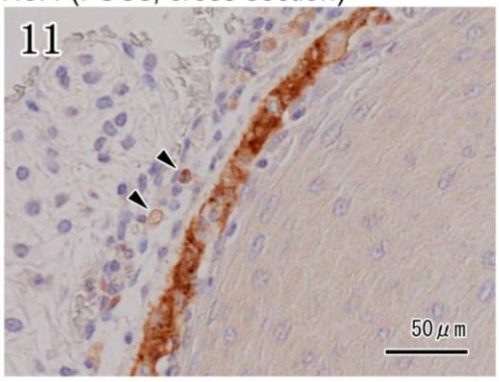

No.3 (FSCs, longitudinal section)

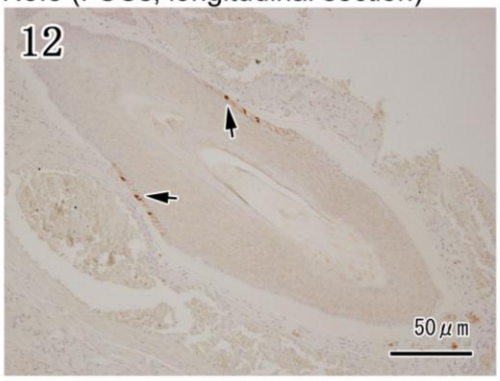

No.3 (FSCs, longitudinal section)

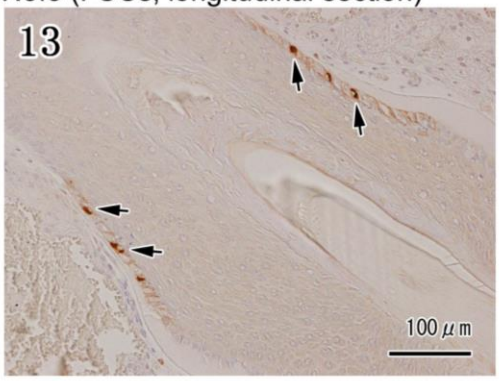

No.3 (FSCs, longitudinal section)

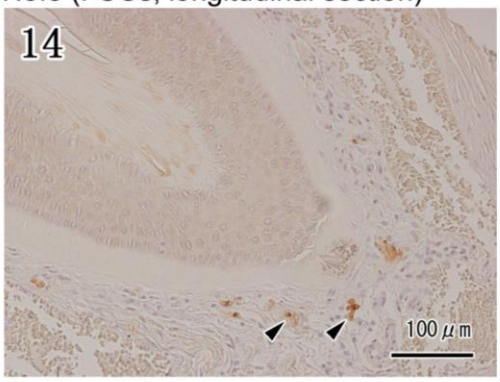

No.4 (primary hair follicle, cross section)

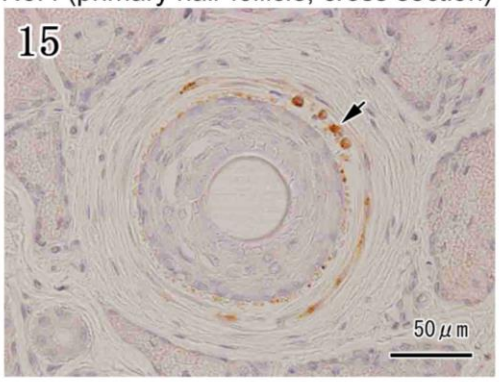

Figs.16-21: Immunohistochemistry (NF, CK20, CAM5.2)

No.4 (FSCs, cross section, NF)

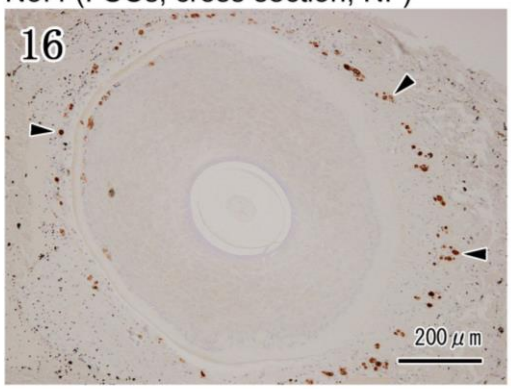

No.4 (FSCs, cross section, NF)

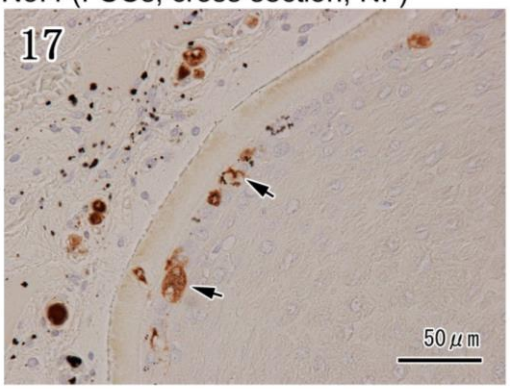

No.4 (FSCs, cross section, CK20)

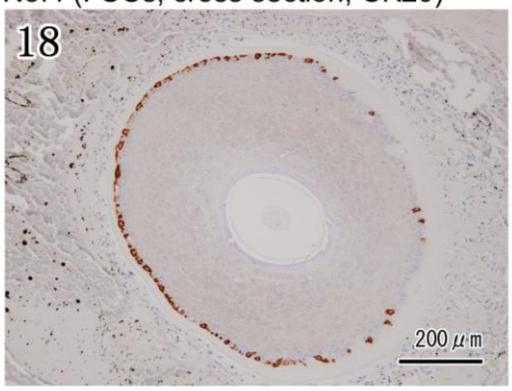

No.4 (FSCs, cross section, CK20)

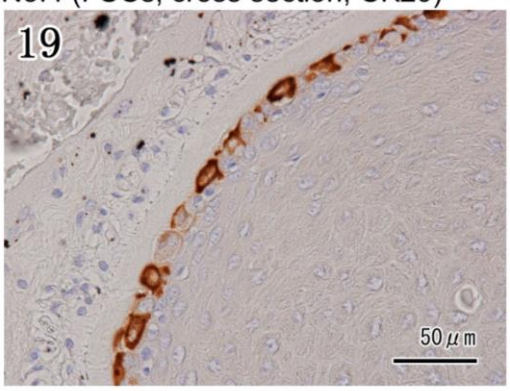

No.4 (FSCs, cross section, CAM5.2)

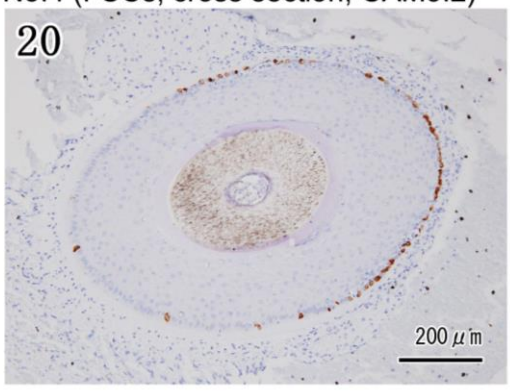

No.4 (FSCs, cross section, CAM5.2)

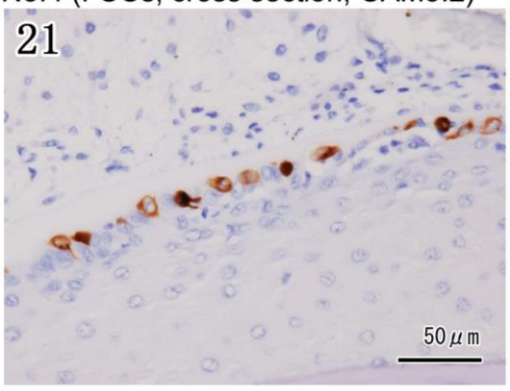

Figs.22-24: Double immunofluorescence staining (CK20 and anti-P)

No.4 (FSCs, cross section, anti-P)

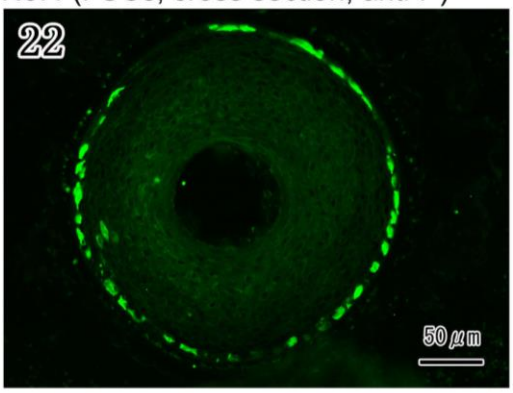

No.4 (FSCs, cross section, CK20)

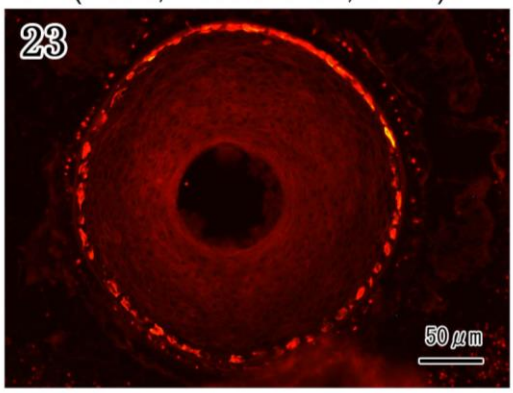

No.4 (FSCs, merge, CK20 and anti-P)

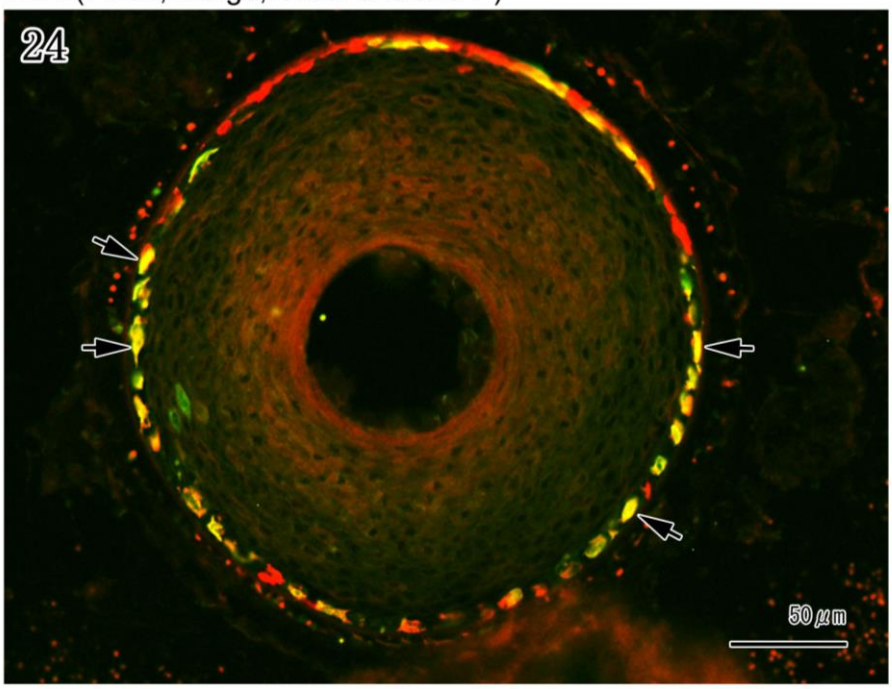

Figs.25-30: Double immunofluorescence staining (CAM5.2 and anti-P)

No.5 (FSCs, longitudinal section, anti-P)

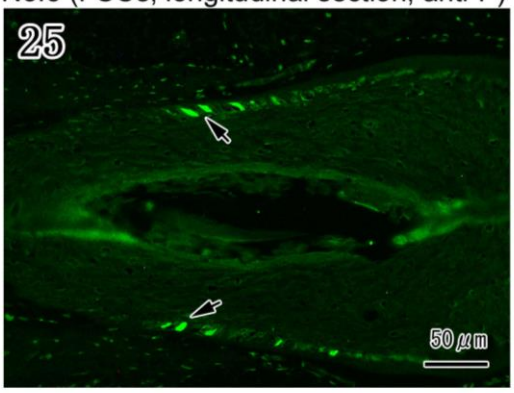

No.5 (FSCs, cross section, anti-P)

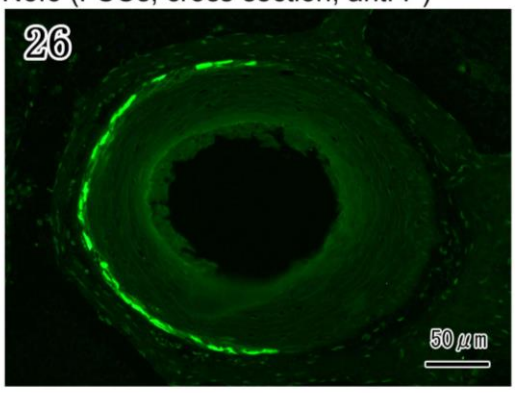

No.5 (FSCs, longitudinal section, CAM5.2)

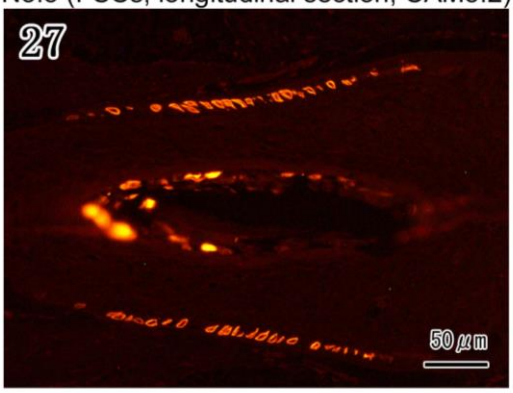

No.5 (FSCs, cross section, CAM5.2)

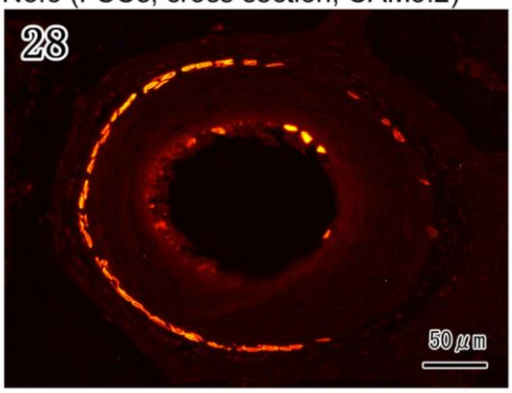

No.5 (FSCs, merge, CAM5.2 and anti-P)

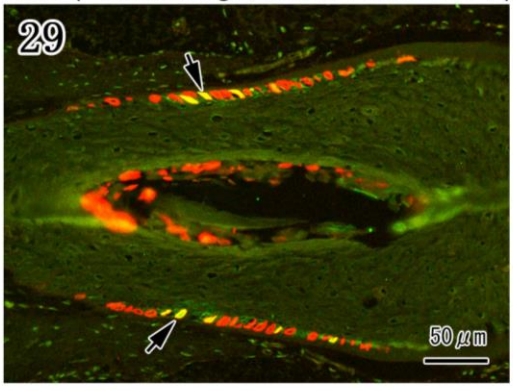

No.5 (FSCs, merge, CAM5.2 and anti-P)

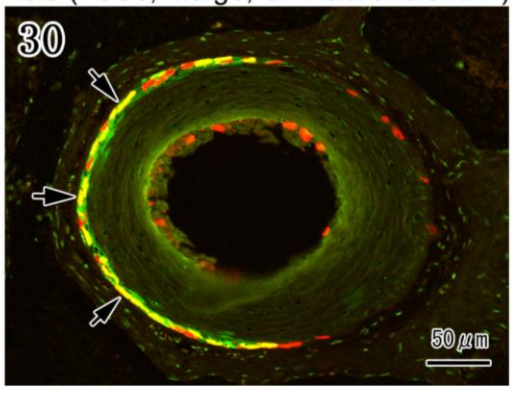

Figs.31-33: Double immunofluorescence staining (CAM5.2 and anti-P)

No.5 (FSCs, cross section, anti-P)

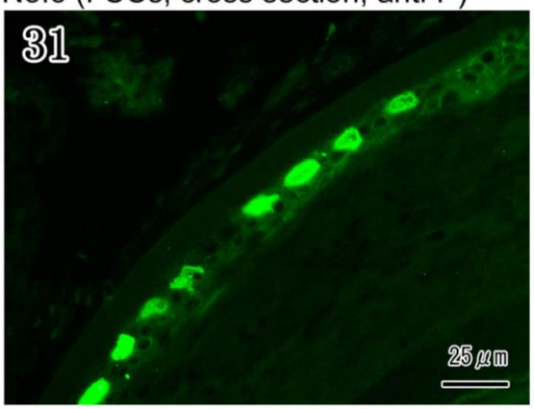

No.5 (FSCs, cross section, CAM5.2)

No.5 (FSCs, merge, CAM5.2 and anti-P)

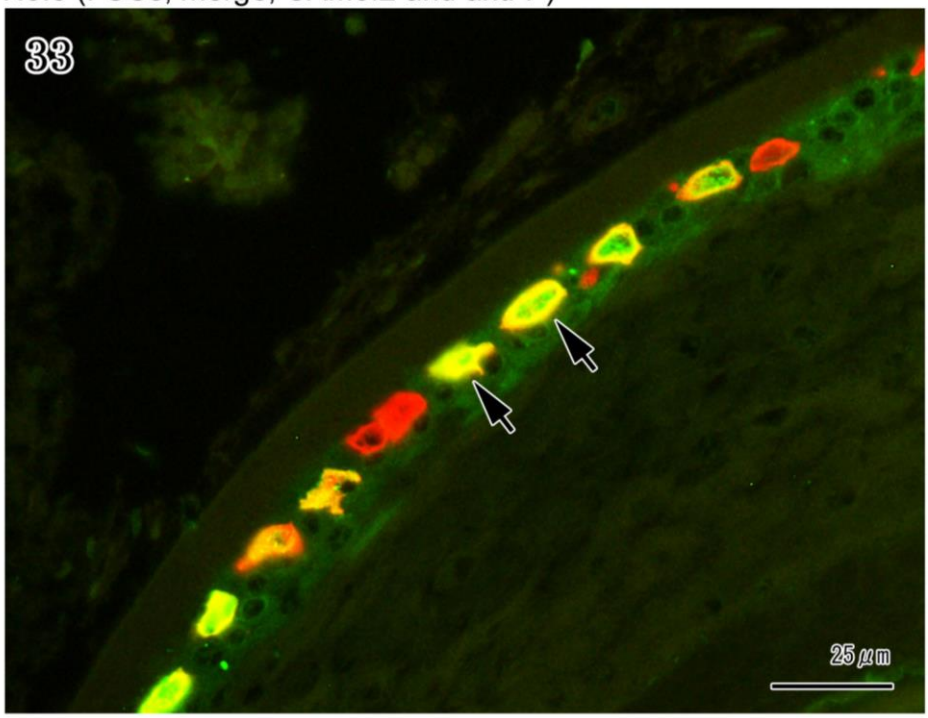

Chapter 3: Comparative pathology about peripheral tissues of mice intramuscularly infected with fixed (CVS-11) and street (1088) rabies strains

Introduction

Rabies virus is an enveloped, negative-stranded neurotropic RNA virus belonging to the genus *Lyssavirus* of the *Rhabdoviridae* family, which usually causes a lethal encephalomyelitis in humans and animals [52]. They have a simple genome of approximately 12 kb in length encoding five viral proteins: the nucleocapsid protein (N), phosphoprotein (P), matrix protein (M), glycoprotein (G), and large polymerase protein (L) [52]. The G protein is the only surface protein that is responsible for binding to specific neural receptors, such as acetylcholine receptors [32], neural cell adhesion molecule [49], or nerve-growth factor receptor (P75NTR) [52] to enter into target cells and the induction of innate immune responses and humoral immune response, such as the production of virus-neutralizing antibodies [27, 60], and also this protein is importance for regulating viral replication [39]. Generally, rabies viruses are categorized into two main groups: street virus strains (field isolates) and fixed virus strains (laboratory-adapted strains). Street strain of rabies viruses are known to be high pathogenic than fixed strains after peripheral infections. The first fixed strain made by Pasteur through serial intracerebral passage of a street strain in rabbits [26]. Although, both fixed and street strains are highly neurotropic laboratory strain and infection leads to the development of fatal acute encephalomyelitis; however, the fixed strains have different characteristics from street strains, such as regularity and shortening incubation period, stability of virulence, a reduction or loss of infectivity and pathogenicity following peripheral inoculations, and increased intracellular propagation and budding of virus particles from infected cells [19, 31].

Previously, several pathological studies of experimental rabies virus infection doing in the experimental mouse models have been performed, but mostly emphasizes the routes of viral spread and the pathological changes of the central nervous system (CNS) after infected with fixed strains or street strains of rabies viruses [15, 29]. The Challenge Virus Standard (CVS) strain of fixed rabies virus is often used for the study of rabies pathogenesis because it has a low risk of infection for human compared with street (wild-type) strains, and displays highly neuropathogenic effects for laboratory animals. Our previous studies have demonstrated that the CVS-11 virus causes severe apoptosis of migratory T lymphocytes and neurons in the brain after mice inoculated intracerebrally, but paralysis was absent [29, 38]. In contrast, paralysis was presented with spinal neurons necrosis when the CVS-11 virus is inoculated into the hind limb muscles [28], which are primary target sites of the rabies virus after infected peripherally [3]. These observations indicate that the CVS virus are susceptible to nerve cells, but different mechanisms exist to induction of cell death as well as the paralytic symptoms associated with necrosis of spinal neurons rather than severe neuronal apoptosis in the brain.

Although animals infected with street rabies virus usually died, there are several studies of resistance and of recover after onset of neurological symptoms [13, 15, 23, 58]. However, the mechanisms mediating this resistance and recover are poorly understood, but viral strain [15, 58], and host immune response [34, 45] factors alone or in combination are suggested as possible explanations. Induction of neuronal apoptosis by attenuated variant of street rabies virus has been reported in experimental mouse models [15]. On the other hand, in the natural infection by the wild-type rabies viruses in dogs [47], humans [25, 50] and mice inoculated with street rabies virus (silver-haired bat variant) via intracerebral route [57] does not induce neuronal apoptosis in the brain. These observations indicate that the degree of neuronal apoptosis was inversely correlated with the pathogenicity of street rabies virus.

The pathogenesis of rabies in natural infection is generally transmitted through infected saliva of mammals. Rarely, transmission has been reported by eating raw meat from infected animals [11], aerosol transmission in caves that are contained by large numbers of bats [51], and organs transplantation from donors with rabies [46]. Previous studies have described that rabies virus replicates in striated myocytes before invaded the axons of motor neurons and sensory nerves via neuromuscular junction [33, 38]. The viruses migrate to the CNS via retrograde axonal transport. There is no viraemia [41]. After reaching the CNS, the rabies virus then spreads centrifugally to the peripheral organs and autonomic nervous system, and is present in neurons throughout the body. In the terminal stage of the infection cycle, rabies virus descends to the salivary glands with secretion of high-titer virus into the saliva [7, 14]. Furthermore, the distribution of rabies virus antigen in peripheral non-nervous tissues has been noted in experimental animal models, but most studies emphasize the salivary gland and the skin [5, 7, 14, 16]. Some studies have been reported in human cases that the rabies virus can be found in the nerve plexus of many peripheral organs including the adrenal gland, kidney, pancreas, heart, and gastrointestinal tract [24, 27, 50]. Similar studies in animals are infrequent it was done in the foxes and skunks [4], bovines [1] and rodents [35].

However, the involvement of the peripheral nervous and non-nervous tissues of the head has not been well characterized. In this study, the histopathological changes and the distribution of viral antigens in peripheral nervous and non-nervous tissues of the head were investigated in adult C57BL/6J and *dd*Y mice that were infected intramuscularly with fixed rabies virus (CVS-11 strain) and street rabies virus (1088-N0 and 1088-N30 strains), respectively.

Materials and methods

Virus, animals, and inoculations

The Challenge Virus Standard-11 (CVS-11) strain of fixed rabies virus, and the street rabies virus 1088-N0 strain and attenuated variant 1088-N30 strain were used in this present study.

The filed isolated street rabies virus (1088 strains)

The street rabies virus 1088 (N0 and N30) strains were kindly provided by Department of Microbiology, Faculty of Medicine, Oita University (Oita, Japan). The parental virus of this strain was isolated from a woodchuck in the Centers for Disease Control in Atlanta, U.S.A. was obtained from the Yale Arbovirus Unit, Yale University, was grown in mouse neuroblastoma C1300 (NA) cells as previously described [58]. The 1088-N0 was passaged in NA cells for 1 time, while the 1088-N30 was passaged in NA cells for 30 times. The genomic sequence analyzed by Department of Microbiology, Faculty of Medicine, Oita University observed on the G protein of 1088-N30 have three potential sequons in the *N*-glycosylation sites, Asparagine (Asn) at positions 37, 319, and 194 (Asn^{37}, Asn^{319}, and Asn^{194}); whereas, the *N*-glycosylation sites of 1088-N0 have only two sequons at Asn^{37}, Asn^{319} [58]. Thirty-six 6-week-old female *dd*Y mice were purchased from Kyudo Co., Ltd., (Saga, Japan). Fifteen mice were inoculated intramuscularly (right *triceps surae* muscle) with viral dose of 10^6 plaque-forming units of each strain suspended in phosphate-buffered saline (PBS, pH7.4) and six uninfected control mice were inoculated with PBS alone. All the procedures were performed according to the guidelines for animal experiments with the approval of the ethics committee of Oita University.

The CVS-11 virus

The CVS-11 rabies virus was obtained from Dr. C. E. Rupprecht (Rabies Section, Virus and Rickettsia Zoonoses Branch, Centers for Disease Control and Preservation, Atlanta, GA, U.S.A.), was grown in mouse A/J (H-2a) neuroblastoma cells. The G protein of CVS-11 virus has three potential sequons in the *N*-glycosylation sites, at Asn^{37}, Asn^{204} and Asn^{319} [58]. Five 6-week-old female C57BL/6J mice were purchased from Japan SLC, Inc. (Shizuoka, Japan). All mice were inoculated intramuscularly (right *triceps surae* muscle) with viral dose of 10^7 plaque-forming units of the CVS-11 strain suspended in PBS. All experiments were performed in level 2 biosafety laboratories according to the committee on biosafety and animal handling and ethical regulation of the National Institute of Infectious Disease, Japan. Animal care, breeding, virus inoculation and observation were performed in accordance with the guideline of institutional committee.

Necropsy and histopathological examination

All experimentally inoculated mice were observed daily for neurological symptoms. Groups of CVS-11 inoculated mice were sacrificed at 7 days post-inoculation (PI) for 3 mice, at 8 and 9 days PI - one mouse per day. Each mouse was anesthetized with chloroform and perfused transcardially with 10-15 ml of PBS, followed by fixed with a 10% neutral buffered formalin (Wako, Japan).

In contrast, groups of 1088-N0 and 1088-N30 inoculated mice were sacrificed and their sera were sampled at 5, 8, and 11 days PI – five mice per day. It was subjected to 3 mice as a negative control in any of the groups. Each mouse was anesthetized with isoflurane or ether and perfused transcardially with 10-15 ml of PBS, followed by fixed with a 10% neutral buffered formalin (Wako).

The carcass and internal organs of each mouse were grossly examined and the brain was removed. The skull samples were decalcified in K-CX (Fujisawa, Pharmaceutical Co., Ltd., Osaka, Japan) solution at room temperature for 12 hours, and then washed in running tap water for 24 hours. Coronal sections of the skulls at the positions of the forehead, including the eyes, circumvallate papilla of the tongue, trigeminal ganglion and trigeminal nerve, infraorbital nerve, major (parotid and mandibular) salivary glands, lingual minor salivary glands, nasolacrimal duct, olfactory bulb, maxillary nerve, optic nerve, hypoglossal nerve, nasal mucosa, lingual mucosa, harderian glands, lacrimal gland, facial muscle and muzzle skin were prepared. For routine histological diagnosis and examination, tissues samples were embedded in paraffin wax, sectioned at 3 μm and dried on a slide dryer machine at 40°C for overnight. Serial sections were then subjected to hematoxylin and eosin, special straining (luxol fast blue staining) and immunohistochemistry, and terminal deoxynucleotidyl transferase-mediated deoxyuridine triphosphate (dUTP) nick end labeling (TUNEL) assay as described below.

Staining with hematoxylin and eosin (HE)

The sections were stained with hematoxylin and eosin for general histopathological examination.

Protocol

Paraffin was removed from the sections by a series of xylene and ethanol rinses. Tissue sections were rinsed in distilled water for 5 minutes and stained with hematoxylin solution for 3 minutes, rinsed in running tap water for 5 minutes and stained with eosin solution for 5 minutes, rinsed in distilled water for three times and dehydrated through a series of ethanol and xylene. The sections were then mounted in microscopy mounting medium.

Staining with luxol fast blue (LFB)

The sections were stained with LFB for myelin or myelinated axons examination.

Protocol

Paraffin was removed from the sections by a series of xylene and ethanol rinses. The tissue sections were rinsed in distilled water for 5 minutes, and then sections were immersed in 0.005% acetic acid solution in 95% ethyl alcohol at room temperature for 5 minutes. Place sections in 0.1% LFB solution for 16 hours in a 60°C oven, rinse off excess strain in 95% ethyl alcohol, rinse briefly in distilled water, sections were differentiated in 0.05% lithium carbonate solution for 15-20 seconds, followed by a final rinse in distilled water. After checking for completion of differentiation under the microscope, sections were counterstained in cresyl violet solution for 1 minute, rinse again in distilled water for 5 minutes, and followed by dehydrated through a series of ethanol and xylene. The sections were mounted in microscopy mounting medium.

Immunohistochemistry

1. For detection of the rabies virus antigens in tissues

The sections were stained using the streptavidin-biotin-peroxidase complex method with rabbit anti-phosphoprotein (P) antibodies.

Protocol

The sections were deparaffinized by a series of xylene and ethanol rinses, rehydrated, and washed twice with distilled water. The sections were treated for the activation of antigen with 0.25% trypsin at room temperature for 30 minutes. After this treatment, sections were washed three times for 5 minutes in distilled water. After washing, to removed endogenous peroxidase activity the sections were immersed with 0.3% H_2O_2 in methanol for 60 minutes; then they were

washed three times for 5 minutes in distilled water once again. The sections were treated with 10% normal goat serum (Nichirei Biosciences, Tokyo, Japan) for 60 minutes to block non-specific reaction. Sections were then incubated with primary antibody for overnight at 4°C in a humidified chamber. Primary antibody was diluted 1:1200. After incubation with primary antibody, sections were washed three times for 5 minutes in phosphate buffer saline (PBS, pH7.4) and incubated for 30 minutes at room temperature with the biotinylated anti-rabbit IgG (Nichirei Biosciences) as a secondary antibody. Sections were again washed three times for 5 minutes in PBS; then incubated for 30 minutes in room temperature with peroxidase-streptavidin enzyme (Nichirei Biosciences) for 30 minutes, washed in PBS three times for 5 minutes. Finally, sections were visualized using 3-3'-diaminobenzidine tetrachloride substrate (DAB substrate; DAKO, Kyoto, Japan), followed by rinsing in distilled water. The sections were counterstained with hematoxylin, and rinsing in running tap water again for 5 minutes. The sections were then dehydrated and mounted in microscopy mounting medium. Negative control was processed with rabbit serum instead of primary antibody.

2. For detection of tissue macrophages

The sections were stained using the polymer-based immunohistochemical method with rabbit anti-ionized calcium-binding adaptor molecule 1 antibodies (Iba1, Wako Ltd., Osaka, Japan).

Protocol

The sections were deparaffinized by a series of xylene and ethanol rinses, rehydrated, and washed twice with distilled water. After washing, the sections were treated for the activation of antigens with 10 mM sodium citrate buffer (pH 6.0) in a water bath at 95°C for 30 minutes; then they were rinsed in distilled water with three changes of 5 minutes each. Incubation for 10 minutes in 3% H_2O_2 in methanol to removed endogenous peroxidase activity, and the sections

were rinsed in distilled water (three changes, 5 minutes each). To block non-specific reaction, the sections were treated with 10% normal goat serum (Nichirei Biosciences, Japan) for 60 minutes at room temperature, followed by incubation with the primary antibody for overnight at 4°C in a humidified chamber. Primary antibody was diluted 1:500. After incubation with the primary antibody, sections were rinsed in PBS (three changes, 5 minutes each), and then incubated for 30 minutes at room temperature with the anti-rabbit IgG (Nichirei Biosciences) as a secondary antibody. Sections were again washed three times for 5 minutes in PBS; then incubated with peroxidase-streptavidin enzyme (Nichirei Biosciences) for 30 minutes at room temperature, washed in PBS three times for 5 minutes. Finally, sections were visualized using DAB substrate, followed by rinsing in distilled water. Sections were counterstained with haematoxylin, and washed again in running tap water for 5 minutes. Slides were then dehydrated and mounted in microscopy mounting medium.

3. For detection of T lymphocytes

The sections were stained using the polymer-based immunohistochemical method with polyclonal rabbit anti-CD3 antibodies (DAKO, Kyoto, Japan) for detection of T lymphocytes.

Protocol

The sections were deparaffinized by a series of xylene and ethanol rinses, rehydrated, and washed twice with distilled water. The sections were treated with Histofine® pH 9.0 (Nichirei Biosciences, Japan) for activation of antigens by microwaving at 750W for 5 minutes; then were washed in distilled water with three changes of 5 minutes each. After washing, incubation for 10 minutes in 3% H_2O_2 in methanol to removed endogenous peroxidase activity, and the sections were rinsed in distilled water (three changes, 5 minutes each). To block non-specific reaction, the sections were treated with 10% normal goat serum (Nichirei Biosciences) for 60 minutes, followed by incubation with the primary antibody for overnight at 4°C in a humidified chamber.

Primary antibody was diluted 1:50. After incubation with the primary antibody, sections were rinsed in PBS (three changes, 5 minutes each), then incubated for 30 minutes at room temperature with the Envision + System Labelled Polymer-HRP anti-rabbit (DAKO), rinsed in PBS (three changes, 5 minutes each) once again. Finally, sections were visualized using DAB substrate, followed by rinsing in distilled water. The sections were counterstained with hematoxylin, and rinsing in running tap water again for 5 minutes. The sections were then dehydrated and mounted in microscopy mounting medium.

4. For detection of B lymphocytes

The sections were stained using the polymer-based immunohistochemical method with polyclonal rabbit anti-CD20 antibodies (Spring Bioscience, Fremont, USA) for detection of B lymphocytes.

Protocol

The sections were deparaffinized by a series of xylene and ethanol rinses, rehydrated, and washed twice with distilled water. The sections were treated with Histofine® pH 9.0 (Nichirei Biosciences) for activation of antigens by microwaving at 750W for 5 minutes; then were washed in distilled water with three changes of 5 minutes each. After washing, incubation for 10 minutes in 3% H_2O_2 in methanol to removed endogenous peroxidase activity, and the sections were rinsed in distilled water (three changes, 5 minutes each). To block non-specific reaction, the sections were treated with 10% normal goat serum (Nichirei Biosciences) for 30 minutes, followed by incubation with the primary antibody for overnight at 4°C in a humidified chamber. After incubation with the primary antibody, sections were rinsed in PBS (three changes, 5 minutes each), then incubated for 30 minutes at room temperature with the Envision + System Labelled Polymer-HRP anti-rabbit (DAKO), rinsed in PBS (three changes, 5 minutes each) once again. Finally, sections were visualized using DAB substrate, followed by rinsing in distilled

water. The sections were counterstained with hematoxylin, and rinsing in running tap water again for 5 minutes. The sections were then dehydrated and mounted in microscopy mounting medium.

5. *For detection of nerve fibers*

The sections were stained using the polymer-based immunohistochemical method with monoclonal mouse anti-neurofilament protein antibodies (NF, DAKO, Kyoto, Japan) for detection of nerve fibers.

Protocol

The sections were deparaffinized by a series of xylene and ethanol rinses, rehydrated, and washed twice with distilled water. After washing, the sections were treated for the activation of antigens with Proteinase-K at room temperature for 30 minutes; then they were rinsed in distilled water with three changes of 5 minutes each. Incubation for 10 minutes in 3% H_2O_2 in methanol to removed endogenous peroxidase activity, and the sections were rinsed in distilled water (three changes, 5 minutes each), followed by incubation with the primary antibody for overnight at 4°C in a humidified chamber. Primary antibody was diluted 1:100. After incubation with the primary antibody, sections were rinsed in PBS (three changes, 5 minutes each), then incubated for 30 minutes at room temperature with the Histofine® Simple Stain MAX-PO (Mouse) (Nichirei Biosciences) rinsed in PBS (three changes, 5 minutes each) once again. Finally, sections were visualized using DAB substrate, followed by rinsing in distilled water. The sections were counterstained with hematoxylin, and rinsing in running tap water again for 5 minutes. The sections were then dehydrated and mounted in microscopy mounting medium.

Terminal deoxynucleotidyl transferase-mediated deoxyuridine triphosphate (dUTP) nick end labeling (TUNEL) assays

The sections were evaluated using TUNEL assay kit (ApopTag® Plug peroxidase In Situ Apoptosis Detection Kit, Millipore Corporation, Billerica, MA, USA) for detection of fragmented DNA of apoptotic cells.

Protocol

The sections were deparaffinized by a series of xylene and ethanol rinses, rehydrated, and washed twice with distilled water. After washing, sections were treated with Proteinase-K (DAKO) for 15 minutes at room temperature to activated antigens, rinsed in PBS (three changes, 5 minutes each). Then, endogenous peroxidase activity was removed with 0.3% H_2O_2 in methanol for 15 minutes at room temperature, rinsed in PBS (three changes, 5 minutes each). After washing in PBS, sections were covered with 50 μl of the TUNEL reaction mixture, which containing terminal deoxynucleotidyl transferase (TdT) and fluorescein-dUTP, and incubated under a coverslip in a humidified chamber for 60 minutes at 37°C. The reaction was stopped by washing sections in PBS. Sections were then incubated with anti-digoxigenin peroxidase for 30 minutes at room temperature. Then, washed in PBS (three changes, 5 minutes each) once again. Finally, sections were visualized using DAB substrate, followed by rinsing in distilled water. The sections were counterstained with hematoxylin, and rinsing in running tap water again for 5 minutes. The sections were then dehydrated and mounted in microscopy mounting medium.

Rapid fluorescent focus inhibition test

Viral neutralizing antibody (VNA) titers against the rabies virus were determined by rapid fluorescent focus inhibition tests (RFFIT) as previously described [43, 58]. VNA titers were represented as international units per ml (IU/ml), which was calculated by comparison

with WHO international standards [RAI: Anti-rabies Immunoglobulin, human, National Institute for Biological Standards & Control (NIBSC)]. A VNA titer of ≥0.5 IU/ml was defined as adequate for protection against rabies [56].

Results

Clinical signs and gross findings

The 1088-N0 virus-infected mice

Mice showed anorexia, emaciation, ruffled fur and hunched backs at 4 to 5 days after inoculation. Mice initially developed signs of rabies including uncoordinated limb movements, ataxia, and paralysis in the inoculated limb before developing into a bilateral hind limb paralysis at 5 days post-inoculation (PI). Paralysis was progressed to quadriparalysis, and subsequently mice became moribund state at 8 days PI. All infected mice died within 11 days PI after onset of symptoms. Conversely, normal control mice did not show any clinical symptoms within 11 days of intramuscular inoculation. No gross findings were observed at necropsy in any of the mice throughout the experimental period.

The 1088-N30 virus-infected mice

At 5 days PI, one of 5 mice showed paralysis in the inoculated limb, but others did not show any clinical signs consistent with rabies virus infection. Progressive neurological symptoms were developed at 8 days PI, one of 5 mice showed bilateral paralysis of the hind limbs, and others showed incoordination with decrease hind limb movement. All mice recovered at 11 days PI. No gross findings were observed at necropsy in any of the mice throughout the experimental period.

The CVS-11 virus-infected mice

Paralysis was found at 4 days PI. Paralysis was initially mild with deceased hind limb movement, but as the disease worsened, the mice became severely paralyzed at 7 days PI and progressed to quadriparalysis and died at 9 days. No gross findings were observed at necropsy in any of the mice throughout the experimental period.

Histopathological examination

Trigeminal ganglion and trigeminal nerve

The 1088-N0 virus-infected mice

At 5 days PI, mild neuronal degeneration and necrosis was observed in all mice. Most affected ganglion neurons showed swollen, pale, with absence of Nissl substance, and some showed nuclear pyknosis and cytoplasmic shrinkage (Figs. 1, 3). Occasional neurons contained cytoplasmic vacuoles. A small number of mononuclear inflammatory cell infiltrates composed mainly of lymphocytes were seen in the ganglia. However, the trigeminal nerves evaluated appeared normal.

At 8 days PI, mild to moderate neuronal degeneration and necrosis was observed in all mice. The numbers of degenerated neurons were increased significantly compared to 5 days PI. Most affected ganglion neurons showed swollen, rounded or angular, pale, with reduction in or absence of Nissl substance, and some showed hypereosinophilic, nuclear pyknosis, cytoplasmic shrinkage, and dispersed chromatin. Nuclei were central or slightly eccentric, and some contained clumped chromatin or undergoing karyorrhexis (Figs 5, 7). Occasional neurons contained cytoplasmic vacuoles. In addition, a small number of lymphocytes infiltrate scattered throughout the ganglia and under the epineurium. The trigeminal nerves exhibited mild non-suppurative neuritis characterized by axonal degeneration, swollen myelin sheaths, minimal myelin disintegration and vacuolization with mild infiltration of lymphocytes.

At 11 days PI, moderate neuronal degeneration and necrosis was observed in all mice. The numbers of degenerated neurons were increased significantly compared to 8 days PI. Many affected ganglion neurons showed hypereosinophilic, cytoplasmic shrinkage, with reduction in or absence of Nissl substance and either a pyknotic nucleus or absence of nuclear detail (Figs 9,

10). In addition, a small number of lymphocytes infiltrate scattered throughout the ganglia, often surrounding necrotic neurons. In the trigeminal nerves, the degree of damage in nerve bundle is higher than in 8 days PI. The trigeminal nerves exhibited mild non-suppurative neuritis characterized by swollen myelin sheaths, moderate myelin disintegration and vacuolization with infiltration of a few lymphocytes (Figs 13, 14).

The 1088-N30 virus-infected mice

At 5 days PI, mild neuronal degeneration and necrosis was observed in all mice. Most affected ganglion neurons showed swollen, pale, with absence of Nissl substance, and some showed nuclear pyknosis and cytoplasmic shrinkage. A small number of mononuclear inflammatory cell infiltrates composed mainly of lymphocytes were seen in the ganglia. However, the trigeminal nerves evaluated appeared normal.

At 8 days PI, mild to moderate neuronal degeneration and necrosis was observed in all mice. The numbers of degenerated neurons were increased significantly compared to 5 days PI. Most affected ganglion neurons showed swollen, rounded or angular, pale, with reduction in or absence of Nissl substance, and some showed nuclear pyknosis, hypereosinophilic, cytoplasmic shrinkage, and dispersed chromatin. Nuclei were central or slightly eccentric, and some contained clumped chromatin or undergoing karyorrhexis. A small number of lymphocytes were seen in the ganglia. The trigeminal nerves exhibited mild non-suppurative neuritis characterized by axonal degeneration, swollen myelin sheaths, minimal myelin disintegration and vacuolization with mild lymphocytic infiltration.

At 11 days PI, moderate neuronal degeneration and necrosis was observed in all mice. The numbers of degenerated neurons were increased significantly compared to 8 days PI. Many affected ganglion neurons showed swollen, hypereosinophilic, cytoplasmic shrinkage, with absence of Nissl substance and either a pyknotic nucleus or absence of nuclear detail. In

addition, a minimal to moderate number of lymphocytes infiltrate was observed diffusely throughout the ganglia. In the trigeminal nerve bundles, the degree of damage in nerve bundles is higher than 8 days PI. The trigeminal nerve bundles showed mild to moderate non-suppurative neuritis characterized by swollen myelin sheaths, moderate myelin disintegration and vacuolization with mild lymphocytic infiltration.

The CVS-11 virus-infected mice

At 7 days PI, mild neuronal degeneration and necrosis was present in the trigeminal ganglia. Most affected ganglion neurons showed swollen, pale, with absence of Nissl substance, and some showed nuclear pyknosis and cytoplasmic shrinkage. A small number of mononuclear inflammatory cell infiltrates composed mainly of lymphocytes was seen in the trigeminal ganglia. The trigeminal nerves the trigeminal nerves evaluated appeared normal.

At 8 days PI, in the trigeminal ganglion exhibited mild to moderate non-suppurative ganglionitis characterized by mild lymphocytic infiltration and moderate neuronal degeneration and necrosis. Most affected ganglion neurons showed nuclear pyknosis and cytoplasmic shrinkage, and occasional ganglion neurons were swollen, pale, with reduction or absence of Nissl substance. The trigeminal nerves showed mild axonal vacuolization.

At 9 days PI, the numbers of necrotic neurons were increased significantly compared to 7 and 8 days PI. Many neurons in the ganglion have a swollen, hypereosinophilic, with reduction or absence of Nissl substance and either a pyknotic nucleus or absence of nuclear detail (Figs. 19, 21). Mild lymphocytic infiltration was scattered throughout the ganglia. The trigeminal nerves exhibited mild axonal degeneration characterized by minimal myelin disintegration and vacuolization.

Optic nerve

The 1088-N0 and 1088-N30 viruses-infected mice

At 5 days PI, mild lymphocytic infiltration was observed in the nerve fibers. The numbers of lymphocytes were gradually increased at 8 and 11 days PI.

The CVS-11 virus-infected mice

At 7 days PI, mild lymphocytic infiltration was observed in the nerve fibers. The optic nerves of 8 and 9 days PI were not found on the sections.

Maxillary nerve and nasolacrimal duct

The 1088-N0 and 1088-N30 viruses-infected mice

At 5 days PI, no histological changes were observed in the maxillary nerves. In nasolacrimal duct, epithelial cells were slightly swollen and sloughed epithelial cells were occasionally present in the duct lumen. In addition, mild hyperplasia of spindle-shaped stromal cells and mild to moderate infiltration of mononuclear inflammatory cells were also seen around the duct.

At 8 days PI, no histological changes were observed in the maxillary nerves. In nasolacrimal duct, mild edema of the lamina propria, mild hyperplasia of spindle-shaped stromal cells, and mild to moderate infiltration of mononuclear inflammatory cells were also seen around the duct. In addition, the mucosal surface was thickened when compared to the 5 days PI, and epithelial cells showed degenerative changes and sloughed into the duct lumen.

At 11 days PI, the maxillary nerves showed mild to moderate axonal vacuolar degeneration. In some of these axons exhibit irregular swelling and fragmentation. In nasolacrimal duct, mild edema of the lamina propria, mild hyperplasia of spindle-shaped stromal cells, and moderate infiltration of mononuclear inflammatory cells were observed

around the duct. Degenerative changes of the epithelial cells were more severe than 8 days PI. In addition, the number of sloughed epithelial cells, cellular debris, and mononuclear inflammatory cells in the duct lumen were much higher than 8 days PI (Fig. 25).

The CVS-11 virus-infected mice

At 7 days PI, the maxillary nerves showed mild axonal degeneration. At 8 and 9 days PI, more advanced lesions appeared, including moderate axonal swelling and fragmentation, and myelin disintegration. In the nasolacrimal ducts, epithelial cells were swollen and dissociated with edematous separation from underlying basal lamina. Some of these epithelial cells showed degenerative changes and sloughed into the duct lumen. In addition, mild hyperplasia of spindle-shaped stromal cells and mild to moderate infiltration of mononuclear inflammatory cells were also observed around the duct.

Olfactory bulb and nasal mucosa

The 1088-N0 and 1088-N30 viruses-infected mice

At 5 days PI, no histological changes were observed in the olfactory bulb. In the nasal septum mucosa, mild infiltration of lymphocytes and a very few neutrophils were observed surrounding the secretory glands in the lamina propria.

At 8 and 11 days PI, no histological changes were observed in the olfactory bulb. In the nasal septum mucosa, mild infiltration of lymphocytes and neutrophils observed surrounding the secretory glands in the lamina propria, while nasal mucosal epithelium appeared intact.

The CVS-11 virus-infected mice

At 7, 8 and 9 days PI, no histological changes were observed in the olfactory bulb. In the nasal septum mucosa, mild infiltration of lymphocytes was observed surrounding the secretory glands in the lamina propria, while nasal mucosal epithelium appeared intact.

Infraorbital nerve, eyes (retina), lacrimal gland and harderian gland

The 1088-N0 virus-infected mice

At 5, 8 and 11 days PI, no histological changes were observed in the retina, lacrimal glands and harderian glands.

At 8 and 11 days PI, infraorbital nerves showed mild axonal vacuolar degeneration. In some of these axons exhibit irregular swelling and fragmentation.

The 1088-N30 virus-infected mice

At 5, 8 and 11 days PI, no histological changes were observed in the infraorbital nerves, lacrimal glands, harderian glands and retina.

The CVS-11 virus-infected mice

At 7, 8 and 9 days PI, no histological changes were observed in the infraorbital nerves, lacrimal glands, harderian glands and retina (Fig. 23).

Hypoglossal nerves, lingual mucosa, circumvallate papillae and lingual minor salivary glands

The 1088-N0 and 1088-N30 viruses-infected mice

At 5 days PI, no histological changes were observed in the hypoglossal nerves, lingual mucosa, circumvallate papillae and lingual minor salivary glands.

At 8 days PI, circumvallate papillae showed mild to moderate degeneration of the taste cells characterized by increased cytoplasmic eosinophilia, nuclear pyknosis, and appear rounded (Fig. 29). Mild inflammatory cell infiltrates composed of lymphocytes and neutrophils were also observed in the lamina propria.

At 11 days PI, more advanced lesions were observed in the circumvallate papillae, including moderate degeneration of taste cells characterized by markedly increased cytoplasmic eosinophilia, cytoplasmic shrinkage and nuclear pyknosis. Mild inflammatory cell infiltrates composed of lymphocytes and neutrophils were also seen in the lamina propria. No pathological findings were observed in the lingual minor salivary glands.

The CVS-11 virus-infected mice

At 7, 8 and 9 days PI, no histological changes were observed in the hypoglossal nerves, lingual mucosa and lingual minor salivary glands. However, circumvallate papillae showed moderate degeneration of the taste cells characterized by densely eosinophilic cytoplasm, cytoplasmic shrinkage and nuclear pyknosis. Mild mononuclear inflammatory cell infiltrates composed of lymphocytes and macrophages were observed in the lamina propria.

Parotid and mandibular salivary glands

The 1088-N0 virus-infected mice

At 5, 8 and 11 days PI, no histological changes were observed in the parotid glands. On the other hand, the mandibular glands showed mild inflammatory cell infiltrates composed mainly of lymphocytes and a few plasma cells surrounded striated ducts and interstitial connective tissue, while the acinar epithelium appeared intact at 8 days PI. Similar findings were observed in the 11 days PI, but numbers of inflammatory cells decreased when compared to the 8 days PI.

The 1088-N30 virus-infected mice

At 5, 8 and 11 days PI, no histological changes were observed in the parotid glands. On the other hand, the mandibular glands showed mild inflammatory cell infiltrates composed mainly of lymphocytes and a few plasma cells surrounded striated ducts and interstitial connective tissue, while the acinar epithelium appeared intact.

The CVS-11 virus-infected mice

At 7, 8, and 9 days PI, no histological changes were observed in the parotid and mandibular glands.

Facial muscle

The 1088-N0 virus-infected mice

No histological changes were observed in the facial muscle at 5 days PI. At 8 days PI, intramuscular nerve fibers showed mild axonal degeneration characterized by slight swelling and mild fragmentation. Mild myelin disintegration and vacuolization were also found in a few nerve fibers.

At 11 days PI, intramuscular nerve fibers showed moderate to severe axonal degeneration characterized by irregular swelling and some axons have ruptured into beaded structures. In addition, the facial muscle bundles showed myofiber degeneration characterized by loss of cross-striations, swollen with pale eosinophilic cytoplasm, and some myofibers were fragmented and hyalinized eosinophilic cytoplasm with nuclear pynknosis (Fig. 31).

The 1088-N30 virus-infected mice

No histological changes were observed in the facial muscle fibers at 5 days PI. At 8 and 11 days PI, intramuscular nerve fibers showed mild axonal vacuolar degeneration and fragmentation, while the muscle fibers appeared intact.

The CVS-11 virus-infected mice

At 7, 8, and 9 days PI, no histological changes were observed in the facial muscle and intramuscular nerve fibers.

Muzzle skin

The 1088-N0 virus-infected mice

No histological changes were observed in the muzzle skin at 5 days PI. At 8 and 11 days PI, the peripheral nerve fibers in the muzzle skin showed mild axonal vacuolar degeneration characterized by slight swelling, and some axons have oval vacuoles or disintegrated into beaded structures. In addition, in the hair follicle epithelium, individual epithelial cells showed mild degeneration characterized by increased eosinophilic granular cytoplasm with vacuolization.

The 1088-N30 virus-infected mice

At 5 and 8 days PI, no histological changes were observed in the muzzle skin. At 11 days PI, the peripheral nerve fibers in the muzzle skin showed mild axonal vacuolar degeneration characterized by slight swelling, and some axons have oval vacuoles or disintegrated into beaded structures.

The CVS-11 virus-infected mice

At 7, 8, and 9 days PI, no histological changes were observed in the muzzle skin.

Immunohistochemical examination

Detection of rabies virus antigens by anti-P antibodies

The anatomical distribution of rabies virus antigens in the peripheral tissues of head in mice infected with 1088-N0, 1088-N30 and CVS-11 viruses was summarized in Table 1.

The 1088-N0 virus-infected mice

At 5 days PI, viral antigens were detected in the trigeminal ganglia (2 mice). In the trigeminal ganglia, viral antigens were observed in the ganglion neurons characterized by a small spots to sparse granularity throughout the cytoplasm of ganglion neurons (Figs 2, 4).

At 8 days PI, viral antigens were detected in the trigeminal ganglia and trigeminal nerves (5 mice), hypoglossal nerves (1 mouse), circumvallate papillae (1 mouse), lingual mucosa (3 mice), retina (2 mice), facial muscle (1 mouse) and muzzle skin (3 mice). In the trigeminal ganglia, viral antigens were observed in the many ganglion neurons characterized by sparse to diffuse granularity throughout the cytoplasm of neurons and their axonal and dendritic processes, the number of viral antigens were significantly increased than 5 days PI (Figs 6, 8). In lingual mucosa, a small number of viral antigens were observed in the epithelial cells of the stratified squamous epithelium (Fig. 27). In circumvallate papillae, viral antigens were seen as small spots in the cytoplasm of taste cells (Fig. 30). In the retina, viral antigens were found in the ganglion cells in the ganglion cell layer, characterized by diffuse granularity throughout the cytoplasm of neurons and their axonal processes in the inner plexiform layer. In the facial muscle, viral antigens were observed as a sparse granularity in the cytoplasm of myoblasts (Fig. 33) and intramuscular nerve fibers. In the muzzle skin, viral antigens were observed as small intracytoplasmic granules at the border of the stratum granulosum and stratum corneum of the

epidermis, peripheral cutaneous nerve fibers and the basal layer of the outer root sheath of hair follicles.

At 11 days PI, viral antigens were detected in the trigeminal ganglia and trigeminal nerves (5 mice), maxillary nerves (5 mice), hypoglossal nerves (3 mice), lingual mucosa (4 mice), lingual minor salivary glands (4 mice), infraorbital nerves (5 mice), facial muscle (5 mice), muzzle skin (5 mice) and the retina (5 mice). In the trigeminal ganglia, the numbers of viral antigens were significantly increased than 8 days PI. In the trigeminal nerves, viral antigens were observed as small spots and prominent in fragmented nerve fibers, and an increase in the number of viral antigen-positive cells compared to 8 days PI. In the lingual mucosa, viral antigens were observed in the epithelial cells of stratified squamous epithelium, and an increase in the number of viral antigens when compared to 8 days PI. In the lingual minor salivary glands, viral antigens were observed in the cytoplasm of the serous acinar cells (Fig. 28). In the infraorbital nerves, viral antigens were seen as small spots and prominent in fragmented nerve fibers. In the retina, viral antigens were found in the ganglion cells in the ganglion cell layer and their axonal processes in the inner plexiform layer. The facial muscle, viral antigens were detected in intramuscular nerve fibers, and an increase in the number of viral antigens when compared to 8 days PI (Fig. 32). In the muzzle skin, viral antigens were observed as small intracytoplasmic granules at the border of the stratum granulosum and stratum corneum of the epidermis, peripheral cutaneous nerve fibers, and the basal layer of the out root sheath of hair follicles (Figs. 34-36).

The 1088-N30 virus-infected mice

No viral antigens detected in all tissues at 5 days PI. At 8 days PI, viral antigens were detected in the trigeminal ganglia and trigeminal nerves (5 mice). In the trigeminal ganglia, viral antigens were observed in the ganglion neurons, characterized by sparse to diffuse granularity

throughout the cytoplasm of neurons and their axonal and dendritic processes. In the trigeminal nerves, viral antigens were seen as small spots and prominent in fragmented nerve fibers.

At 11 days PI, viral antigens were detected in the trigeminal nerves (2 mice), maxillary nerves (4 mice), hypoglossal nerves (1 mouse), lingual mucosa (3 mice), lingual minor salivary gland (4 mice) and muzzle skin (3 mice). In the trigeminal nerves, viral antigens were observed as small spots and prominent in fragmented nerve fibers. In the maxillary nerves, viral antigens were seen as small spots and prominent in fragmented nerve fibers. In the lingual mucosa, viral antigens were found in the epithelial cells of the stratified squamous epithelium. In the muzzle skin, viral antigens were observed as small intracytoplasmic granules at the border of the stratum granulosum and stratum corneum of the epidermis, peripheral cutaneous nerve fibers, and positive cells were also found in the basal layer of the external root sheath of hair follicles.

The CVS-11 virus-infected mice

At 7 days PI, viral antigens were detected in the trigeminal ganglia and trigeminal nerves (3 mice), lingual mucosa (2 mice), and the retina (3 mice). In the trigeminal ganglia, viral antigens were observed in the ganglion neurons characterized by sparse to diffuse granularity throughout the cytoplasm of neurons and their axonal and dendritic processes. In lingual mucosa, a small number of positive cells were observed in the epithelial cells of the stratified squamous epithelium. In the retina, viral antigens were observed in the ganglion cells in the ganglion cell layer characterized by diffuse granularity throughout the cytoplasm and their axonal processes in the inner plexiform layer (Fig. 24).

At 8 days PI, in the trigeminal ganglia, viral antigens were detected mainly in the cytoplasm, dendrites and axons of ganglion neurons (1 mouse). Viral antigens were sparse to diffuse granularity throughout the cytoplasm of ganglion neurons, but no viral antigens were detected in other tissues.

At 9 days PI, viral antigens were detected in the ganglion neurons of the trigeminal ganglia and lingual mucosa (1 mouse). Viral antigens were diffuse granularity throughout the cytoplasm of ganglion neurons (Figs. 20, 22). In lingual mucosa, a small number of positive cells were observed in the stratified squamous epithelium.

Detection of nerve fibers by anti-neurofilament protein (NF) and for identification of the myelin sheath of the myelinated nerve fibers by luxol fast blue (LFB) staining

The 1088-N0 and 1088-N30 viruses-infected mice

At 8 days PI, anti-NF immunoreactivity showed a slight decrease of axonal density in the trigeminal ganglia and trigeminal nerves.

At 11 days PI, anti-NF immunoreactivity showed weak and irregular positive reaction, and diffusely loss of both small- and large-diameter axons in the trigeminal ganglia (Fig. 12), trigeminal nerves (Figs 17, 18), maxillary nerves and infraorbital nerves. In trigeminal ganglia, LFB staining revealed a decrease density of myelinated nerve fibers and extensive axonal demyelination, and degenerated ganglion neurons were pale because of depletion of Nissl substance (Fig. 11). Likewise, in trigeminal nerves, LFB staining revealed a decrease density of myelinated nerve fibers and extensive axonal demyelination (Figs. 15, 16).

The CVS-11 virus-infected mice

At 8 and 9 days PI, anti-NF immunoreactivity showed diffusely loss of both small- and large-diameter axons in the maxillary nerves, trigeminal nerves, and trigeminal ganglia. In addition, LFB-stained sections showing a decrease density of myelinated nerve fibers and extensive axonal demyelination in the maxillary nerves and trigeminal nerves.

Detection of tissue macrophages by anti-Iba1 antibodies

The 1088-N0 virus-infected mice

At 5 days PI, a small number of anti-Iba1 positive cells appeared in the lumen and lamina propria of the nasolacrimal ducts. At 8 and 11 days PI, an increase in the number of anti-Iba1 positive cells appeared in the lumen of the nasolacrimal ducts.

The 1088-N30 virus-infected mice

At 5 days PI, a small number of anti-Iba1 positive cells appeared in the lumen and lamina propria of the nasolacrimal ducts. At 8 and 11 days PI, an increase in the number of anti-Iba1 positive cells appeared in the lumen and lamina propria of the nasolacrimal ducts.

The CVS-11 virus-infected mice

At 7, 8 and 9 days PI, a small number of anti-Iba1 positive cells appeared in the lumen and in the lamina propria of the nasolacrimal ducts.

Detection of T lymphocytes by anti-CD3 antibodies

The 1088-N0 and 1088-N30 viruses-infected mice

At 5, 8 and 11 days PI, a small numbers of anti-CD3 positive cells appeared in the trigeminal ganglia, trigeminal nerves and optic nerves.

The CVS-11 virus-infected mice

At 7 days PI, a small number of anti-CD3 positive cells appeared in the optic nerves. At 8 and 9 days PI, a small number of anti-CD3 positive cells were also seen in the trigeminal ganglia.

Detection of B lymphocytes by anti-CD20 antibodies

The 1088-N0 virus-infected mice

At 5 days PI, a small number of anti-CD20 positive cells appeared in the lumen of the nasolacrimal ducts. Increased numbers of anti-CD20 positive cells appeared in the submucosa at 8 and 11 days PI.

The 1088-N30 virus-infected mice

At 5, 8 and 11 days PI, a small number of anti-CD20 positive cells appeared in the lamina propria and lumen of the nasolacrimal ducts.

The CVS-11 virus-infected mice

At 8 and 9 days PI, a small number of anti-CD20 positive cells appeared in the submucosa of the nasolacrimal ducts.

Detection of apoptotic cells by TUNEL assays

The CVS-11 virus-infected mice

There are no TUNEL-positive cells observed in any of the anatomical areas.

The 1088-N0 and 1088-N30 viruses-infected mice

There are no TUNEL-positive cells observed in any of the anatomical areas.

Determination of viral neutralizing antibody (VNA) titer by rapid fluorescent focus inhibition tests

The VNA titer in the serum of the 1088-N0 and 1088-N30 viruses-infected mice was shown in Table 2 and Table 3, respectively. At 5 days PI, the VNA titer was significantly higher

in mice infected with 1088-N30 viruses compared to 1088-N0 virus-infected mice. Four of five mice infected with 1088-N30 viruses had a VNA titer of more than 0.5 IU/ml, whereas only one of five mice infected with 1088-N0 viruses had a VNA titer of more than 0.5 IU/ml. The trend for the variants to induce a greater response than 1088-N0 viruses was also observed at 8 and 11 days PI, even though all of the mice infected with 1088-N0 viruses had a VNA titer above 0.5 IU/ml.

Discussion

In this chapter, the mouse model was used to investigate virus distribution in different regions of the peripheral nervous and non-nervous tissues of head, with the exception of brain following peripheral intramuscular inoculation with fixed and street rabies virus. After intramuscular inoculation, C57BL/6J mice that were infected with the fixed rabies virus strain CVS-11 exhibited paralysis, became moribund and died during the terminal stage of infection. Similar symptoms occurred in *dd*Y mice were infected with 1088-N0 viruses. On the other hand, *dd*Y mice infected with attenuated virus strain 1088-N30 developed hind limb paralysis, but recovered from infection at the same time. The VNA titers in the serum of mice infected with 1088-N30 viruses were significantly higher than mice infected with 1088-N0 viruses (see Tables 2 and 3). These findings are consistent with those for mice that were inoculated with the CVS-11 viruses intramuscularly [28], as well as, infection of mice with an attenuated strain of rabies virus triggers a strong specific immune response that results in a non-lethal infection [58].

Several studies have demonstrated factors that affect various aspects of rabies pathogenesis include route of inoculation [23, 38], viral strain [15, 44], host immunocompetence [9, 37], and species of the host [18], but not all of these appear to influence the distribution of virus in the CNS. Interestingly, Yamada *et al*. [58] demonstrated that the G protein determines the distribution pattern of rabies virus in the brain, and a strong humoral immune response induced by the attenuated virus strain 1088-N30 is mainly responsible for restricted virus spread within the CNS. However, the street rabies virus elicited weaker innate immune responses compared with an attenuated fixed virus [54]. In the present study, viral antigens were detected in the trigeminal ganglia, trigeminal nerve, maxillary nerve, infraorbital nerve, hypoglossal nerve, retina, lingual mucosa, taste cells of the circumvallate papillae, lingual minor salivary glands, facial muscle and muzzle skin of mice infected with 1088-N0 viruses. On the other hand, the 1088-N30 viruses had infected the trigeminal ganglia, trigeminal nerve, maxillary nerve,

hypoglossal nerve, lingual mucosa, lingual minor salivary glands and muzzle skin. The CVS-11 viruses had restrictively infected the trigeminal ganglia, trigeminal nerve, lingual mucosa, and the retina (see Table. 1). These findings demonstrate that, although three strains of rabies virus grew in the CNS, the street strains spread rapidly to the peripheral nervous tissues and non-nervous tissues of the head. In addition, early induction of inflammation and VNA are an important role to prevent the virus spread from the CNS to peripheral tissues.

In the present study, the trigeminal ganglia and trigeminal nerves were consistently infected even at the early stage of the infection with the CVS-11, 1088-N0 and 1088-N30 viruses. In addition, bilateral non-suppurative trigeminal ganglioneuritis, characterized by neuronal necrosis, Nissl substance dissolution, occasional nuclear pyknosis, cytoplasmic shrinkage, axonal demyelination, and mononuclear cells infiltration were also found in all experimental groups. Similar findings have been reported in bats experimentally infected with attenuated fixed viruses [40] and bovines naturally infected with street (wild-type) rabies viruses [1]. Previous studies have described the morphological structure of trigeminal ganglion of rodent that contains a number of sensory neurons and provides sensory innervation to the head and face [12]. Thus, these injuries can cause reduction or loss of skin sensation and loss or reductions in reflections on the head and face [10].

In this study, infection of the epidermal cells and external root sheath cells of tactile hair follicles was found in the muzzle skin of mice infected with 1088-N0 and 1088-N30 viruses. These findings are consistent with previous report of skunks and foxes infected with street rabies virus [4]. Previous studies have documented the muzzles skin contains many tactile hair follicles that are surrounded by an abundant nerve supply [5, 55], which is receive sensory innervation by the infraorbital branch of the trigeminal nerve [12]. Thus, centrifugal viral propagation to the tactile hair follicles in muzzle skin is probably mediated by trigeminal ganglion neurons that supply tactile hairs (via trigeminothalamic axons).

The salivary gland and tongue are known to be important as portals of exit for the rabies virus into the saliva [8, 42]. It is essential in most natural rabies vectors for horizontal transmission of the virus to other hosts by biting, and previous study indicated virus can appears in the saliva of dogs up to 14 days before appearance of clinical symptoms [14]. In this study, during observes clinical symptoms, the viral antigen was detected in the lingual mucosal epithelium in all of experimental groups; however, only the 1088-N0 group, viral antigens were detected in the taste cells of circumvallate papillae and also found in the serous acinar epithelium of the lingual minor salivary glands, whereas no viral antigens detected in both parotid and mandibular salivary glands. Similar observations have been demonstrated in humans that lack of viral antigens in the major salivary glands [24, 50], but appeared in the taste cells and acini of the minor salivary gland of tongue. On the other hand, in chapter 1, I found abundant acinar infection in the mandibular glands of naturally infected rabid dogs. Therefore, it was suggested that acinar infection of the major salivary glands only be prominent in natural rabies vectors, where excretion of high-titer virus in the saliva is important for transmission of the infection, whereas the tongue and lingual minor salivary gland in mice appears to be a preferred location for virus replication and responsible for the production of saliva that contains lower amounts of infectious rabies virus.

The hypoglossal nerve provides motor supply to the skeletal muscle of the tongue and for controls all tongue movements. Retrograde transneuronal infection by rabies virus in the hypoglossal nerve affects ability to control tongue movements [53]. Smart and Charlton [44] reported that the amount of viral antigen appeared in the hypoglossal nuclei higher in street virus-infected skunks than in CVS virus infected-skunks. In the present study supported the former case because viral antigen was detected in the hypoglossal nerves in some mice that were infected with street rabies virus, but did not detected in CVS-11 virus-infected mice. These findings indicate that after the street rabies virus replicates within the hypoglossal nuclei,

located in the medulla oblongata [47], the virus then spreads centrifugally along the hypoglossal nerve to reach skeletal muscle fibers of the tongue [24], meanwhile it may causes of the hypoglossal nerve dysfunction associated with tongue paralysis and dysphagia that are common symptoms of rabies in small animals.

The involvements of the ocular structures in rabies virus infection have been reported previously [16, 17, 59]. Infection was observed in the corneal epithelial cells, and in ganglion cell layer of the retina, which is innervates by sensory afferents via the optic nerve [30]. Histology also showed lymphoplasmacytic infiltration in the retina, ciliary body and in the choroid [17]. Camelo *et al.* [6] described that T lymphocyte plays an important role in the protection of the eye against rabies virus ocular infection. In the present study, viral antigens were detected in the retinal ganglion cells of mice infected with CVS-11 and 1088-N0 viruses, whereas in the corneal epithelial cells and photoreceptor did not become infected until the late stage of infection. In addition, small numbers of T lymphocytes were observed in the optic nerves, but no viral antigen was detected here. Thus, centrifugal viral propagation progress from the CNS to the retina via the optic nerve, but an inflammatory response may lead to the clearance of the pathogen in nerve fibers.

Within the CNS, infiltration of T lymphocytes has been reported to play a major role not only in blocking rabies virus spread [3], but also in clearing rabies virus from the CNS [20]. Nevertheless, the other outcome of the infiltrating T lymphocytes that may release of cytotoxic cytokines such as interferon (IFN)-γ to kill virus-infected cells [26]. Recently, some studies have shown that both fixed and street rabies viruses induce apoptosis in inflammatory cells in the CNS [29, 48], suggesting that interfering with release of cytotoxic cytokines and against inflammatory cell-mediated cell lysis. In this study, virus infected trigeminal ganglion neurons exhibited necrotic features by light microscopy and they were negative for TUNEL staining and also infiltrating T lymphocytes did not undergo apoptosis. These findings suggest that

degeneration of ganglion neurons may be associated with T lymphocytes infiltration in the trigeminal ganglion, and their cytokine likely serve to promote the necrosis of ganglion neurons, which might also contribute to the loss of facial sensation.

Previous studies have documented the evidence of the extra-cranial tissues inflammation, including the lung, heart, liver, and kidney in human and mice infected with street rabies virus associated with tissue macrophages infiltration [21, 35]. After rabies virus infection, the activated tissue macrophages express inducible nitric oxide synthase (iNOS), which stimulate the secretion various kinds of proinflammatory cytokines, such as interleukin (IL)-1β, tumor necrosis factor (TNF)-α, interferon (IFN)-γ, and nitric oxide (NO) [2, 35]. High NO levels are cytotoxic that can activate protease and inactivate anti-proteases which lead to increase in breakdown of the extracellular matrix, and direct injury to epithelial cells [36]. In the present study, mild to moderate number of macrophages positive to anti-Iba1 antibody were detected in the nasolacrimal ducts in all experimental groups, and also the nasolacrimal ducts exhibited degeneration and sloughing of the epithelial cells. Therefore, it was suggested that the tissue macrophages and their cytokines play an important role in the formation of tissue inflammation in this study.

References

1. Abreu, C. C., Nakayama, P. A., Nogueira, C. I., Mesquita, L. P., Lopes, P. F., Wouters, F., Varaschin, M. S. and Bezerra, Jr. P. S. 2014. Histopathology and immunohistochemistry of tissues outside central nervous system in bovine rabies. *J. Neuroviral.* **20**: 388-397.
2. Akaike, T. and Maeda, H. 2000. Nitric oxide and virus infection. *Immunology* **101**: 300-308.
3. Baloul, L. and Lafon, M. 2003. Apoptosis and rabies virus neuroinvasion. *Biochimie.* **85**: 777-788.
4. Balachandran, A. and Charlton, K. 1994. Experimental rabies infection of non-nervous tissues in skunks (*Mephitis mephitis*) and foxes (*Vulpes vulpes*). *Vet. Pathol*. **31**: 93-102.
5. Blenden, D. C., Bell, J. F., Tsao, A. T. and Umoh, J. U. 1983. Immunofluorescent examination of the skin of rabies-infected animals as a means of early detection of rabies virus antigen. *J. Clin. Microbiol.* **18**: 631-636.
6. Camelo, S., Castellanos, J., Lafage, M. and Lafon, M. 2001. Rabies virus ocular disease: T-cell-dependent protection is under the control of signaling by the p55 tumor necrosis factor alpha receptor, p55TNFR. *J. Virol.* **75**: 3427-3434.
7. Charlton, K. M., Casey, G. A. and Cambell, J. B. 1983. Experimental rabies in skunks: mechanisms of infection of the salivary glands. *Can. J. Comp. Med.* **47**: 363-369.
8. Charlton, K. M., Casey, G. A. and Webster, W. A. 1984. Rabies virus in the salivary glands and nasal mucosa of naturally infected skunks. *Can. J. Comp. Med.* **48**: 338-339.
9. Chopy, D., Pothlichet, J., Lafage, M., Mégret, F., Fiette, L., Si-Tahar, M. and Lafon, M. 2011. Ambivalent role of the innate immune response in rabies virus pathogenesis. *J. Virol.* **85**: 6657-6668.

10. De Lahunta, A. and Glass, E. 2009. *In*: Veterinary Neuroanatomy and Clinical Neurology. Elsevier, St. Louis.

11. Dimaano, E. M., Scholand, S. J., Alera, M. P. and Belandres, D. B. 2011. Clinical and epidemiological features of human rabies cases in the Philippines: a review from 1987 to 2006. *Int. J. Infect. Dis.* **15**: 495-499.

12. Erzurumlu, R. S., Murakami, Y. and Rijli, F. M. 2010. Mapping the face in the somatosensory brainstem. *Nat. Rev. Neurosci.* **11**: 252-63.

13. Fekadu, M. and Baer, G. M. 1980. Recovery from clinical rabies of 2 dogs inoculated with a rabies virus strain from Ethiopia. *Am. J. Vet. Res.* **41**: 1632-1634.

14. Fekadu, M. and Shaddock, J. H. 1984. Peripheral distribution of virus in dogs inoculated with two strains of rabies virus. *Am. J. Vet. Res.* **45**: 724-729.

15. Feng, Y. J., Lin, D. Y., Ying, H., Yan, T. X., Hao, L., Cheng, Y. P., Xin, S. X., Tao, J. W., Dong, L. G., Qing, T. and Long, W. F. 2014. Comparative analysis of the pathogenetic mechanisms of street rabies virus strains with different virulence levels. *Biomed. Environ. Sci.* **27**: 749-762.

16. Fischman, H. R. and Schaeffer, M. 1971. Pathogenesis of experimental rabies as revealed by immunofluorescence. *Ann. N. Y. Acad. Sci.* **177**: 78-97.

17. Haltia, M., Tarkkaken, A. and Kivelä, T. 1989. Rabies: ocular pathology. *Br. J. Ophthalmol.* **73**: 61-67.

18. Hamir, A. N., Moser, G. and Rupprecht, C. E. 1996. Clinicopathologic variation in raccoons infected with different street rabies virus isolates. *J. Vet. Diag. Invest.* **8**: 31-37.

19. Hamamoto, N., Uda, A., Noguchi, A., Okutani, A., Kaku, Y., Park, C. H., Morikawa, S. and Inoue, S. 2015. Different intracellular localization of G protein between Kyoto strain (street virus) and CVS-26 strain (fixed virus) was associated with N-glycosylation

of G protein at the site of 204. Proceeding of the 17th International Conference on Emerging Infectious Diseases; 2015 Jan 25-29; Taipei, Taiwan.

20. Hooper, D. C., Morimoto, K., Bette, M., Whihe, E., Koprowski, H. and Dietzschold, B. 1998. Collaboration of antibody and inflammation in clearance of rabies virus from the central nervous system. *J. Virol.* **72**: 3711-3719.

21. Hsu, Y. H. and Chen, H. I. 2008. Acute respiratory distress syndrome associated with rabies. *Pathology* **40**: 647-650.

22. Jackson, A. C., Reimer, D. L. and Ludwin, S. K. 1989. Spontaneous recovery from the encephalomyelitis in mice caused by street rabies virus. *Neuropathol. Appl. Neurobiol.* **15**: 459-475.

23. Jackson, A. C. and Reimer, D. L. 1989. Pathogenesis of experimental rabies in mice: an immunohistochemical study. *Acta Neuropathol.* **78**: 159-165.

24. Jackson, A. C., Ye, H., Phelan, C. C., Ridaura-Sanz, C., Zheng, Q., Li, Z., Wan, X. and Lopez-Corella, E. 1999. Extraneural organ involvement in human rabies. *Lab. Invest.* **79**: 945-951.

25. Jackson, A. C., Randle, E., Lawrance, G. and Rossiter, J. P. 2008. Neuronal apoptosis does not play an important role in human rabies encephalitis. *J. Neuroviral.* **14**: 368-375.

26. Jackson, A. C. 2013. pp: 394-395. *In*: Rabies, 3rded., Elsevier Saunders, Philadelphia.

27. Jogai, S., Radotra, B. D. and Banerjee, A. K. 2002. Rabies viral antigen in extracranial organs: a post-mortem study. *Neuropathol. Appl. Neurobiol.* **28**: 334-338.

28. Kojima, D., Park, C. H., Satoh, Y., Inoue, S., Noguchi, A. and Oyamada, T. 2009. Pathology of the spinal cord of C57BL/6J mice infected with rabies virus (CVS-11). *J. Vet. Med. Sci.* **71**: 319-324.

29. Kojima, D., Park, C. H., Tsujikawa, S., Kohara, K., Hatai, H., Oyamada, T., Noguchi, A. and Inoue, S. 2010. Lesions of the central nervous system induced by intracerebral

inoculation of BALB/c mice with rabies virus (CVS-11). *J. Vet. Med. Sci.* **72**: 1011-1016.

30. Kučera, P., Dolivo, M., Coulon, P. and Flamand, A. 1985. Pathways of the early propagation of virulent and avirulent rabies strains from the eye to the brain. *J. Virol.* **55**: 158-162.

31. Lepine, P. 1938. On the evolution of fixed strains of rabies virus. *J. Hyg.* (Lond). **38**: 180-184.

32. Lentz, T. L., Burrage, T. G., Smith, A. L., Crick, J. and Tignor, G. H. 1982. Is the acetylcholine receptor a rabies virus receptor? *Science* **215**: 182-184.

33. Lewis, P., Fu, Y. and Lentz, T. L. 2000. Rabies virus entry at the neuromuscular junction in nerve-muscle cocultures. *Muscle Nerve* **23**: 720-730.

34. Lodmell, D. L., Wiedbrauk, D. L. and Ewalt, L. C. 1989. Interferon induced within the central nervous system during infection is inconsequential as a mechanism responsible for murine resistance to street rabies virus. *J. Gen. Virol.* **70**: 473-478.

35. Liao, P. H., Hsu, Y. H., Yang, H. H., Wang, M. H. and Chen, L. K. 2012. Involvement of extraneural tissues and upregulation of inducible nitric oxide synthase after experiment infection with rabies virus in BALB/c mice and LEW/SsN rats. *Pathol. Int.* **62**: 619-627.

36. McGavin, M. D. and Zachary, J. F. 2007. pp. 133-134. *In*: Pathologic basis of veterinary disease, 4th ed., Mosby Elsevier, St. Louis.

37. Mitrabhakdi, E., Shuangshoti, S., Wannakrairot, P., Lewis, R. A., Susuki, K., Laothamatas, J. and Hemachudha, T. 2005. Difference in neuropathogenetic mechanism in human furious and paralytic rabies. *J. Neurol. Sci*. **238**: 3-10.

38. Park, C. H., Kondo, M., Inoue, S., Noguchi, A., Oyamada, T., Yoshikawa, H. and Yamada, A. 2006. The histopathogenesis of paralytic rabies in six-week-old C57BL/6J

mice following inoculation of the CVS-11 strain into the right triceps surae muscle. *J. Vet. Med. Sci.* **68**: 589-595.

39. Pulmanausahakul, R., Li, J., Schnell, M. J. and Dietzschold, B. 2008. The glycoprotein and the matrix protein of rabies virus affect pathogenicity by regulating viral replication and facilitating cell-to-cell spread. *J. Virol.* **82**: 2330-2338.

40. Reid, J. E. and Jackson, A. C. 2001. Experimental rabies virus infection in *Artibeus jamaicensis* bats with CVS-24 variants. *J. Neurovirol.* **7**: 511-517.

41. Reaves, E. J., Salmon-Mulanovich, G., Guevara, C., Kochel, T. J., Steinbach, D. E. and Montgomery, J. M. 2012. Susceptibility and lack of evidence for a viremic state of rabies in the night owl monkey, *Aotus nancymaae*. *Virol. J.* **9**: 95.

42. Schatz, J., Teifke, J. P., Mettenleiter, T. C., Aue, A., Stiefel, D., Müller, T. and Freuling, C. M. 2014. Lyssavirus distribution in naturally infected bats from Germany. *Vet. Microbiol.* **169**: 33-41.

43. Shiota, S., Mannen, K., Matsumoto, T., Yamada, K., Yasui, T., Takayama, K., Kobayashi, Y., Khawplod, P., Gotoh, K., Ahmed, K., Iha, H. and Nishizono, A. 2009. Development and evaluation of a rapid neutralizing antibody test for rabies. *J. Virol. Methods* **161**: 58-62.

44. Smart, N. L. and Charlton, K. M. 1992. The distribution of challenge virus standard rabies virus versus skunk street rabies virus in the brains of experimentally infected rabid skunks. *Acta Neuropathol.* **84**: 501-508.

45. Souza, A. and Madhusudana, S. N. 2014. Survival from rabies encephalitis. *J. Neurol. Sci.* **339**: 8-14.

46. Srinivasan, A., Burton, E. C., Kuehnert, M. J., Rupprecht, C., Sutker, W. L., Ksiazek, T. G., Paddock, C. D., Guarner, J., Shieh, W. J., Goldsmith, C., Hanlon, C. A., Zoretic, J., Fischbach, B., Niezgoda, M., El-Feky, W. H., Orciari, L., Sanchez, E. Q., Likos, A.,

Klintmalm, G. B., Cardo, D., LeDue, J., Chamberland, M. E., Jernigan, D. B. and Zaki, S. R. 2005. Transmission of rabies virus from an organ donor to four transplant recipients. *N. Engl. J. Med.* **352**: 1103-1111.

47. Suja, M. S., Mahadevan, A., Madhusudhana, S. N., Vijayasarathi, S. K. and Shankar, S. K. 2009. Neuroanatomical mapping of rabies nucleocapsid viral antigen distribution and apoptosis in pathogenesis in street dog rabies–an immunohistochemical study. *Clin. Neuropathol.* **28**: 113-124.

48. Suja, M. S., Mahadevan, A., Madhusudana, S. N. and Shankar, S. K. 2011. Role of apoptosis in rabies viral encephalitis: a comparative study in mice, canine, and human brain with a review of literature. *Pathol. Res. Int.* **2011**: 374286.

49. Thoulouze, M. I., Lafage, M., Schachner, M., Hartmann, U., Cremer, H. and Lafon, M. 1998. The neural cell adhesion molecule is a receptor for rabies virus. *J. Virol.* **72**: 7181-7190.

50. Tobiume, M., Sato, Y., Katano, H., Nakajima, N., Tanaka, K., Noguchi, A., Inoue, S., Hasegawa, H., Iwasa, Y., Tanaka, J., Hayashi, H., Yoshida, S., Kurane, I. and Sata, T. 2009. Rabies virus dissemination in neural tissues of autopsy cases due to rabies imported into Japan from the Philippines: immunohistochemistry. *Pathol. Int.* **59**: 555-566.

51. Tselis, A. C. and Booss, J. 2014. Rabies. *In*: Handbook of Clinical Neurology. Vol. **123** (3rd series) Neurovirology. Elsevier Saunders, Philadelphia.

52. Tuffereau, C., Benejean, J., Blondel, D., Kieffer, B. and Flamand, A. 1998. Low-affinity nerve-growth factor receptor (P75NTR) can serve as a receptor for rabies virus. *EMBO J.* **17**: 7250-7259.

53. Ugolini, G. 1995. Specificity of rabies virus as a transneuronal tracer of motor network: transfer from hypoglossal motoneurons to connected second-order and higher order central nervous system cell groups. *J. Comp. Neurol.* **356**: 457-80.

54. Wang, Z. W., Sarmento, L., Wang, Y., Li, X., Dhingra, V., Tseggai, T., Jiang, B. and Fu, Z. F. 2005. Attenuated rabies virus activates, while pathogenic rabies virus evades, the host innate immune response in the central nervous system. *J. Virol.* **79**: 12554-12565.

55. Wacharapluesadee, S., Tepsumethanon, V., Supavonwong, P., Kaewpom, T., Intarut, N. and Hamachudha, T. 2012. Detection of rabies viral RNA by TaqMan real-time RT-PCR using non-neural specimens from dogs infected with rabies virus. *J. Virol. Methods* **184**: 109-112.

56. WHO Expert consultation on rabies. Second report. 2013. *World Health Organ Tech. Rep. Ser*. **982**: 1-139.

57. Yan, X., Prosniak, M., Curtis, M. T., Weiss, M. L., Faber, M., Dietzschold, B. and Fu, Z. F. 2001. Silver-haired bat rabies virus variant does not induce apoptosis in the brain of experimentally infected mice. *J. Neuroviral*. **7**: 518-527.

58. Yamada, K., Park, C. H., Noguchi, K., Kojima, D., Kubo, T., Komiya, N., Matsumoto, T., Mitui, M. T., Ahmed, K., Morimoto, K., Inoue, S. and Nishizono, A. 2012. Serial passage of a street rabies virus in mouse neuroblastoma cells resulted in attenuation: potential role of the additional *N*-glycosylation of viral glycoprotein in the reduced pathogenicity of street rabies virus. *Virus Res.* **165**: 34-45.

59. Zaidman, G. W. and Billingsley, A. 1998. Corneal impression test for the diagnosis of acute rabies encephalitis. *Ophthalmology* **105**: 249-251.

60. Zhang, G., Wang, H., Mahmood, F. and Fu, Z. F. 2013. Rabies virus glycoprotein is an important determinant for the induction of innate immune responses and the pathogenic mechanism. *Vet. Microbiol.* **162**: 601-613.

Table 1. Summary of anatomical distribution of rabies viral antigens in the peripheral nervous and non-nervous tissues of the head in mice infected with CVS-11, 1088-N0 and 1088-N30 viruses

Anatomical Area	CVS-11 virus			1088-N0 virus			1088-N30 virus		
	7 DPI (n=3)	8 DPI (n=1)	9 DPI (n=1)	5 DPI (n=5)	8 DPI (n=5)	11 DPI (n=5)	5 DPI (n=5)	8 DPI (n=5)	11 DPI (n=5)
Trigeminal ganglion	3	1	1	2	5	5	-	5	-
Trigeminal nerve	3	1	1	2	5	5	-	5	2
Optic nerve	-	-	NA	-	-	-	-	-	-
Maxillary nerve	-	-	-	-	-	5	-	-	4
Nasolacrimal duct	-	-	-	-	-	-		-	-
Olfactory bulb	-	-	-	-	-	-	-	-	-
Nasal mucosa	-	-	-	-	-	-	-	-	-
Retina	3	-	-	-	2	5	-	-	-
Lacrimal glands	-	-	NA	-	NA	NA	-	NA	NA
Harderian glands	-	-	-	-	-	-	-	-	-
Infraorbital nerve	-	-	-	-	-	5	-	-	-
Hypoglossal nerve	-	-	-	-	1	3	-	-	1
Lingual mucosa	2	-	1	-	3	4	-	-	3
Circumvallate papillae (taste cells)	-	NA	-	-	1	-	NA	-	-
Lingual minor salivary glands	-	-	-	-	-	4	-	-	4
Parotid salivary glands	-	-	-	-	-	-	-	-	-
Mandibular salivary glands	-	-	-	-	-	-	-	-	-
Facial muscle	-	-	-	-	1	5	-	-	-
Muzzle skin	-	-	-	-	3	5	-	-	3

DPI: days post inoculation, NA: not available due to distortion/fragmentation, -: no antigen detected

Table 2. The titer of viral neutralizing antibodies (VNA) of mice-infected with 1088-N0 viruses detected by rabid fluorescent focus inhibition tests

5 days PI			8 days PI			11 days PI		
Mouse No.	VNA (IU/ml)		Mouse No.	VNA (IU/ml)		Mouse No.	VNA (IU/ml)	
1		0.55	1		1.35	1		2.83
2		0.14	2		2.0	2		0.59
3		0.4	3		3.35	3		18.21
4		0.16	4		4.16	4		9.11
5		0.25	5		0.71	5		0.92
	Ave.	0.262		Ave.	1.929		Ave.	3.029
Control		0.12	Control		0.2	Control		0.19
Control		0.12	Control		0.2	Control		0.19
Control		0.12	Control		0.2	Control		0.19
	Ave.	0.12		Ave.	0.2		Ave.	0.19

PI: post inoculation, IU: international units

Table 3. The titer of viral neutralizing antibodies (VNA) of mice-infected with 1088-N30 viruses detected by rabid fluorescent focus inhibition tests

5 days PI			8 days PI			11 days PI		
Mouse No.	VNA (IU/ml)		Mouse No.	VNA (IU/ml)		Mouse No.	VNA (IU/ml)	
1		1.54	1		8.7	1		7.98
2		1.41	2		3.82	2		21.65
3		0.35	3		12.86	3		51.45
4		1.14	4		11.77	4		19.81
5		3.08	5		2.27	5		0.92
	Ave.	1.2169		Ave.	6.4793		Ave.	20.71
Control		0.12	Control		0.2	Control		0.19
Control		0.12	Control		0.2	Control		0.19
Control		0.12	Control		0.2	Control		0.19
	Ave.	0.12		Ave.	0.2		Ave.	0.19

PI: post inoculation, IU: international units

Figure legends

Figs. 1-4. Histology and immunohistochemistry of trigeminal ganglion of mice infected with 1088-N0 viruses at 5 days PI. Nuclear pyknosis and cytoplasmic vacuolation (arrow, Fig. 3), and viral antigens (Figs. 2 and 4) were observed in ganglion neurons.

Figs. 5-8. Histology and immunohistochemistry of trigeminal ganglion of mice infected with 1088-N0 viruses at 8 days PI. Nuclear pyknosis, cytoplasmic shrinkage and swollen with Nissl substance dissolution (arrows, Fig. 7), and viral antigens (Figs. 6 and 8) were observed in ganglion neurons and their axonal and dendritic processes.

Figs. 9-10. Trigeminal ganglion of mice infected with 1088-N0 viruses at 11 days PI. A small number of lymphocytes infiltrate throughout the ganglion (Fig. 9). Many ganglion neurons showed nuclear pyknosis and cytoplasmic shrinkage (arrows, Fig. 10).

Fig. 11. Trigeminal ganglion of mice infected with 1088-N0 viruses at 11 days PI. LFB staining revealed a decrease density of myelinated nerve fibers and extensive axonal demyelination (asterisk), and degenerated ganglion neurons were pale because of depletion of Nissl substance (arrows).

Fig. 12. Trigeminal ganglion of mice infected with 1088-N0 viruses at 11 days PI. Anti-NF immunoreactivity revealed weak and irregular positive reaction, and diffusely loss of both small- and large-diameter axons (asterisk).

Figs. 13-14. Trigeminal nerve of mice infected with 1088-N0 viruses at 11 days PI. Axonal degeneration, swollen myelin sheaths, myelin disintegration and vacuolization were observed (arrows, Fig. 14).

Figs. 15-16. Trigeminal nerve of mice infected with 1088-N0 viruses at 11 days PI. LFB staining revealed a decrease density of myelinated nerve fibers and extensive axonal demyelination.

Figs. 17-18. Trigeminal nerve of mice infected with 1088-N0 viruses at 11 days PI. Anti-NF immunoreactivity revealed weak and irregular positive reaction of axons.

Figs. 19-22. Histology and immunohistochemistry of trigeminal ganglion of mice infected with CVS-11 viruses at 9 days PI. Nuclear pyknosis, cytoplasmic shrinkage and swollen with Nissl substance dissolution (arrows, Fig. 21), and viral antigens (Figs. 20 and 22) were observed in many ganglion neurons and their axonal and dendritic processes.

Figs. 23-24. Histology and immunohistochemistry of the retina of mice infected with CVS-11 viruses at 7 days PI. There was no morphological changes were observed in the retina (Fig. 23) and lens (asterisk). Viral antigens were detected in the ganglion cells and their axonal processes in the inner plexiform layer (Fig. 24).

Figs. 25-26. Histology and immunohistochemistry of the maxillary nerve (M) and nasolacrimal duct (asterisk) of mice infected with 1088-N0 viruses at 11 days PI. The maxillary nerve revealed mild to moderate axonal vacuolar degeneration. In nasolacrimal duct revealed mild to moderate infiltration of mononuclear inflammatory cells appeared in submucosa. In addition, the mucosal surface was slightly thickened and epithelial cells showed degenerative changes (arrow) and sloughed into the duct lumen admixed with numerous necrotic inflammatory debris (Fig. 25). Viral antigens were detected in the axons of maxillary nerve (arrows, Fig. 26).

Fig. 27. Immunohistochemistry of tongue of mice infected with 1088-N0 viruses at 8 days PI. Viral antigens were detected in the lingual mucosa, circumvallate papillae and lingual minor salivary gland (asterisk).

Fig. 28. Immunohistochemistry of the lingual minor salivary glands of mice infected with 1088-N0 viruses at 11 days PI. Viral antigens were detected in the cytoplasm of the serous acinar epithelium (arrows).

Figs. 29-30. Histology and immunohistochemistry of the circumvallate papillae of mice infected with 1088-N0 viruses at 8 days PI. Cytoplasmic shrinkage and nuclear pyknosis (arrow, Fig. 29), and viral antigens were observed in taste cells (Fig. 30).

Figs. 31-32. Histology and immunohistochemistry of the facial muscle of mice infected with 1088-N0 viruses at 11 days PI. The facial muscle showed myofiber degeneration characterized by loss of cross-striations, hyalinized eosinophilic cytoplasm, intramuscular nerve fibers exhibited axonal degeneration, and occasional myoblasts were also seen (asterisk, Fig. 31). Viral antigens were detected in the intramuscular nerve fibers (Fig. 32).

Fig. 33. Immunohistochemistry of the facial muscle of mice infected with 1088-N0 viruses at 8 days PI. Viral antigens were detected in the cytoplasm of myoblasts.

Figs. 34-35. Immunohistochemistry of the muzzle skin of mice infected with 1088-N0 viruses at 11 days PI. Viral antigens were detected in the epithelial cells of epidermis, peripheral cutaneous nerve fibers and basal layer of the out root sheath of tactile hair follicles.

Fig. 36. Immunohistochemistry of the muzzle skin of mice infected with 1088-N0 viruses at 11 days PI. High magnification of Fig. 35. Viral antigens were detected in the epithelial cells of the epidermis.

Figs.1-6: Trigeminal ganglion, N0 strain

Trigeminal ganglion, 5 DPI, HE

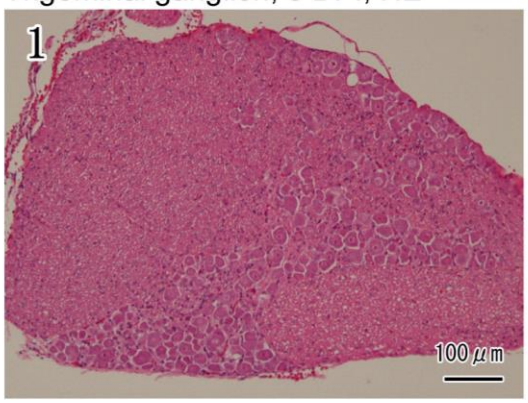

Trigeminal ganglion, 5 DPI, anti-P

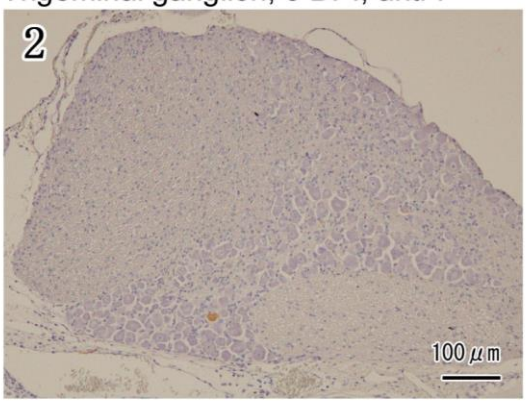

Trigeminal ganglion, 5 DPI, HE

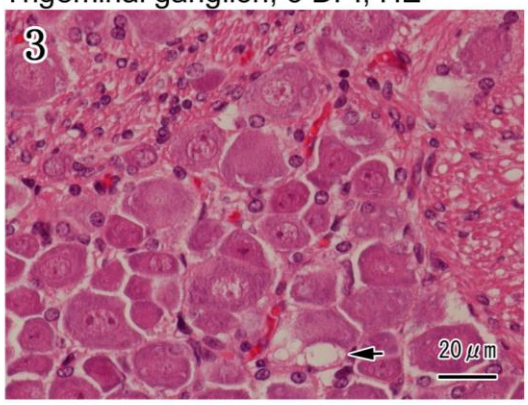

Trigeminal ganglion, 5 DPI, anti-P

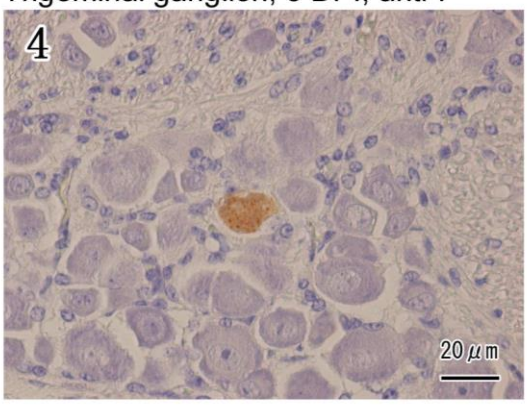

Trigeminal ganglion, 8 DPI, HE

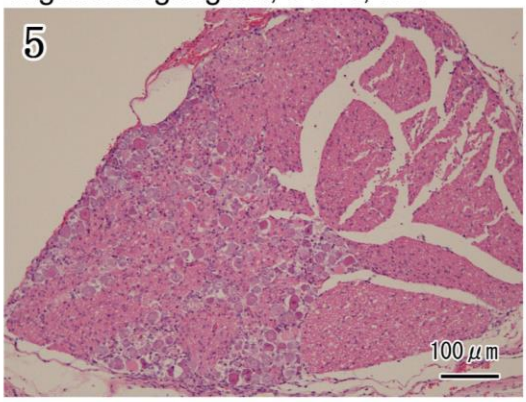

Trigeminal ganglion, 8 DPI, anti-P

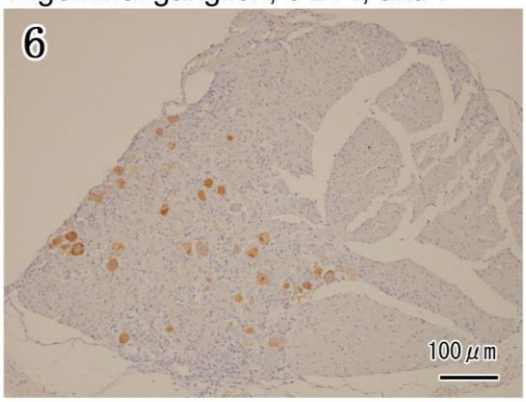

Figs.7-12: Trigeminal ganglion, N0 strain

Trigeminal ganglion, 8 DPI, HE

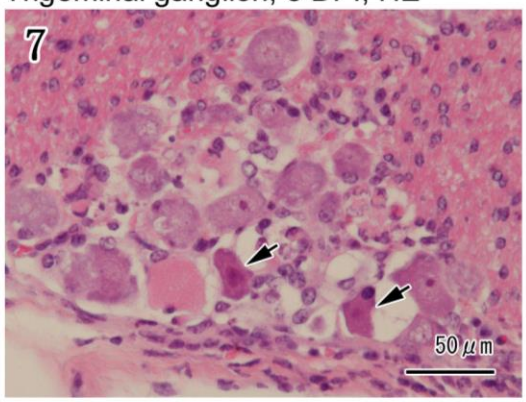

Trigeminal ganglion, 8 DPI, anti-P

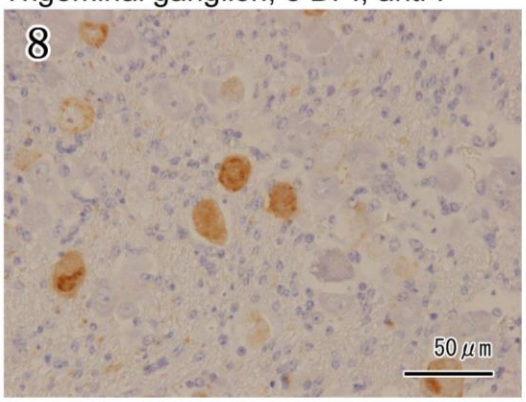

Trigeminal ganglion, 11 DPI, HE

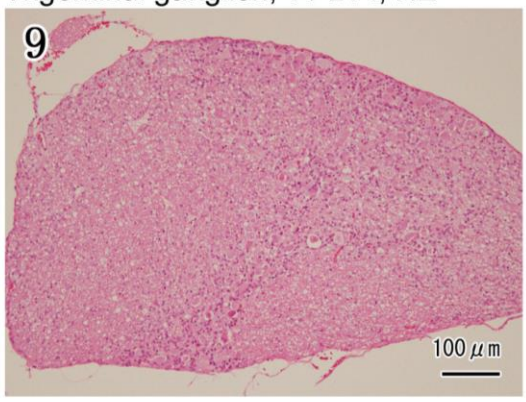

Trigeminal ganglion, 11 DPI, HE

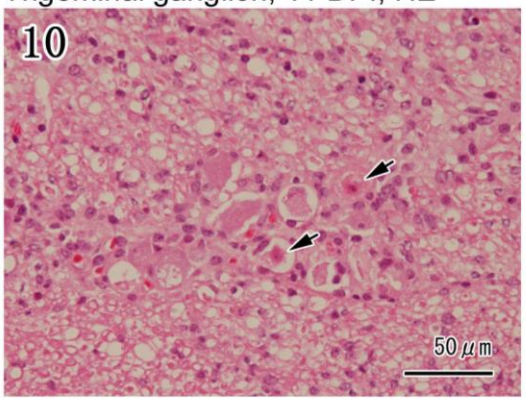

Trigeminal ganglion, 11 DPI, LFB

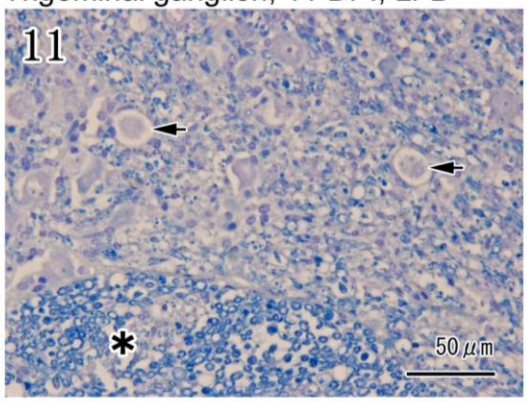

Trigeminal ganglion, 11 DPI, NF

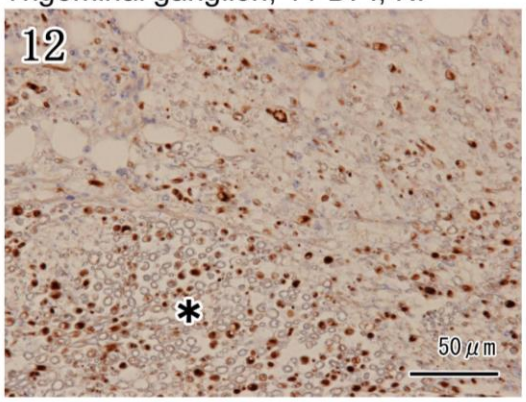

Figs.13-18: Trigeminal nerve, N0 strain

Trigeminal nerve, 11 DPI, HE

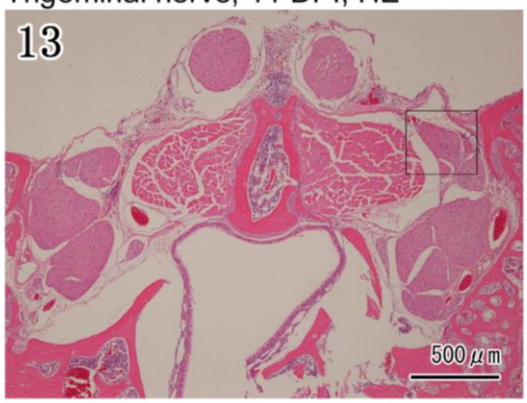

Trigeminal nerve, 11 DPI, HE

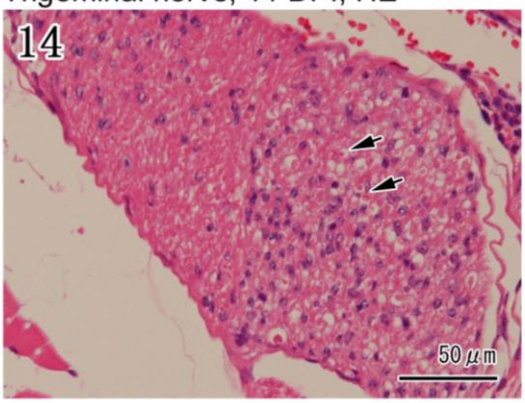

Trigeminal nerve, 11 DPI, LFB

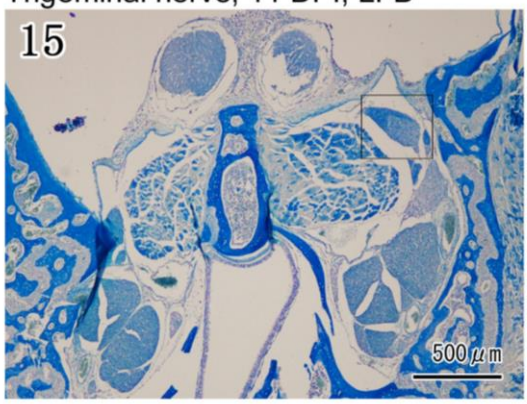

Trigeminal nerve, 11 DPI, LFB

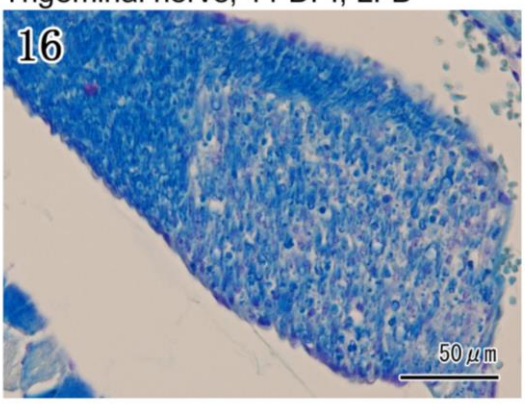

Trigeminal nerve, 11 DPI, NF

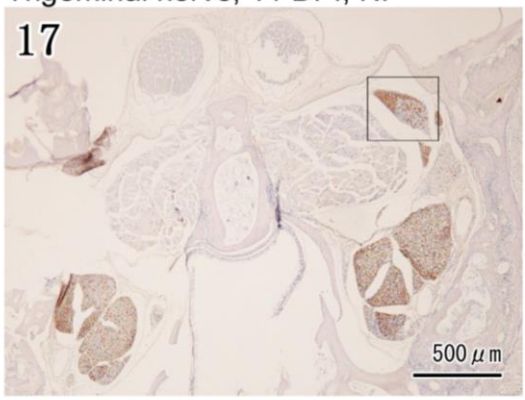

Trigeminal nerve, 11 DPI, NF

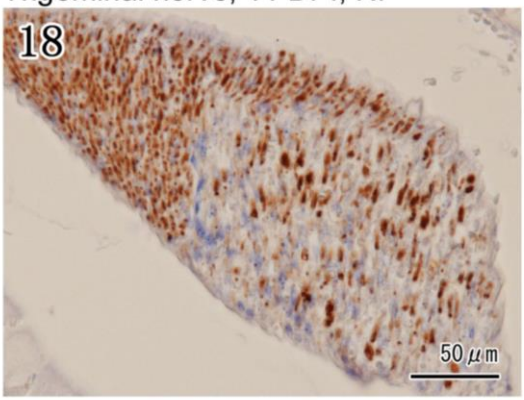

Figs.19-24: Trigeminal ganglion・retina, CVS-11 strain

Trigeminal ganglion, 9 DPI, HE

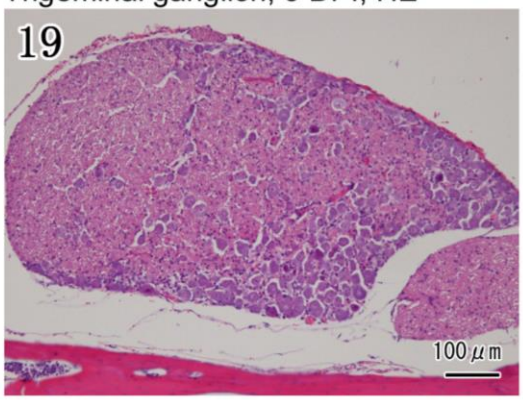

Trigeminal ganglion, 9 DPI, anti-P

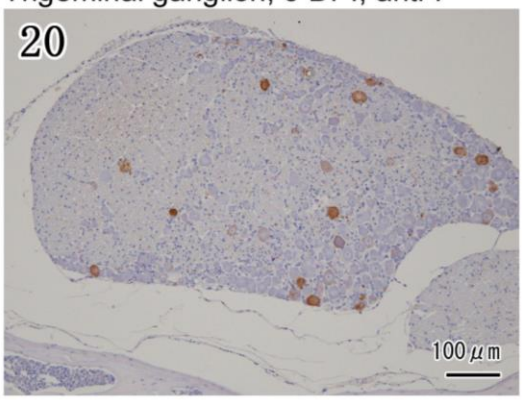

Trigeminal ganglion, 9 DPI, HE

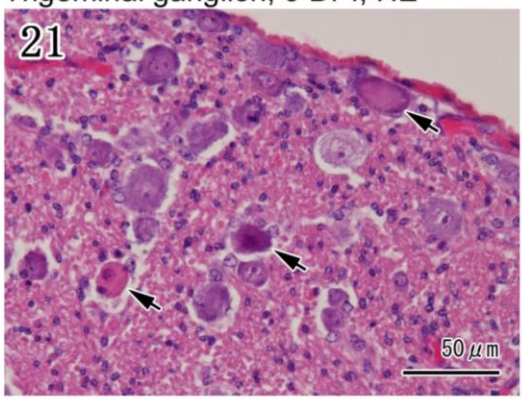

Trigeminal ganglion, 9 DPI, anti-P

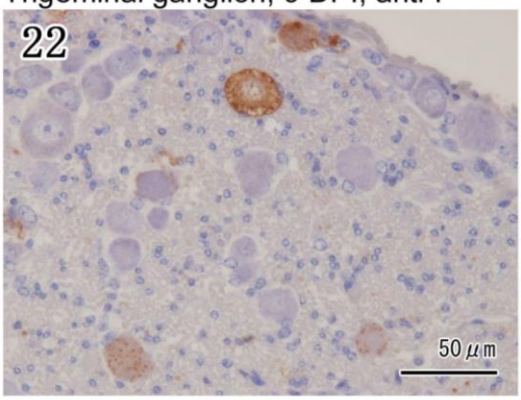

Retina, 7 DPI, HE

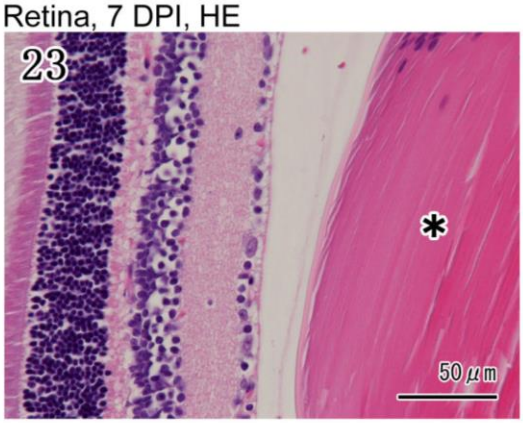

Retina, 7 DPI, anti-P

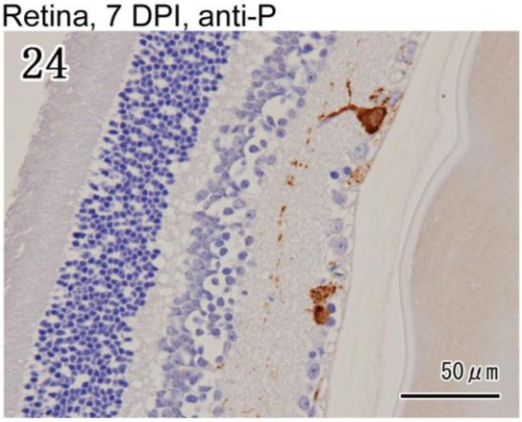

Figs.25-30: Maxillary nerve・nasolacrimal duct・tongue, N0 strain

Maxillary nerve, 11 DPI, HE

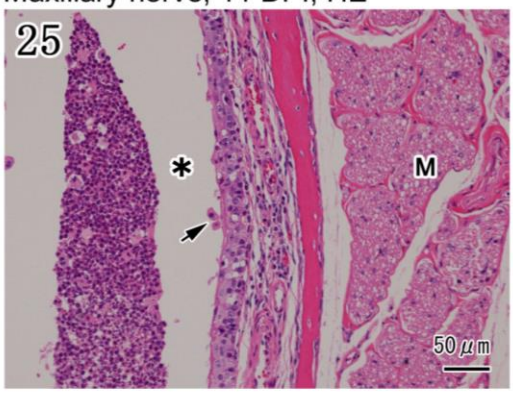

Maxillary nerve, 11 DPI, anti-P

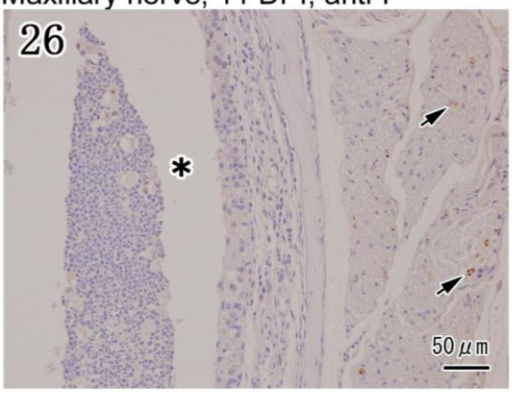

Tongue, 8 DPI, anti-P

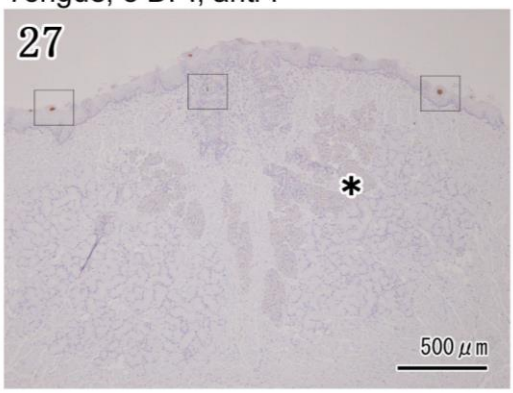

Minor salivary gland, 11 DPI, anti-P

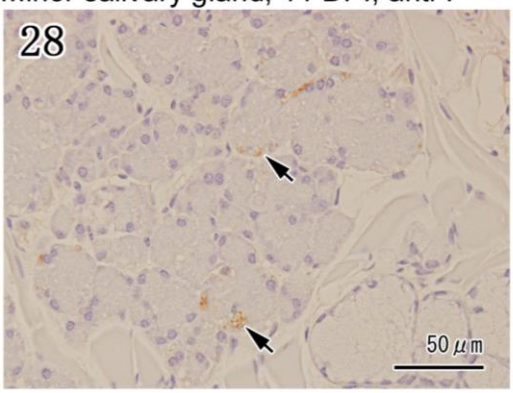

Circumvallate papillae, 8 DPI, HE

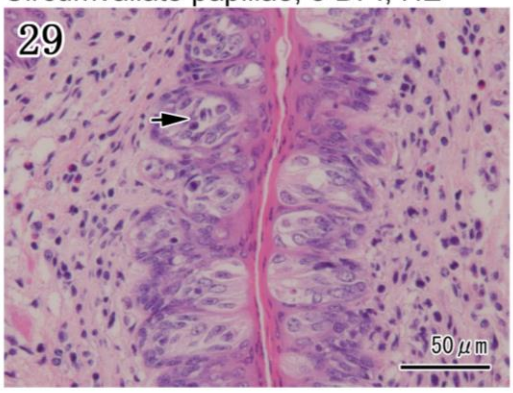

Circumvallate papillae, 8 DPI, anti-P

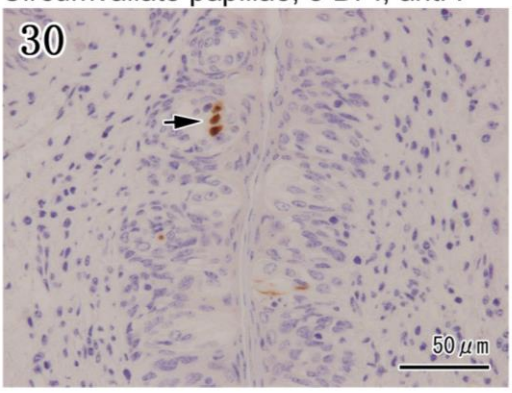

Figs.31-36: Facial muscle・muzzle skin, N0 strain

Facial muscle, 11 DPI, HE

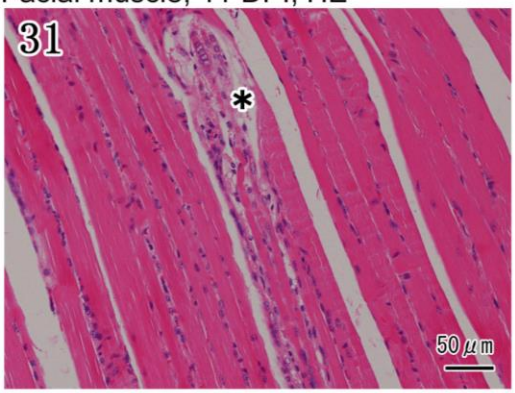

Facial muscle, 11 DPI, anti-P

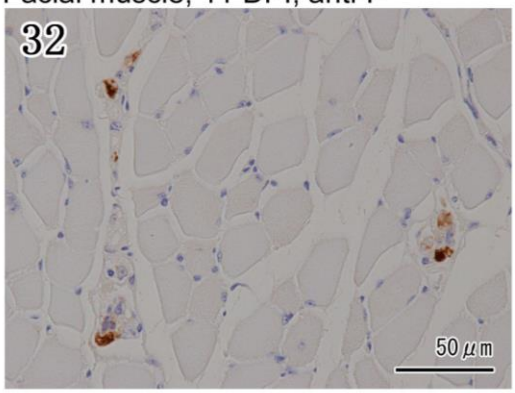

Facial muscle, 8 DPI, anti-P

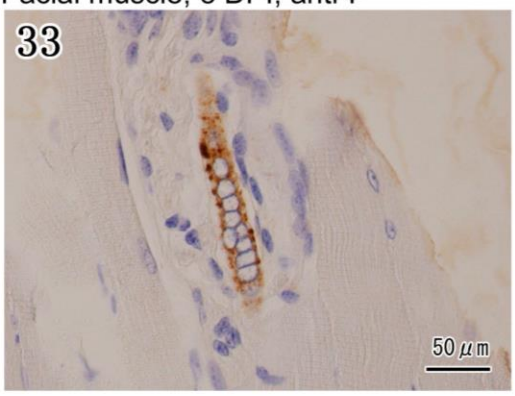

Muzzle skin, 11 DPI, anti-P

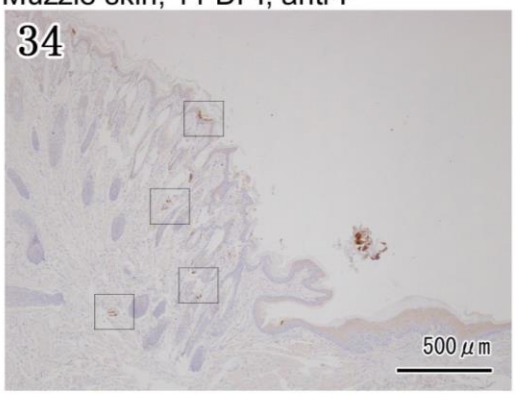

Muzzle skin, 11 DPI, anti-P

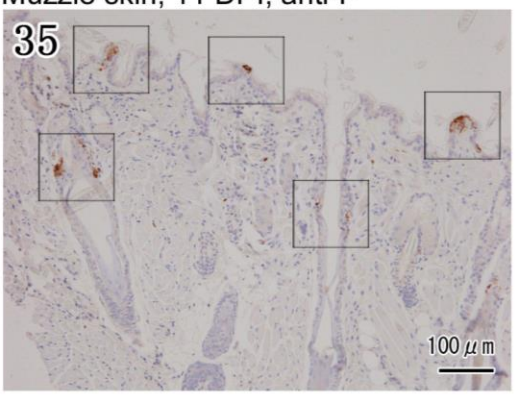

Muzzle skin, 11 DPI, anti-P

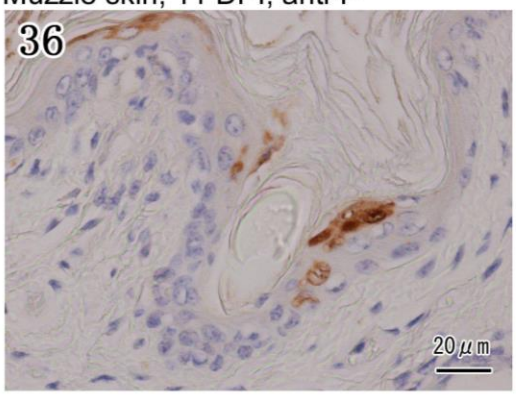

Chapter 4 Pathological study on the central nervous system and peripheral tissues of *dd*Y mice intramuscularly infected with street rabies virus (1088-N0 strain)

Introduction

Rabies is a fatal zoonotic disease caused by the rabies virus that affects all mammalian species [17]. An unexpected case of naturally acquired rabies infection in a chicken has been reported recently in India [4]. According to the World Health Organization, estimates 55,000 human deaths of rabies were accounted every year worldwide and 34,500 of these deaths come from Asia [37]. Rabies virus is a neurotropic virus that initially targets the central nervous system (CNS), resulting in fatal encephalomyelitis, the histopathological changes observed in the CNS are typically relatively mild, showing varying degrees of mononuclear inflammatory cell infiltration of the leptomeninges, perivascular lymphocyte cuffing, microglial activation, and neuronophagia. However, a precise understanding of the invasion pathways from the periphery to the CNS remains poorly understood. It was hypothesized that the virus inoculated at the periphery entry to CNS only via a motor neuron through the neuromuscular junction [13, 35]. However, some experimental studies have demonstrated that the virus migrates directly into the CNS via sensory nerve through nerve spindles and dorsal root ganglia sensory neurons after replication at the infection site [25, 36]. Neuroanatomical studies of neuronal cells infected by rabies virus following peripheral inoculation have shown that the virus disseminates in the CNS within axons by trans-synaptic propagation [8, 20, 35, 40].

The street strains of rabies virus are highly neuroinvasive that isolated from naturally infected animals, and have incubation periods varying from 2 weeks to more than 1 year and variable clinical effects [38]. Within the CNS, this virus causes extensive dendritic injury and decreased number of dendritic spines in hippocampal neurons after intracranial inoculation in

the mouse [28]. Feng *et al*. [11] proposed that most of neurons in the brain of mice infected with attenuated rabies virus strain are intact and have few abnormalities in organelle structure, while infection with highly neurovirulent strain of street rabies virus showed marked neuronal damage and structural abnormalities. On the other hand, street rabies virus (canine rabies virus variant) does not cause damage to neurons in the brain in natural rabies vectors [12]. These observations indicate that the pathological changes observed in these experimental infection models greatly differ between the various virus strains studied.

Previously, our laboratory used the CVS-11 strain of fixed virus for the study of rabies pathogenesis in mice [18, 19, 25]. However, infection with fixed rabies virus in the laboratory does not fully represent the pathogenesis in animals which infected with wild-type or street rabies virus under natural conditions. To obtain the more information about neuropathogenesis of rabies in mice, in this study, street rabies virus (1088-N0 strain) was inoculated into the right hind limb of *dd*Y mice, and the primary target cells and the sequential involvement during infection in the peripheral tissues and CNS were investigated.

Materials and methods

Virus, animals, and inoculations

The filed isolated street rabies virus 1088-N0 strain

The street rabies virus 1088-N0 strain was kindly provided by the Department of Microbiology, Faculty of Medicine, Oita University (Oita, Japan). The parental virus of this strain was isolated from a woodchuck in the Centers for Disease Control in Atlanta, U.S.A. was obtained from the Yale Arbovirus Unit, Yale University, and was replicated in mouse neuroblastoma C1300 (NA) cells as previously described [39]. The 1088-N0 was passaged in mouse brain for 2 generations. The genomic sequence analyzed by Department of Microbiology, Faculty of Medicine, Oita University observed on the surface glycoprotein (G protein) of 1088-N0 have two potential sequons in the *N*-glycosylation sites, Asparagine (Asn) at positions 37, 319 (Asn^{37}, Asn^{319}) [39]. Twenty-four 6-week-old female *dd*Y mice were purchased from Kyudo Co., Ltd., (Saga, Japan), 15 mice were inoculated intramuscularly (right *triceps surae* muscle) with viral dose of 10^6 plaque-forming units suspended in phosphate-buffered saline (PBS, pH 7.4) and nine uninfected control mice were inoculated intramuscularly with PBS alone. All experiments were performed in level-3 biosafety laboratories according to the guidelines for animal experiments with the approval of the ethics committee of Oita University.

Necropsy and preparation of tissue sections

All experimentally inoculated mice were observed daily for neurological conditions. The mice were sacrificed at 5, 8, and 11 days post-inoculation (PI) – five mice per day and their sera, and brain, spinal cord and muscle were sampled. It was subjected to 3 mice as a negative control in any of the groups. Each mouse was anesthetized with an inhalation anesthetic (isoflurane) and perfused intracardially with 10-15 ml of PBS, followed by fixed with 10% neutral buffered

formalin. The brain, spinal and muscle samples were removed and postfixed in 10% neutral buffered formalin at room temperature (RT) for less than 24 hours. The spinal samples were decalcified in K-CX (Fujisawa, Pharmaceutical Co., Ltd., Osaka, Japan) solution at RT for 12 hours, and then washed in running tap water for 12 hours. Coronal sections of the brains at the positions of olfactory bulb, forebrain, mammillary body and pons and transverse sections of spinal cords at the cervical (C3-C4), thoracic (T1-T3), lumbar (L1-L2), and sacral (S1-S3) vertebrae were prepared. For routine histological evaluation, tissues samples were embedded in paraffin wax, serially sectioned (3 μm thickness), and mounted on glass slides and dried on a slide dryer machine at 40°C for overnight. Serial sections were then subjected to haematoxylin and eosin, and luxol fast blue staining, to immunohistochemistry and to *in situ* terminal deoxynucleotidyl-transferase-mediated (dUTP) nick end labeling (TUNEL) assays.

Staining with hematoxylin and eosin (HE)

The sections were stained with hematoxylin and eosin for general histopathological examination.

Protocol

Paraffin was removed from the sections by a series of xylene and ethanol rinses. Tissue sections were rinsed in distilled water for 5 minutes and stained with hematoxylin solution for 3 minutes, rinsed in running tap water for 5 minutes and stained with eosin solution for 5 minutes, rinsed in distilled water for three times and dehydrated through a series of ethanol and xylene. The sections were then mounted in microscopy mounting medium.

Staining with luxol fast blue (LFB)

The sections were stained with LFB for myelin or myelinated axons examination.

Protocol

Paraffin was removed from the sections by a series of xylene and ethanol rinses. The tissue sections were rinsed in distilled water for 5 minutes, and then sections were immersed in 0.005% acetic acid solution in 95% ethyl alcohol at room temperature for 5 minutes. Place sections in 0.1% LFB solution for 16 hours in a 60°C oven, rinse off excess strain in 95% ethyl alcohol, rinse briefly in distilled water, sections were differentiated in 0.05% lithium carbonate solution for 15-20 seconds, followed by a final rinse in distilled water. After checking for completion of differentiation under the microscope, sections were counterstained in cresyl violet solution for 1 minute, rinse again in distilled water for 5 minutes, and followed by dehydrated through a series of ethanol and xylene. The sections were mounted in microscopy mounting medium.

Immunohistochemistry

2. For detection of the rabies virus antigens in tissues

The sections were stained using the streptavidin-biotin-peroxidase complex method with rabbit anti-phosphoprotein (P) antibodies.

Protocol

The sections were deparaffinized by a series of xylene and ethanol rinses, rehydrated, and washed twice with distilled water. The sections were treated for the activation of antigen with 0.25% trypsin at room temperature for 30 minutes. After this treatment, sections were washed three times for 5 minutes in distilled water. After washing, to removed endogenous peroxidase activity the sections were immersed with 0.3% H_2O_2 in methanol for 60 minutes; then they were washed three times for 5 minutes in distilled water once again. The sections were treated with 10% normal goat serum (Nichirei Biosciences, Tokyo, Japan) for 60 minutes to block non-

specific reaction. Sections were then incubated with primary antibody for overnight at 4°C in a humidified chamber. Primary antibody was diluted 1:1200. After incubation with primary antibody, sections were washed three times for 5 minutes in phosphate buffer saline (PBS, pH 7.4) and incubated for 30 minutes at room temperature with the biotinylated anti-rabbit IgG (Nichirei Biosciences) as a secondary antibody. Sections were again washed three times for 5 minutes in PBS; then incubated for 30 minutes in room temperature with peroxidase-streptavidin enzyme (Nichirei Biosciences) for 30 minutes, washed in PBS three times for 5 minutes. Finally, sections were visualized using 3-3'-diaminobenzidine tetrachloride substrate (DAB substrate; DAKO, Kyoto, Japan), followed by rinsing in distilled water. The sections were counterstained with hematoxylin, and rinsing in running tap water again for 5 minutes. The sections were then dehydrated and mounted in microscopy mounting medium. Negative control was processed with rabbit serum instead of primary antibody.

2. For detection of microglia

The sections were stained using the polymer-based immunohistochemical method with rabbit anti-ionized calcium-binding adaptor molecule 1 antibodies (Iba1, Wako Ltd., Osaka, Japan) for detection of microglia.

Protocol

The sections were deparaffinized by a series of xylene and ethanol rinses, rehydrated, and washed twice with distilled water. After washing, the sections were treated for the activation of antigens with 10 mM sodium citrate buffer (pH 6.0) in a water bath at 95°C for 30 minutes; then they were rinsed in distilled water with three changes of 5 minutes each. Incubation for 10 minutes in 3% H_2O_2 in methanol to removed endogenous peroxidase activity, and the sections were rinsed in distilled water (three changes, 5 minutes each). To block non-specific reaction, the sections were treated with 10% normal goat serum (Nichirei Biosciences, Japan) for 60

minutes at room temperature, followed by incubation with the primary antibody for overnight at 4°C in a humidified chamber. Primary antibody was diluted 1:500. After incubation with the primary antibody, sections were rinsed in PBS (three changes, 5 minutes each), and then incubated for 30 minutes at room temperature with the anti-rabbit IgG (Nichirei Biosciences) as a secondary antibody. Sections were again washed three times for 5 minutes in PBS; then incubated with peroxidase-streptavidin enzyme (Nichirei Biosciences) for 30 minutes at room temperature, washed in PBS three times for 5 minutes. Finally, sections were visualized using DAB substrate, followed by rinsing in distilled water. Sections were counterstained with haematoxylin, and washed again in running tap water for 5 minutes. Slides were then dehydrated and mounted in microscopy mounting medium.

3. For detection of T lymphocytes

The sections were stained using the polymer-based immunohistochemical method with polyclonal rabbit anti-CD3 antibodies (DAKO, Kyoto, Japan) for detection of T lymphocytes.

Protocol

The sections were deparaffinized by a series of xylene and ethanol rinses, rehydrated, and washed twice with distilled water. The sections were treated with Histofine® pH 9.0 (Nichirei Biosciences, Japan) for activation of antigens by microwaving at 750W for 5 minutes; then were washed in distilled water with three changes of 5 minutes each. After washing, incubation for 10 minutes in 3% H_2O_2 in methanol to removed endogenous peroxidase activity, and the sections were rinsed in distilled water (three changes, 5 minutes each). To block non-specific reaction, the sections were treated with 10% normal goat serum (Nichirei Biosciences) for 60 minutes, followed by incubation with the primary antibody for overnight at 4°C in a humidified chamber. Primary antibody was diluted 1:50. After incubation with the primary antibody, sections were rinsed in PBS (three changes, 5 minutes each), then incubated for 30 minutes at room

temperature with the Envision + System Labelled Polymer-HRP anti-rabbit (DAKO), rinsed in PBS (three changes, 5 minutes each) once again. Finally, sections were visualized using DAB substrate, followed by rinsing in distilled water. The sections were counterstained with hematoxylin, and rinsing in running tap water again for 5 minutes. The sections were then dehydrated and mounted in microscopy mounting medium.

4. For detection of B lymphocytes

The sections were stained using the polymer-based immunohistochemical method with polyclonal rabbit anti-CD20 antibodies (Spring Bioscience, Fremont, USA) for detection of B lymphocytes.

Protocol

The sections were deparaffinized by a series of xylene and ethanol rinses, rehydrated, and washed twice with distilled water. The sections were treated with Histofine® pH 9.0 (Nichirei Biosciences) for activation of antigens by microwaving at 750W for 5 minutes; then were washed in distilled water with three changes of 5 minutes each. After washing, incubation for 10 minutes in 3% H_2O_2 in methanol to removed endogenous peroxidase activity, and the sections were rinsed in distilled water (three changes, 5 minutes each). To block non-specific reaction, the sections were treated with 10% normal goat serum (Nichirei Biosciences) for 30 minutes, followed by incubation with the primary antibody for overnight at 4°C in a humidified chamber. After incubation with the primary antibody, sections were rinsed in PBS (three changes, 5 minutes each), then incubated for 30 minutes at room temperature with the Envision + System Labelled Polymer-HRP anti-rabbit (DAKO), rinsed in PBS (three changes, 5 minutes each) once again. Finally, sections were visualized using DAB substrate, followed by rinsing in distilled water. The sections were counterstained with hematoxylin, and rinsing in running tap water

again for 5 minutes. The sections were then dehydrated and mounted in microscopy mounting medium.

5. *For detection of nerve fibers*

The sections were stained using the polymer-based immunohistochemical method with monoclonal mouse anti-neurofilament protein antibodies (NF, DAKO, Kyoto, Japan) for detection of nerve fibers.

Protocol

The sections were deparaffinized by a series of xylene and ethanol rinses, rehydrated, and washed twice with distilled water. After washing, the sections were treated for the activation of antigens with Proteinase-K at room temperature for 30 minutes; then they were rinsed in distilled water with three changes of 5 minutes each. Incubation for 10 minutes in 3% H_2O_2 in methanol to removed endogenous peroxidase activity, and the sections were rinsed in distilled water (three changes, 5 minutes each), followed by incubation with the primary antibody for overnight at 4°C in a humidified chamber. Primary antibody was diluted 1:100. After incubation with the primary antibody, sections were rinsed in PBS (three changes, 5 minutes each), then incubated for 30 minutes at room temperature with the Histofine® Simple Stain MAX-PO (Mouse) (Nichirei Biosciences) rinsed in PBS (three changes, 5 minutes each) once again. Finally, sections were visualized using DAB substrate, followed by rinsing in distilled water. The sections were counterstained with hematoxylin, and rinsing in running tap water again for 5 minutes. The sections were then dehydrated and mounted in microscopy mounting medium.

6. For detection of astrocytes

The tissue sections were stained using the polymer-based immunohistochemical method with anti-glial fibrillary acidic protein antibody (GFAP; Nichirei Bioscience, Tokyo, Japan) for detection of astrocytes.

Protocol

The tissue sections were deparaffinized by a series of xylene and ethanol rinses, rehydrated, and washed twice with distilled water. To remove endogenous peroxidase, tissue sections were treated with 3% H_2O_2 in methanol for 15 minutes, and sections were then rinsed in distilled water (three changes, 5 minutes each). To block non-specific reaction, sections were treated with 10% normal goat serum (Nichirei Biosciences) for 30 minutes at room temperature, followed by incubation with the primary antibody at room temperature for 60 minutes in a humidified chamber. After incubation with the primary antibody, sections were rinsed in PBS (three changes, 5 minutes each), then incubated for 30 minutes at room temperature with Histofine® simple stain MAX-PO (Rabbit) (Nichirei Biosciences) as a secondary antibody, and then rinsed in PBS (three changes, 5 minutes each) once again. Finally, sections were visualized using DAB substrate, followed by rinsing in distilled water. The sections were counterstained with hematoxylin, and rinsing in running tap water again for 5 minutes. The sections were then dehydrated and mounted in microscopy mounting medium.

Terminal deoxynucleotidyl transferase-mediated deoxyuridine triphosphate (dUTP) nick end labeling (TUNEL) assay

The sections were evaluated using TUNEL assay kit (ApopTag® Plug peroxidase In Situ Apoptosis Detection Kit, Millipore Corporation, Billerica, MA, USA) for detection of fragmented DNA of apoptotic cells.

Protocol

The sections were deparaffinized by a series of xylene and ethanol rinses, rehydrated, and washed twice with distilled water. After washing, sections were treated with Proteinase-K (DAKO) for 15 minutes at room temperature to activated antigens, rinsed in PBS (three changes, 5 minutes each). Then, endogenous peroxidase activity was removed with 0.3% H_2O_2 in methanol for 15 minutes at room temperature, rinsed in PBS (three changes, 5 minutes each). After washing in PBS, sections were covered with 50 µl of the TUNEL reaction mixture, which containing terminal deoxynucleotidyl transferase (TdT) and fluorescein-dUTP, and incubated under a coverslip in a humidified chamber for 60 minutes at 37°C. The reaction was stopped by washing sections in PBS. Sections were then incubated with anti-digoxigenin peroxidase for 30 minutes at room temperature. Then, washed in PBS (three changes, 5 minutes each) once again. Finally, sections were visualized using DAB substrate, followed by rinsing in distilled water. The sections were counterstained with hematoxylin, and rinsing in running tap water again for 5 minutes. The sections were then dehydrated and mounted in microscopy mounting medium.

Results

Clinical observations and gross findings

Mice showed anorexia, emaciation, ruffled fur and hunched backs at 4 to 5 days after inoculation. Mice initially developed signs of rabies including uncoordinated limb movements, ataxia, and paralysis in the inoculated limb before developing into a bilateral hind limb paralysis at 5 days post-inoculation (PI). Paralysis was progressed to quadriparalysis, and subsequently mice became moribund state at 8 days PI. All infected mice died within 11 days PI after onset of symptoms. Conversely, normal control mice did not show any clinical symptoms within 11 days of intramuscular inoculation. No gross findings were observed at necropsy in any of the mice throughout the experimental period.

Histopathological examination

The spinal cord and dorsal root ganglion

At 5 days PI, mild degeneration of neurons in the spinal cord and dorsal root ganglion was observed. Neuronal degeneration was characterized by swollen (rounded) and lightly stained cytoplasm with a dissolution of the Nissl substance (Figs. 1, 3). Some affected ganglion neurons exhibited necrotic changes, characterized by condensation of nuclear chromatin, nuclear pyknosis, and cytoplasmic shrinkage. In addition, a small number of inflammatory mononuclear cells composed mainly of lymphocytes were observed surrounding blood vessels (perivascular cuffing), under the leptomeninges of spinal cords and under epineurium of dorsal root ganglia.

At 8 days PI, the numbers of degenerated neurons were significantly increased in the spinal cords and dorsal root ganglia. Most affected ganglion neurons showed swollen (rounded) or angular, pale, with reduction in or absence of Nissl substance, and some showed

hypereosinophilic, nuclear pyknosis, cytoplasmic shrinkage, and dispersed chromatin. Nuclei were central or slightly eccentric, and some contained clumped chromatin or undergoing karyorrhexis. Mild lymphocytic infiltration was observed around small vessels in the spinal cords (Fig. 5) and scattered throughout dorsal root ganglia. Large activated microglial cells and gliosis were scattered throughout the parenchyma of the spinal cord. In addition, axonal degeneration, swollen myelin sheaths, minimal myelin disintegration and vacuolization were observed in dorsal root fibers (Figs. 7, 9).

At 11 days PI, the numbers of degenerated neurons were significantly increased in the spinal cords and dorsal root ganglia when compared to 8 days PI mice. Axonal degeneration, swollen myelin sheaths, minimal myelin disintegration and vacuolization were observed in dorsal root fibers. In the spinal cord, moderate lymphocyte infiltration was observed around the small blood vessels and under the leptomeninges (Fig. 41), and large activated microglial cells and gliosis were scattered throughout the parenchyma. On the other hand, no histological changes were observed in the nerve fibers of the ventral root throughout the experiments.

The brain

At 5 days PI, mild inflammatory cells composed of lymphocytes were observed throughout under the leptomeninges of the cerebrum and cerebellum. No histological changes were observed in pyramidal neurons of any area, including the cerebral cortex, thalamus, medulla oblongata, and cerebellum.

At 8 days PI, the nuclear pyknosis and fragmentation, cytoplasmic shrinkage, Negri body-like inclusions were first seen in the pyramidal neurons of the cerebral cortex (Figs. 11, 12, 46, 48), medulla oblongata (Figs. 16, 18). Lesser changes were observed in the neurons of the cerebellum Purkinje cells (Fig. 20), and thalamus neurons. In addition, moderate inflammatory

cells composed of lymphocytes were observed under the leptomeninges and around the small vessels (Fig. 50), and the majority of lymphocytes showed nuclear fragmentation and pyknosis.

At 11 days PI, the numbers of degenerated neurons were significantly increased particularly in the pyramidal cells of the cerebral cortex, medulla oblongata, hypothalamus, cerebellum Purkinje cells and thalamus neurons. In addition, moderate infiltration of lymphocytes were observed under the leptomeninges (Fig. 40), around blood vessels (Fig. 42) and in the cerebral ventricles (Fig. 44), and large activated microglial cells and gliosis were found in multiple areas, including the cerebral cortex, thalamus, medulla oblongata and cerebellum. Frequently, the majority of lymphocytes showed nuclear fragmentation and pyknosis.

Immunohistochemical examination

Detection of rabies virus antigens by anti-P antibodies

At 5 days PI, Viral antigens were initially detected in muscles and intramuscular nerve fibers at site of inoculation, and neurons of the dorsal root ganglia (Figs. 2, 4) and spinal cord (motor neurons in the ventral horns). Virus positive neurons were occasionally observed in the red nuclei, medulla oblongata and cerebral cortex (M1 motor area, Fig. 13).

At 8 days PI, viral antigens were widely distributed in the neurons throughout the brain (Fig. 14), including cerebral cortex, thalamus, hippocampus, medulla oblongata (Figs. 17, 19) and cerebellum Purkinje cells and their dendrites (Fig. 21). Virus positive neurons were also observed particularly in the sensory neurons of the dorsal horns (Fig. 6), dorsal root ganglia and their nerve fibers, but no viral antigens were found in the ventral root fibers (Figs. 8, 10).

At 11 days PI, virus positive neurons were more numerous and widely distributed throughout the brain (Fig. 15), including cerebral cortex, thalamus, hippocampus, medulla

oblongata, and cerebellum Purkinje cells. In addition, antigen positive reactions were found in the sensory neurons in the dorsal horns and dorsal root ganglia neurons.

The localization of viral antigens in the cerebral cortex, hippocampus, thalamus, medulla oblongata, cerebellum, spinal cord, dorsal root ganglion and muscle were summarized in Table 1, and also the anatomical distribution of viral antigens in mouse brain coronal section, including cerebrum, hippocampus and thalamus was showed in schematic data.

Detection of microglia by anti-Iba1 antibodies

At 5 days PI, rod-like small microglia were scattered throughout the spinal cord (Figs. 22, 23), brain (Figs. 28, 29) and dorsal root ganglia. In dorsal root ganglia, microglia were seen predominantly around degenerated neurons. At 8 and 11 days PI, the number of microglia significantly increased and their morphology changed from rod to ramified or amoeboid, and scattered throughout the spinal cord (Figs. 24-27) and brain (Figs. 30-33).

Detection of astrocytes by anti-GFAP antibodies

At 5 days PI, astrocytes were scattered throughout the parenchyma, under the leptomeninges, around the small blood vessels and the central canal of the brain and spinal cord (Figs. 34, 35). At 8 and 11 days PI, the number of astrocytes significantly increased and scattered throughout the parenchyma of the brain and spinal cord (Figs. 36-39). In addition, astrocytes were activated in the brain and spinal cord, and their morphology changed. The process of fibrous astrocytes elongated from the leptomeninges to the deep parenchyma and many large protoplasmic astrocytes were observed concurrently in the parenchyma of the spinal cord, particularly around necrotic neurons.

Detection of lymphocytes by anti-CD3 and anti-CD20 antibodies

At 5 days PI, small numbers of CD3-positive T lymphocytes appeared in the dorsal root ganglion, under the leptomeninges and around blood vessels and ventricles of the brain and spinal cord. At 8 and 11 days PI, the number of CD3-positive T lymphocytes significantly increased and scattered throughout the parenchyma of the brain and spinal cord, particularly around blood vessels (Fig. 43) and central canal of the brain (Fig. 45). On the other hand, CD20-positive B lymphocytes were not detected in the CNS throughout the experimental period.

Detection of apoptotic cells by TUNEL assays

At 5 days PI, small numbers of TUNEL-positive cells appeared in the cerebral cortex, thalamus and medulla oblongata. At 8 and 11 days PI, the numbers of TUNEL-positive cells were significantly increased, and were detected widely distributed in spinal cord and brain, particularly in cerebral cortex (Figs. 47, 49), hippocampus, medulla oblongata and thalamus, and few positive cells found in dorsal root ganglion. Staining was prominent in lymphocytes under the leptomeninges and in the perivascular area (Fig. 51), and glial cells in the cerebral cortex (Figs. 52, 53) that exhibited apoptotic features, such nuclear fragmentation and pyknosis. TUNEL-positive neurons were rarely seen in the cerebral cortex, thalamus and medulla oblongata, but TUNEL-positive signals were not detected in the spinal neurons and dorsal root ganglion neurons in spite of strong immunostaining for the viral antigen.

The mean of the number of glial cells around degenerated neurons, lymphocytes and TUNEL-positive cells in multiples areas (cerebral cortex, thalamus, hippocampus, medulla oblongata) of brain and cervical, thoracic, lumbar, sacral spinal cords at time course was summarized in Table 2.

Detection of nerve fibers by anti-neurofilament protein (NF) and for identification of the myelin sheath of the myelinated nerve fibers by luxol fast blue (LFB) staining

At 8 and 11 days PI, anti-NF immunoreactivity showed weak and irregular positive reaction, and diffusely loss of both small- and large-diameter axons in the in the dorsal root fibers (Figs. 54, 55). In addition, LFB staining revealed a decrease density of myelinated nerve fibers and extensive axonal demyelination of the dorsal root ganglion and dorsal root of spinal nerve, while the ventral root fibers appeared intact (Figs. 56-59).

Discussion

In this study, *dd*Y mice that were inoculated intramuscularly with the street rabies virus strain 1088-N0 isolated from a woodchuck exhibit paralytic signs and the pathological changes are more severe in the dorsal root ganglion neurons than those found in the nerve cells of the brain and spinal cord. Therefore, it was suggested that the possibility that the selective vulnerability of dorsal root ganglion neurons and their nerve fibers in mice infected with 1088 virus deeply participated in clinical signs.

The centripetal propagation of rabies virus from peripheral nerve to reach CNS have been described occurs only via the motor route by binding to the nicotinic acetylcholine receptors at the motor endplates [7, 8, 13, 21, 22, 34]. On the other hand, Park *et al.* [25] and Valandia-Romero *et al*. [36] reported evidence of replication in the muscle spindles and dorsal root ganglia, suggesting that the virus preferentially entered the CNS through sensory nerve fibers. The present study, viral antigens were initially detected in the hind limb muscle at the site of inoculation and dorsal root ganglion neurons, and were then detected in motor neurons in the ventral horns, medulla oblongata neurons, red nuclei, and pyramidal cells in the cerebral cortex (motor M1 area). These results suggested that 1088 virus ascended the CNS in a centripetal propagation via mainly afferent fibers at early stage of infection and move to cerebral cortex using descending spinal tract.

Recently, previous studies have reported that the neurons in the brain of mice-infected with rabies virus can secrete chemokines/cytokines such as gamma interferon (IFN-γ)-inducible protein 10 (CXCL10) that lead to the activation of microglia and astrocytes, infiltration of inflammatory cells, and enhancement of blood-brain barrier permeability [6]. In addition, activated astrocytes and microglia cells can also produce CXCL10, and responsible as a chemoattractant for activated T lymphocytes [9]. In the present study, virus-infected neurons in

spinal cord and brain were first detected at 5 days PI as well as the number of activated microglia cells, astrocytes and inflammatory T lymphocytes increased as the infection progressed. These findings suggested that virus-infected neurons release a chemoattractant chemokines for activated microglia cells and astrocytes, as well as attracting infiltration of inflammatory T lymphocytes into the CNS.

Iba1 is a microglial surface marker, and increased staining for Iba1 can indicate microglial activation in the CNS [1]. Microglia changes their morphological forms such as ramified (resting) and amoeboid (activated) types after CNS injury [26, 30]. Activated microglia produce various proinflammatory cytokines and chemokines, such as interleukin (IL)-1, CXCL10, tumor necrosis factor alpha (TNF-α), matrix metalloproteinases (MMPs), superoxide and nitric oxide (NO) [26], which mediate nerve cell death both directly and indirectly via the induction of NO and free radicals [15], and also NO-induced cytotoxicity via oxidative injury result in immunosuppression and immunopathology [2]. In addition, MMPs are secretory products of activated microglia, which can contribute to breakdown of the blood-brain barrier, leukocyte emigration into the nervous system, and tissue destruction [26]. IL-1 and TNF-α were released by microglia and macrophages, and play an important role in coordinating the inflammatory response associated with rabies encephalopathy [24]. In this study, the number of microglia positive to anti-Iba1 antibody increased significantly from 8 days PI and their morphological changed to a ramified to amoeboid form in the areas where many virus-infected cells and necrotic cells were present. Therefore, it was suggested that activated microglia and their inflammatory cytokines related to neuronal necrosis in the spinal cord and brain.

Within the CNS, astrocytes play potential roles in neuroprotective functions, synaptic transmission, and provide structural, metabolic and trophic support for neurons. As might be expected from their wide range of functions, both beneficial and detrimental effects are attributed to activate astrocytes [3, 10, 29]. Furthermore, astrocytes activated by chemokines

that released from infected nerve cells as above mentioned [6]. In the present study, fibrous and protoplasmic astrocytes increased in the brain and spinal cord from 8 days PI. Subsequently, the numbers of necrotic neurons increased as disease progressed. These findings are consistent with a previous study of our laboratory in which mice were inoculated with fixed rabies virus (CVS-11 strain) intramuscularly, we observed that numerous spinal neurons underwent necrosis and that number of astrocytes increased as the infection progressed [18]. Therefore, it was suggested that the number of astrocytes increased and their morphological changed in response to neuronal cell death by necrosis.

Apoptosis plays a protective role in eliminating virus-infected cells. There are many different pathways that initiate apoptosis [25, 27, 32], of which Fas/Fas ligand apoptotic partway is one of the most important. In the present study, a very few virus-infected nerve cells in the cerebral cortex, thalamus and medulla oblongata were positive for TUNEL staining. However, virus-infected dorsal root ganglion neurons, spinal neurons, and most of nerve cells in the other areas of brain exhibited fragmentation and cytolysis, but these cells were negative against TUNEL. These findings indicate that most of virus-infected nerve cells died by necrosis. These aspects are partially in accordance with those of previous reported by Park *et al.* [25], in which mouse spinal neurons and dorsal root ganglion neurons were more resistant to apoptosis than cerebellum Purkinje cells after CVS-11 strain infection. In addition, in chapter 1, we demonstrated that virus-infected ganglion neurons in the mandibular gland of rabid dogs did not underwent apoptosis. Therefore, it was suggested that absence of neuronal apoptosis in mice infected by street rabies virus may promote prolonged infection within dorsal root ganglion neurons and continuously supply virus to the spinal cord and subsequent propagates centripetally to the brain.

T lymphocytes play an important role in cellular immunity by blocking viral spread and clearing rabies virus from the CNS [5, 14, 23]. Nevertheless, infiltration of T lymphocytes may

release of cytotoxic cytokines such as IFN-γ to kill virus-infected cells [17]. In this study, the CD3-positive T lymphocytes were present in the brain, spinal cord and dorsal root ganglion. These findings suggested that cell-mediated immune response was important for the clearance of rabies virus from the CNS. In addition, infiltrating T lymphocytes were positive for TUNEL staining, similar to results reported in experimental infection of mice and natural infection of dogs and humans by a street rabies virus strain [16, 31, 32]. Thus, it was suggested that street rabies virus may trigger apoptosis in inflammatory cells through the Fas/Fas ligand pathway, thereby interfering with release of cytotoxic cytokines and preventing cell lysis [32].

In conclusion, these results suggested that 1088-N0 virus ascended the spinal cord via mainly afferent fibers and progress to cerebral cortex using descending spinal tract. Furthermore, virus-infected nerve cells died by necrosis, whereas T lymphocytes died by apoptosis. This was accompanied by increased numbers and morphological changes of glial cells associated with the pathogenesis of the experimental rabies.

References

1. Adle-Biassette, H., Bourhy, H., Gisselbrecht, M., Chrétien, F., Wingertsmann, L., Baudrimont, M., Rotivel, Y., Godeau, B. and Gray, F. 1996. Rabies encephalitis in a patient with AIDS: a clinicopathological study. *Acta Neuropathol.* **92**: 415-420.
2. Akaike, T. and Maeda, H., 2000. Nitric oxide and virus infection. *Immunology* **101**: 300-308.
3. Aschner, M. 1998. Astrocytes as mediators of immune and inflammatory responses in the CNS. *Neurotoxicology* **19**: 269-282.
4. Baby, J., Mani, R. S., Abraham, S. S., Thankappan, A. T., Pillai, P. M., Anand, A. M., Madhusudana, S. N., Ramachandran, J. and Sreekumar, S. 2015. Natural rabies infection in a domestic fowl (*Gallus domesticus*): a report from India. *PLoS Negl. Trop. Dis.* **9**: e0003942.
5. Baloul, L. and Lafon, M. 2003. Apoptosis and rabies virus neuroinvasion. *Biochimie* **85**: 777-788.
6. Chai, Q., She, R., Huang, Y. and Fu, ZF. 2015. Expression of neuronal CXCL10 induced by rabies virus infection initiates infiltration of inflammatory cells, production of chemokines and cytokines, and enhancement of blood-brain barrier permeability. *J. Virol.* **89**: 870-876.
7. Coulon, P., Bras, H. and Vinay, L. 2011. Characterization of last-order premotor interneurons by transneuronal tracing with rabies virus in the neonatal mouse spinal cord. *J. Comp. Neurol.* **519**: 3470-3487.
8. Dietzschold, B., Li, J., Faber, M. and Schnell, M. 2008. Concept in the pathogenesis of rabies. *Future Virol*. **3**: 481-490.

9. Dufour, J. H., Dziejman, M., Liu, M. T., Leung, J. H., Lane, T. E. and Luster, A. D. 2002. IFN-gamma-inducible protein 10 (IP-10; CXCL10)-deficient mice reveal a role for IP-10 in effector T cell generation and trafficking. *J. Immunol.* **168**: 3195-3204.

10. Faulkner, J. R. Herrmann, J. E., Woo, M. J., Tansey, K. E., Doan, N. B. and Sofroniew, M. V. 2004. Reactive astrocytes protect tissue and preserve function after spinal cord injury. *J. Neurosci*. **24**: 2143-2155.

11. Feng, Y. J., Lin, D. Y., Ying, H., Yan, T. X., Hao, L., Cheng, Y. P., Xin, S. X., Tao, J. W., Dong, L. G., Qing, T. and Long, W. F. 2014. Comparative analysis of the pathogenetic mechanisms of street rabies virus strains with different virulence levels. *Biomed. Environ. Sci.* **27**: 749-762.

12. Hamir, A. N., Moser, G. and Rupprecht, C. E. 1996. Clinicopathologic variation in raccoons infected with different street rabies virus isolates. *J. Vet. Diag. Invest.* **8**: 31-37.

13. Hemachudha, T., Ugolini, G., Wacharapluesadee, S., Sungkarat, W., Shuangshoti, S. and Laothamatas, J. 2013. Human rabies: neuropathogenesis, diagnosis, and management. *Lancet Neurol.* **12**: 498-513.

14. Hooper, D. C., Morimoto, K., Bette, M., Whihe, E., Koprowski, H. and Dietzschold, B. 1998. Collaboration of antibody and inflammation in clearance of rabies virus from the central nervous system. *J. Virol.* **72**: 3711-3719.

15. Hu, S., Peterson, P. K. and Chao, C. C. 1997. Cytokine-mediated neuronal apoptosis. *Neurochem. Int.* **30**: 427-431.

16. Jackson, A. C., Randle, E., Lawrance, G. and Rossiter, J. P. 2008. Neuronal apoptosis does not play an important role in human rabies encephalitis. *J. Neuroviral.* **14**: 368-375.

17. Jackson, A. C. 2013. pp: 394-395. *In*: Rabies, 3rd ed., Elsevier Saunders, Philadelphia.

18. Kojima, D., Park, C. H., Satoh, Y., Inoue, S., Noguchi, A. and Oyamada, T. 2009. Pathology of the spinal cord of C57BL/6J mice infected with rabies virus (CVS-11). *J. Vet. Med. Sci.* **71**: 319-324.

19. Kojima, D., Park, C. H., Tsujikawa, S., Kohara, K., Hatai, H., Oyamada, T., Noguchi, A. and Inoue, S. 2010. Lesions of the central nervous system induced by intracerebral inoculation of BALB/c mice with rabies virus (CVS-11). *J. Vet. Med. Sci.* **72**: 1011-1016.

20. Koyuncu, O. O., Hogue, I. B. and Enquist, L. W. 2013. Virus infections in the nervous system. *Cell Host Microbe.* **13**: 379-393.

21. Lentz, T. L., Burrage, T. G., Smith, A. L., Crick, J. and Tignor, G. H. 1982. Is the acetylcholine receptor a rabies virus receptor? *Science* **215**: 182-184.

22. Lewis, P., Fu, Y. and Lentz, T. L. 2000. Rabies virus entry at the neuromuscular junction in nerve-muscle cocultures. *Muscle Nerve* **23**: 720-730.

23. Li, X. Q., Sarmento, L. and Fu, Z. F. 2005. Degeneration of neuronal processes after infection with pathogenic, but not attenuated, rabies viruses. *J. Virol.* **79**: 10063-10068.

24. Marquette, C., Van Dam, A. M., Ceccaldi, P. E., Weber, P., Haour, F. and Tsiang, H. 1996. Induction of immunoreactive interleukin-1 beta and tumor necrosis factor-alpha in the brains of rabies virus infected rats. *J. Neuroimmunol*. **68**. 45-51.

25. Park, C. H., Kondo, M., Inoue, S., Noguchi, A., Oyamada, T., Yoshikawa, H. and Yamada, A. 2006. The histopathogenesis of paralytic rabies in six-week-old C57BL/6J mice following inoculation of the CVS-11 strain into the right triceps surae muscle. *J. Vet. Med. Sci.* **68**: 589-595.

26. Rock, R. B., Gekker, G., Hu, S., Sheng, W. S., Cheeran, M., Lokensgard, J. R. and Peterson, P. K. 2004. Role of microglia in central nervous system infections. *Clin. Microbiol. Rev.* **17**: 942-964.

27. Sarmento, L., Tseggai, T., Dhingra, V. and Fu, Z. F. 2006. Rabies virus-induced apoptosis involves caspase-dependent and casepase-independent pathways. *Virus Res.* **121**: 144-151.

28. Song, Y., Hou, J., Qiao, B., Li, Y., Xu, Y., Duan, M., Guan, Z., Zhang, M. and Sun, L. 2013. Street rabies virus causes dendritic injury and F-actin depolymerization in the hippocampus. *J. Gen. Virol.* **94**: 276-283.

29. Sofronniew, M. V. and Vinters, H. V. 2010. Astrocytes: biology and pathology. *Acta Neuropathol.* **119**: 7-35.

30. Streit, W. J. 2002. Microglia as neuroprotective, immunocompetent cells of the CNS. *Glia* **40**: 133-139.

31. Suja, M. S., Mahadevan, A., Madhusudhana, S. N., Vijayasarathi, S. K. and Shankar, S. K. 2009. Neuroanatomical mapping of rabies nucleocapsid viral antigen distribution and apoptosis in pathogenesis in street dog rabies–an immunohistochemical study. *Clin. Neuropathol.* **28**: 113-124.

32. Suja, M. S., Mahadevan, A., Madhusudana, S. N. and Shankar, S. K. 2011. Role of apoptosis in rabies viral encephalitis: a comparative study in mice, canine, and human brain with a review of literature. *Pathol. Res. Int.* **2011**: 374286.

33. Tobiume, M., Sato, Y., Katano, H., Nakajima, N., Tanaka, K., Noguchi, A., Inoue, S., Hasegawa, H., Iwasa, Y., Tanaka, J., Hayashi, H., Yoshida, S., Kurane, I. and Sata, T. 2009. Rabies virus dissemination in neural tissues of autopsy cases due to rabies imported into Japan from the Philippines: immunohistochemistry. *Pathol. Int.* **59**: 555-566.

34. Ugolini, G. 2010. Advances in viral transneuronal tracing. *J. Neurosci. Methods* **194**: 2-20.

35. Ugolini, G. 2011. Rabies virus as a transneuronal tracer of neuronal connections. *Adv. Virus Res.* **79**: 165-202.

36. Velandia-Romero, M. L., Castellanos, J. E. and Martínez-Gutiérrez, M. 2013. In vivo differential susceptibility of sensory neurons to rabies virus infection. *J. Neurovirol.* **19**: 367-375.

37. WHO Expert consultation on rabies. Second report. 2013. *World Health Organ Tech. Rep. Ser*. **982**: 1-139.

38. Woldehiwet, Z. 2002. Rabies: recent developments. *Res. Vet. Sci.* **73**: 17-25.

39. Yamada, K., Park, C. H., Noguchi, K., Kojima, D., Kubo, T., Komiya, N., Matsumoto, T., Mitui, M. T., Ahmed, K., Morimoto, K., Inoue, S. and Nishizono, A. 2012. Serial passage of a street rabies virus in mouse neuroblastoma cells resulted in attenuation: potential role of the additional *N*-glycosylation of viral glycoprotein in the reduced pathogenicity of street rabies virus. *Virus Res.* **165**: 34-45.

40. Zampieri, N., Jessell, T. M. and Murray, A. J. 2013. Mapping sensory circuits by anterograde transsynaptic transfer of recombinant rabies virus. *Neuron* **81**: 766-778.

Table 1. Anatomical distribution of 1088-N0 virus antigens in mice infected intramuscularly

Anatomical Area	5 days PI (n=5)	8 days PI (n=5)	11 days PI (n=5)
Brain			
Cerebral cortex	+	+++++	+++++
Hippocampus	-	++	++++
Thalamus	+	+++++	+++++
Medulla oblongata	+	++++	++++
Cerebellum (Purkinje cells)	-	++++	++++
Spinal cord			
Cervical	+	++	++
Thoracic	+	++	++
Lumbar	+	++	++
Sacral	-	-	+
Dorsal root ganglion			
Cervical	-	+	+
Thoracic	+	+	+
Lumbar	+	+	+
Sacral	+	+	+
Other			
Muscle$^{\xi}$	+	+	+
Intramuscular peripheral nerve$^{\#}$	+	+	+

-: Negative, +: positive ≤ 10 cells, ++: 11-30 cells, +++: 31-50 cells, ++++: 51-100 cells, +++++: >101 cells, PI: post inoculation, $^{\xi}$: right triceps surae muscle, $^{\#}$: intramuscular peripheral nerves around infected muscle.

Table 2. The mean of the number of glial cells, lymphocytes and TUNEL-positive cells in five mice infected with 1088-N0 virus

Cerebral cortex, thalamus, medulla and hippocampus	5 days PI (n=5)	8 days PI (n=5)	11 days PI (n=5)	Control
Iba1	974	1,732	2,045	528
GFAP	67	272	454	59
CD3	24	76	294	0
CD20	0	0	0	0
TUNEL	0	47	156	0
Spinal cord (C, T, L, S)				
Iba1	37	124	148	29
GFAP	16	21	36	15
CD3	15	45	83	0
CD20	0	2	3	0
TUNEL	0	36	67	0

PI: post inoculation, Iba1: microglial cell (ramified or amoeboid microglial cells type only counted), GFAP: astroglial cell (protoplasmic astroglial cells type only counted), CD3: T lymphocyte, CD20: B lymphocyte, C: cervical, T: thoracic, L: lumbar, S: sacral.

Figure legends

Figs. 1-4. Histology and immunohistochemistry of lumbar dorsal root ganglion at 5 days PI. Degenerated ganglion neurons (arrows, Fig. 3) were observed. Viral antigens were found in the cytoplasm of ganglion neurons (Figs. 2 and 4).

Figs. 5-6. Histology and immunohistochemistry of thoracic spinal cord at 8 days PI. Small numbers of lymphocytes were observed surrounding blood vessels (arrows, Fig. 5). Viral antigens were found mainly in the sensory neurons of the dorsal horns (Fig. 6).

Figs. 7-10. Histology and immunohistochemistry of cervical dorsal root ganglion and their fibers at 8 days PI. The number of degenerated ganglion neurons increased (Fig. 7) and some axon exhibited vacuolated changes (arrows, Fig. 9). Viral antigens were observed in the cytoplasm of ganglion neurons and dorsal root fibers (arrows, Figs. 8 and 10), whereas no viral antigens detected in ventral root fibers.

Figs. 11-12. Histology of cerebral cortex (M1 motor area) at 8 days PI. Hypereosinophilic cytoplasm and nuclear pyknosis were observed in pyramidal neurons (arrow heads, Fig. 12).

Figs. 13-15. Brain. At 5 days PI, viral antigens were observed in the pyramidal neurons of cerebral cortex (M1 motor area) (inset, Fig. 13). At 8 (Fig. 14) and 11 (Fig. 15) days PI, viral antigens were widely distributed throughout the brain. Immunohistochemistry.

Figs. 16-19. Histology and immunohistochemistry of medulla oblongata at 8 days PI. Nuclear pyknosis and cytoplasmic shrinkage in the pyramidal neurons were observed (arrows, Fig. 18). Viral antigens were found in the cytoplasm of pyramidal neurons and their axons throughout tissue (Figs. 17 and 19).

Figs. 20-21. Histology and immunohistochemistry of cerebellum at 8 days PI. Necrotic Purkinje cells were observed (arrows, Fig. 20). Viral antigens were found in the cytoplasm of Purkinje cells and their axons in the molecular layer (Fig. 21).

Figs. 22-27. Lumbar spinal cord. Many Iba1-positive rod-like small microglial cells were detected in the gray matter of spinal cord at 5 days PI (arrows, Figs. 22 and 23), and they changed their morphology to be ramified or amoeboid shapes at 8 days PI (arrows, Figs. 24 and 25) and 11 (arrows, Figs. 26 and 27) days PI. Immunohistochemistry.

Figs. 28-33. Cerebrum. Many Iba1-positive rod-like small microglial cells were detected in the cerebral cortex at 5 days PI (arrow heads, Figs. 28 and 29), and they changed their morphology to be ramified or amoeboid shapes at 8 (arrows, Figs. 30 and 31) and 11 (arrows, Figs. 32 and 33) days PI. Immunohistochemistry.

Figs. 34-39. Lumbar spinal cord. At 5 days PI, GFAP-positive astrocytes elongated to reach the deep white matter (arrow, Figs. 34 and 35). Many protoplasmic astrocytes were observed in the

gray matter at 8 days PI (arrows, Figs. 36 and 37), and they changed their morphology to a ramified shape at 11 days PI (arrows, Figs. 38 and 39). Immunohistochemistry.

Fig. 40. Cerebrum. Small numbers of lymphocytes were present under the leptomeniges at 11 days PI (arrows).

Fig. 41. Cervical spinal cord. Small numbers of lymphocytes were present under the leptomeniges at 11 days PI (arrows).

Fig. 42. Cerebral cortex. Small numbers of lymphocytes were present around blood vessel at 11 days PI (arrows).

Fig. 43. Cerebral cortex. At 11 days PI, CD3-positve T lymphocytes appeared around blood vessel at 11 days PI. Immunohistochemistry.

Fig. 44. Cerebrum. Small numbers of lymphocytes were observed around cerebral ventricle (asterisk) at 11 days PI.

Fig. 45. Cerebrum. At 11 days PI, CD3-positve T lymphocytes appeared around cerebral ventricle (asterisk) at 11 days PI. Immunohistochemistry.

Figs. 46-51. Cerebral cortex (M1 motor area). Histology and TUNEL assays at 8 days PI. Hypereosinophilic cytoplasm and nuclear pyknosis was observed in glial cells (Fig. 48) and lymphocytes around blood vessel (arrows, Fig. 50). Marked TUNEL staining was evident in

glial cells (arrows, Fig. 49) and lymphocytes around blood vessel (arrows, Fig. 51), but not in the pyramidal neurons.

Figs. 52-53. Cerebral cortex (M1 motor area). TUNEL positive glial cells were more significantly observed at 11 days PI.

Figs. 54-55. Sacral dorsal root ganglia at 11 days PI. Anti-NF immunoreactivity revealed weak and irregular positive reaction, and diffusely loss of both small- and large-diameter axons (asterisk, Fig. 55).

Figs. 56-59. Sacral dorsal root ganglion and spinal nerve at 11 days PI. Fig. 56, dorsal root ganglion (1) and spinal nerve (2). LFB staining revealed a decrease density of myelinated nerve fibers and extensive axonal demyelination of the dorsal root ganglion (Figs. 57 and 58) and dorsal root of spinal nerve, whereas ventral root fibers appeared intact (asterisk, Fig. 59).

Schematic representation of the anatomical distribution of 1088-N0 virus antigens in mouse brain coronal sections

5 days PI	8 days PI	11 days PI
No.16	**No.33**	**No.50**

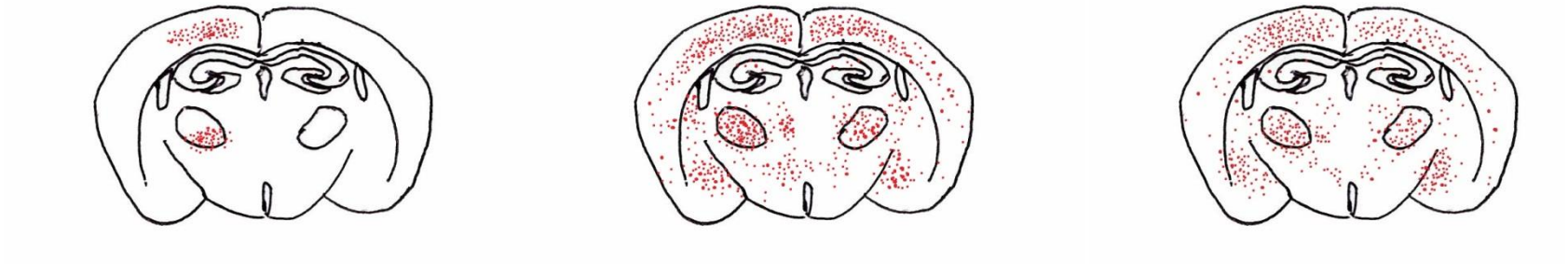

: Virus antigens

Figs.1-6: Spinal cord・dorsal root ganglion

Dorsal root ganglion, lumbar, 5DPI, HE

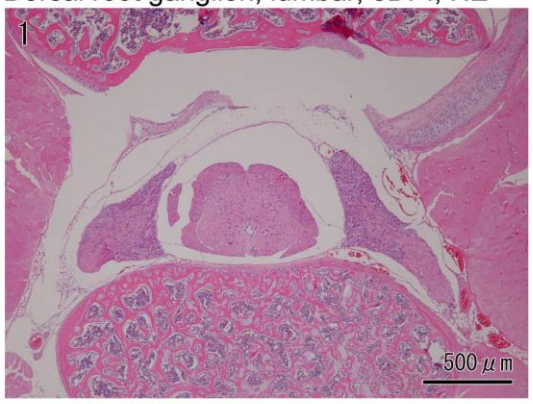

Dorsal root ganglion, lumbar, 5DPI, anti-P

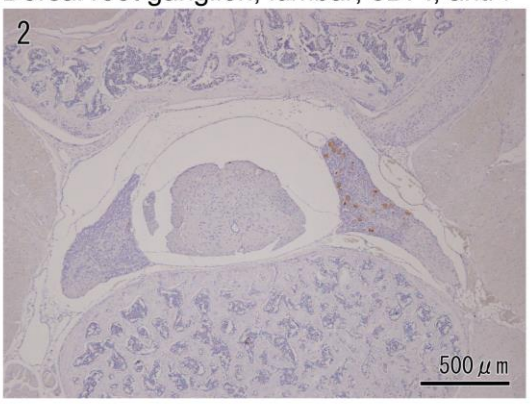

Dorsal root ganglion, lumbar, 5DPI, HE

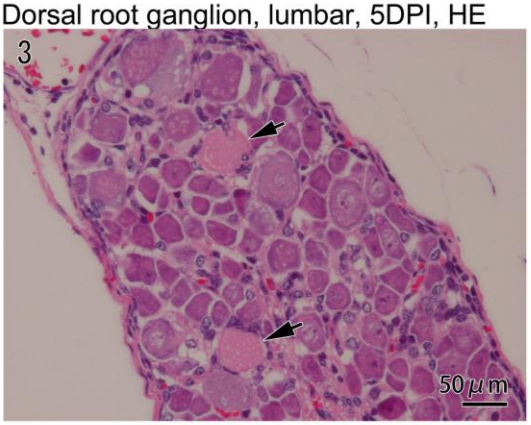

Dorsal root ganglion, lumbar, 5DPI, anti-P

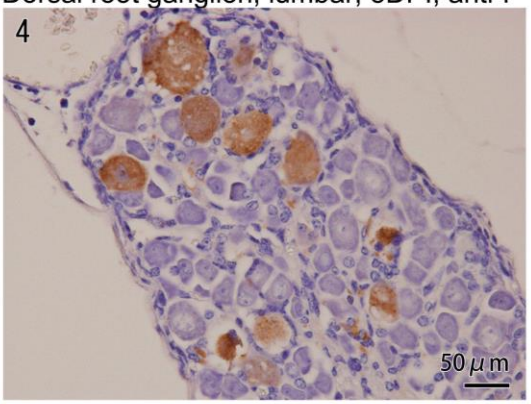

Spinal cord, thoracic, 8DPI, HE

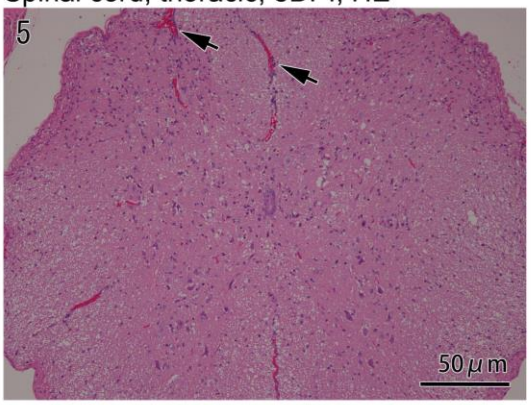

Spinal cord, thoracic, 8DPI, anti-P

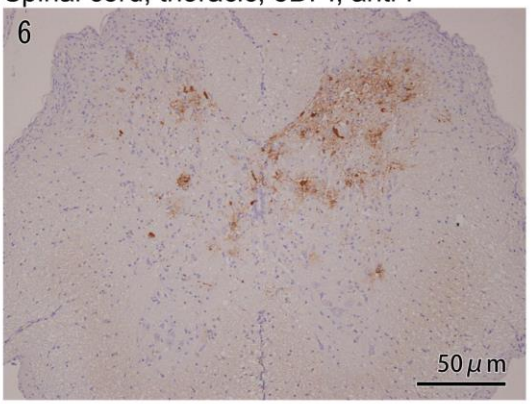

Figs. 7-12: Dorsal root ganglion・brain

Dorsal root ganglion, cervical, 8DPI, HE

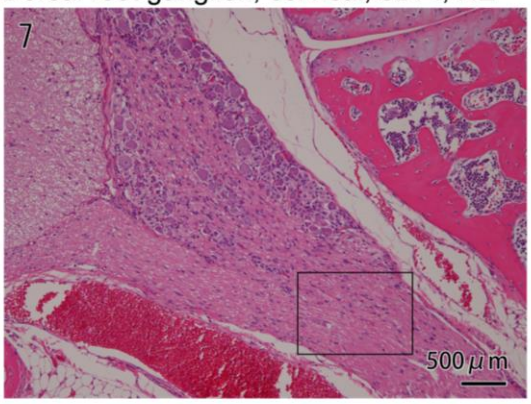

Dorsal root ganglion, cervical, 8DPI, anti-P

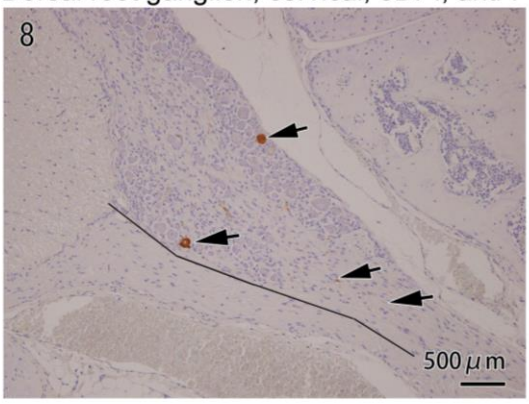

Dorsal root fiber, cervical, 8DPI, HE

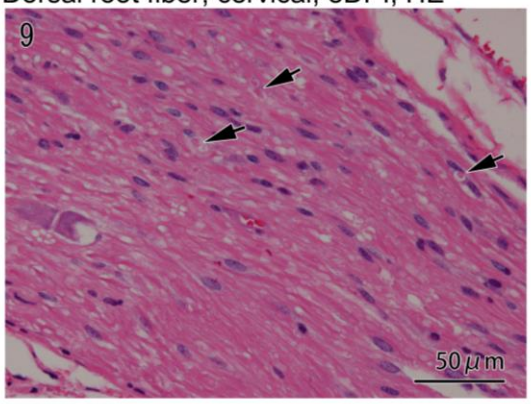

Dorsal root fiber, cervical, 8DPI, anti-P

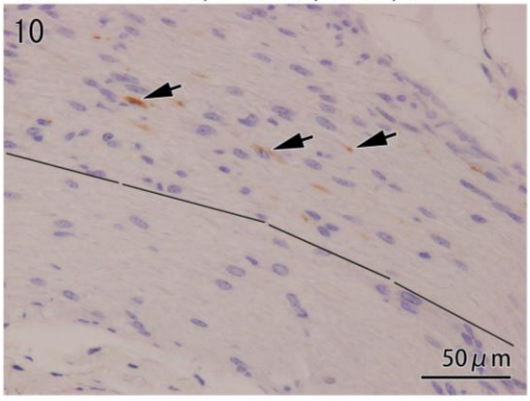

Cerebral cortex, 8 DPI, HE

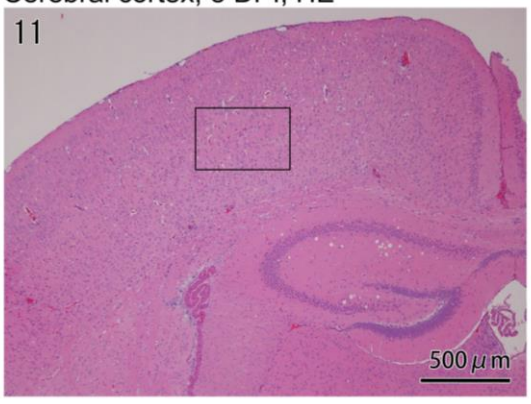

Cerebral cortex, 8 DPI, HE

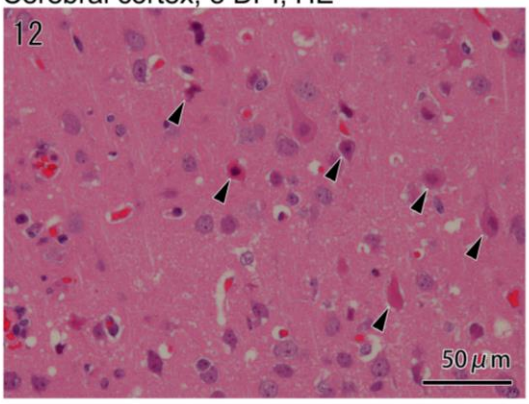

Figs. 13-15: Brain

Brain, 5 DPI, anti-P

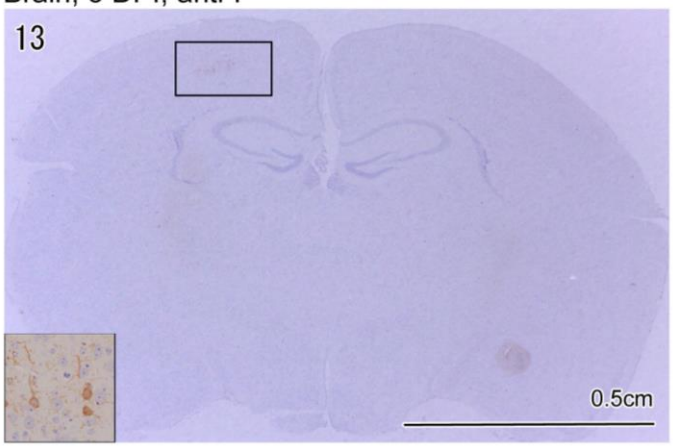

Brain, 8 DPI, anti-P

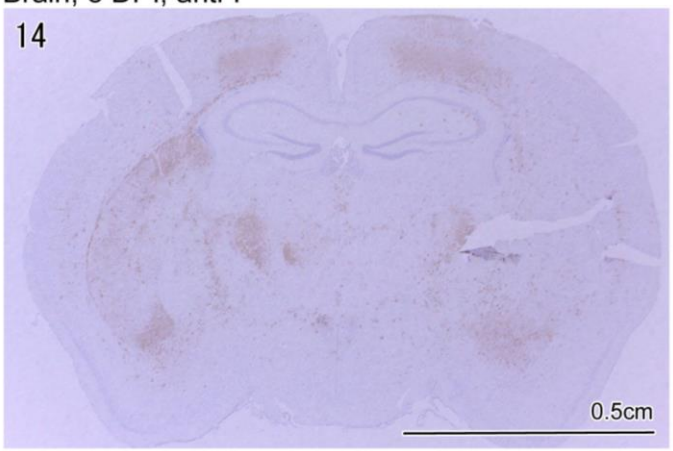

Brain, 11 DPI, anti-P

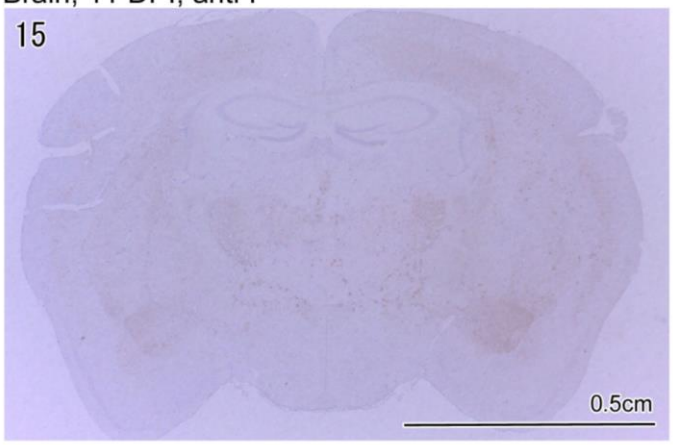

Figs. 16-21: Medulla oblongata・cerebellum

Medulla oblongata, 8DPI, HE

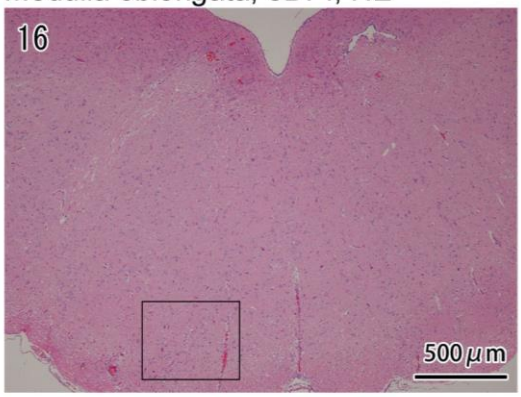

Medulla oblongata, 8DPI, anti-P

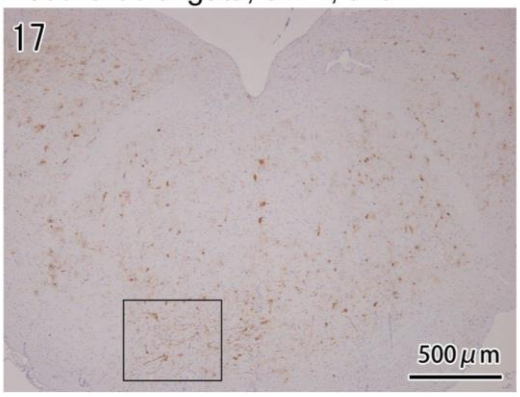

Medulla oblongata, 8DPI, HE

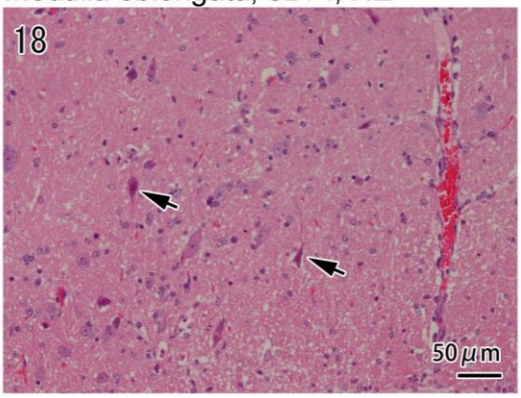

Medulla oblongata, 8DPI, anti-P

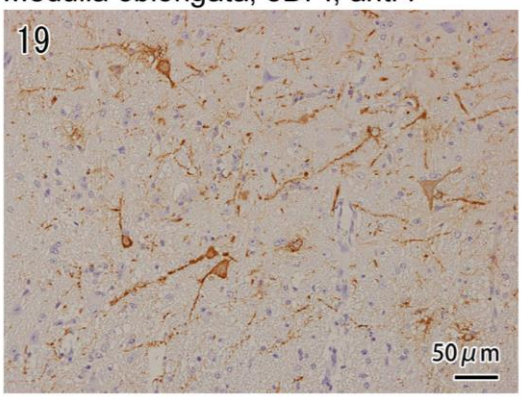

Cerebellum, 8DPI, HE

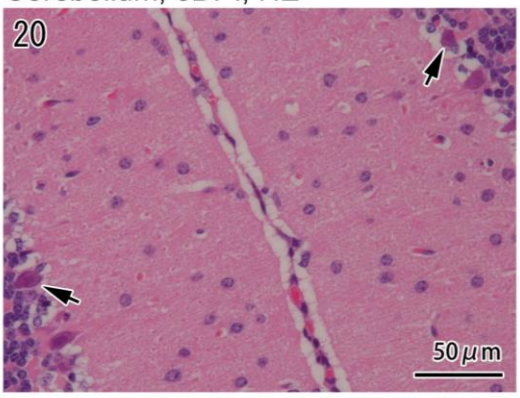

Cerebellum, 8DPI, anti-P

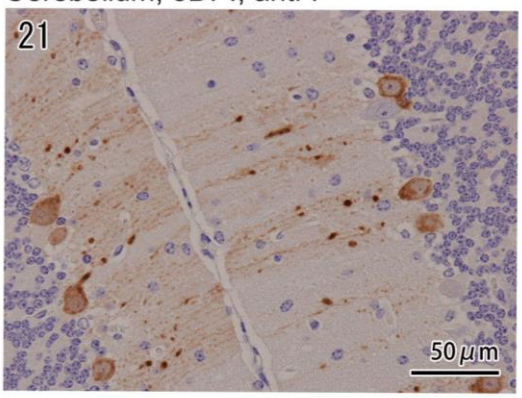

Figs. 22-27: Spinal cord

Spinal cord, lumbar, 5DPI, Iba1

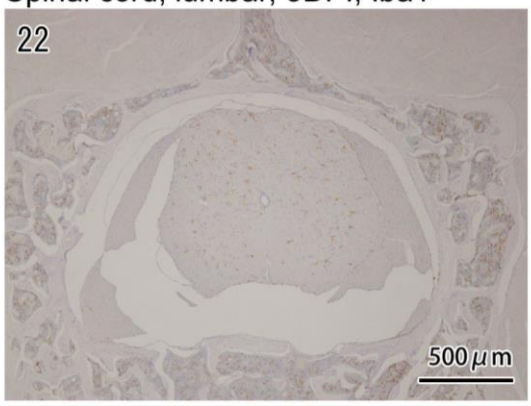

Spinal cord, lumbar, 5DPI, Iba1

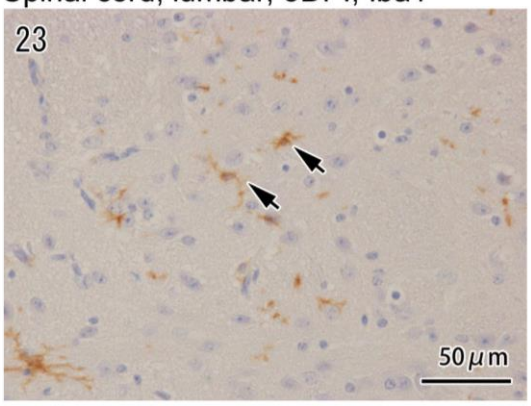

Spinal cord, lumbar, 8DPI, Iba1

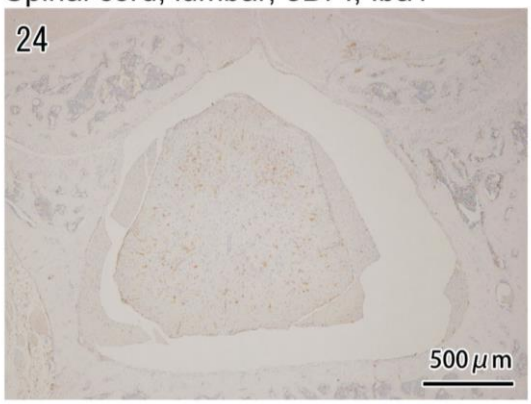

Spinal cord, lumbar, 8DPI, Iba1

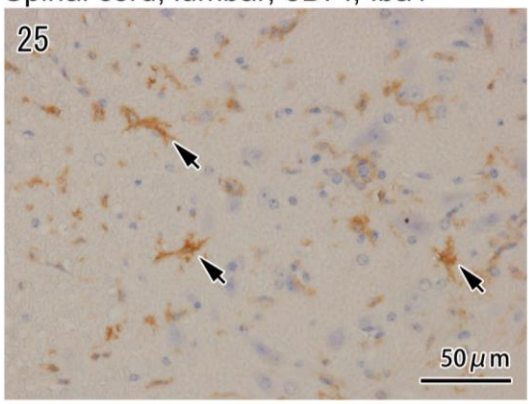

Spinal cord, lumbar, 11DPI, Iba1

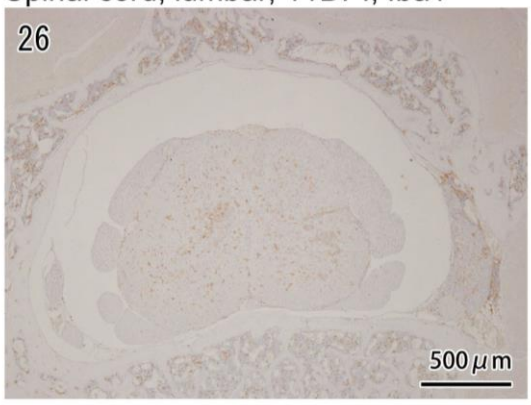

Spinal cord, lumbar, 11DPI, Iba1

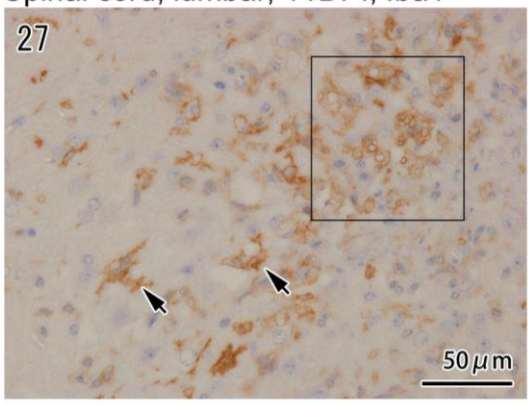

Fig.28-33: Cerebral cortex

Cerebral cortex, 5DPI, Iba1

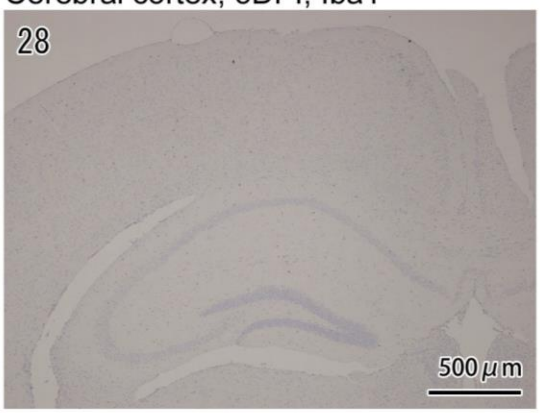

Cerebral cortex, 5DPI, Iba1

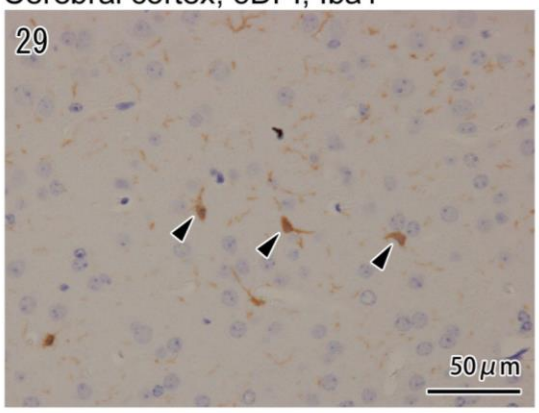

Cerebral cortex, 8DPI, Iba1

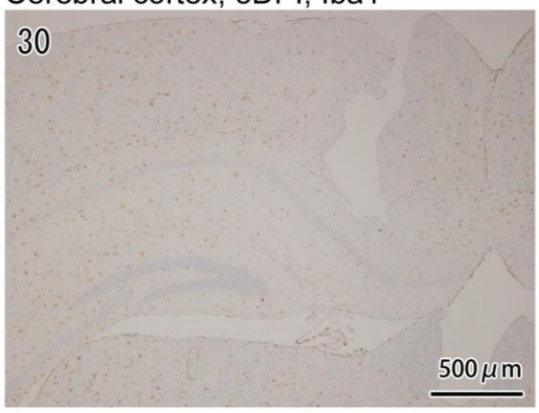

Cerebral cortex, 8DPI, Iba1

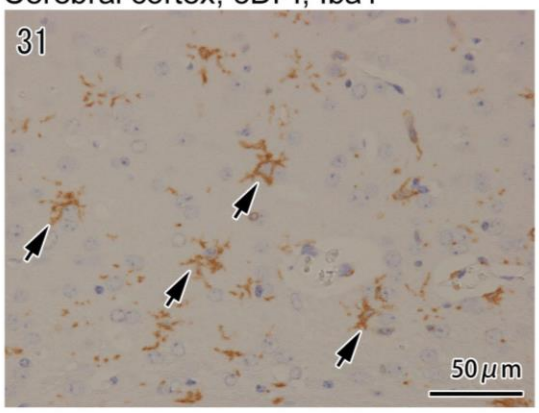

Cerebral cortex, 11DPI, Iba1

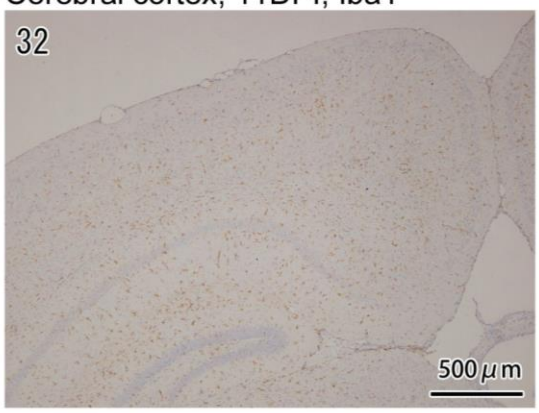

Cerebral cortex, 11DPI, Iba1

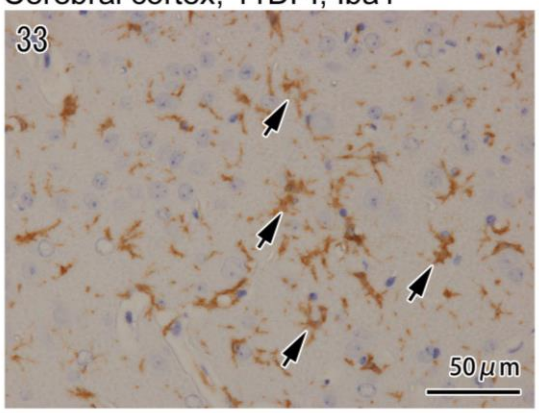

Figs. 34-39: Spinal cord

Spinal cord, lumbar, 5DPI, GFAP

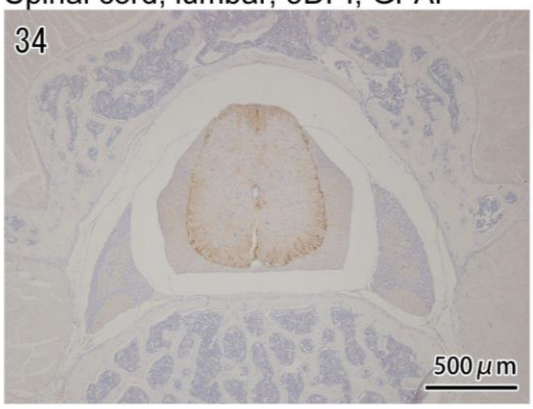

Spinal cord, lumbar, 5DPI, GFAP

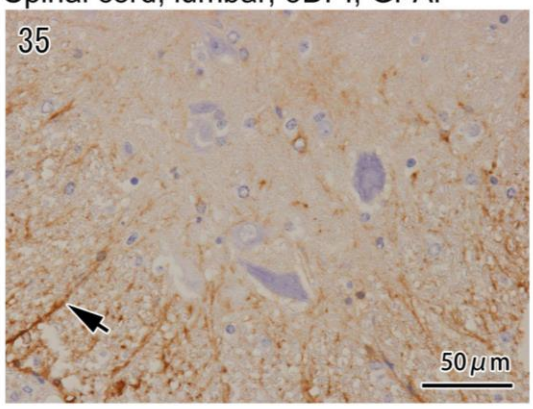

Spinal cord, lumbar, 8DPI, GFAP

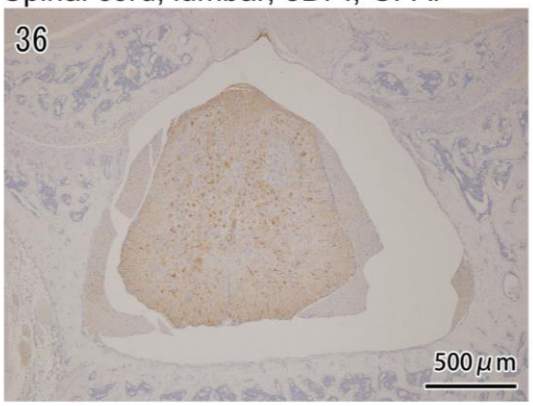

Spinal cord, lumbar, 8DPI, GFAP

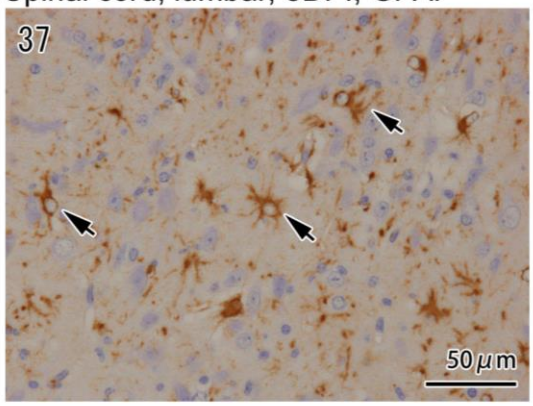

Spinal cord, lumbar, 11DPI, GFAP

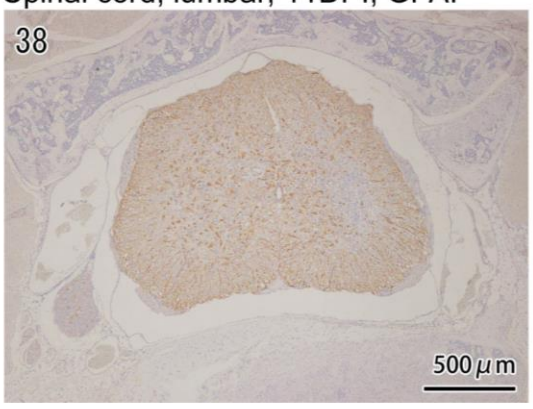

Spinal cord, lumbar, 11DPI, GFAP

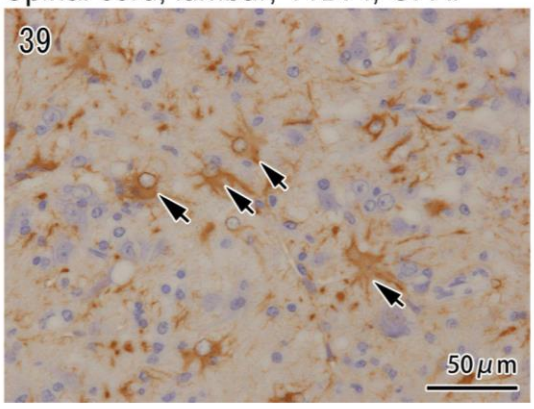

Figs. 40-45: Brain・Spinal cord

Cerebrum, 11DPI, HE

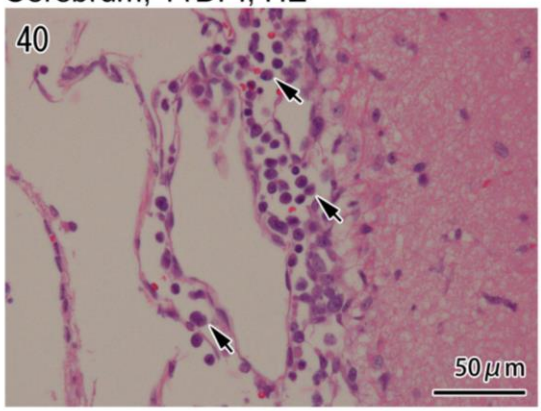

Spinal cord, cervical, 11DPI, HE

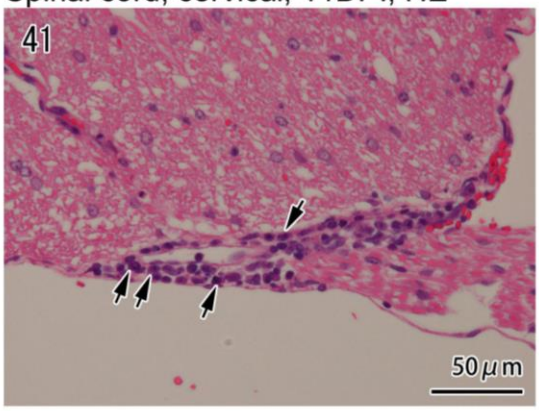

Cerebral cortex, 11DPI, HE

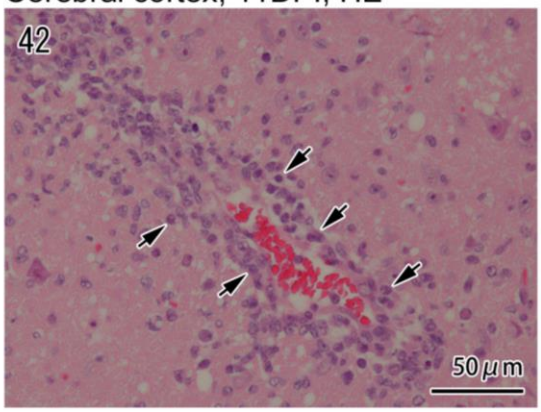

Cerebral cortex, 11DPI, CD3

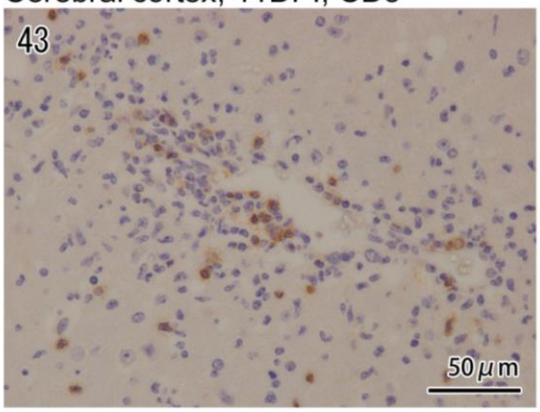

Cerebrum, 11DPI, HE

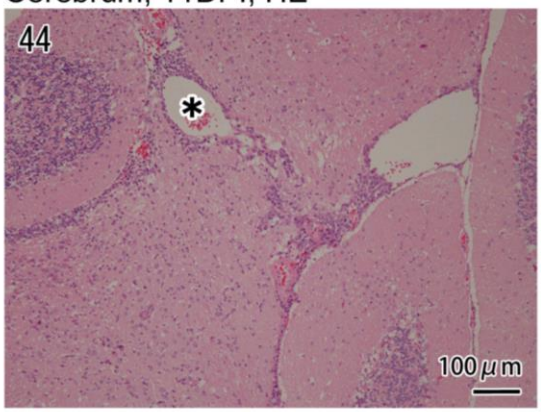

Cerebrum, 11DPI, CD3

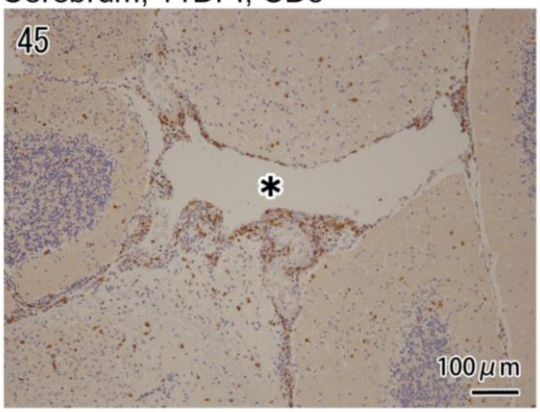

Figs. 46-51: Cerebrum

Cerebral cortex, 8DPI, HE

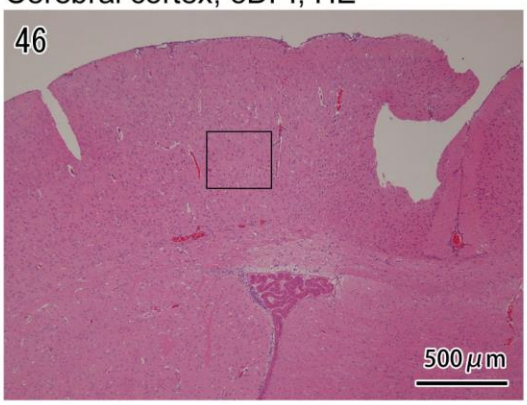

Cerebral cortex, 8DPI, TUNEL

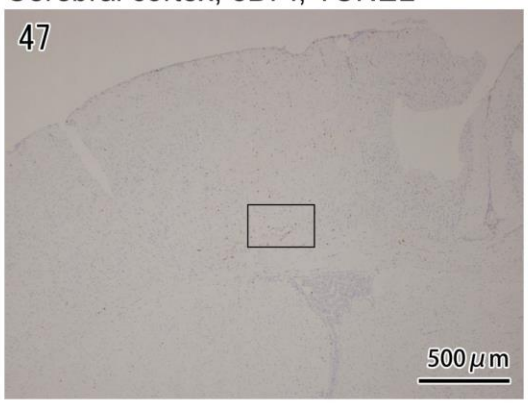

Cerebral cortex, 8DPI, HE

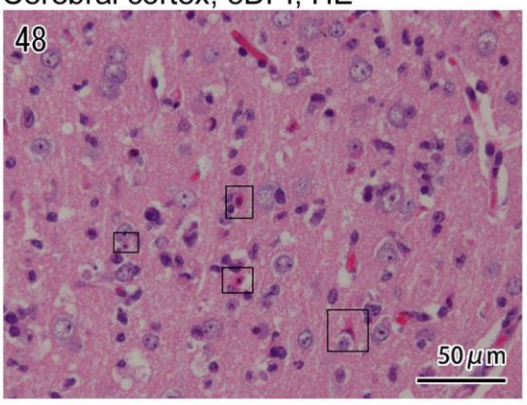

Cerebral cortex, 8DPI, TUNEL

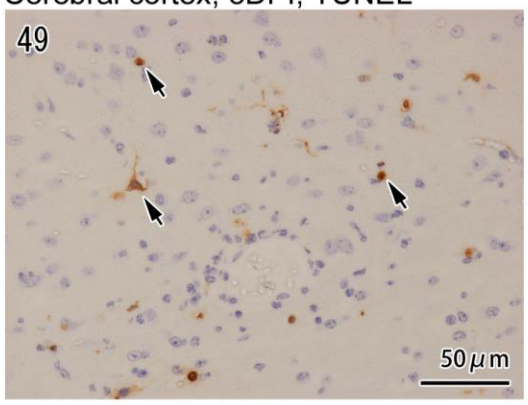

Cerebral cortex, 8DPI, HE

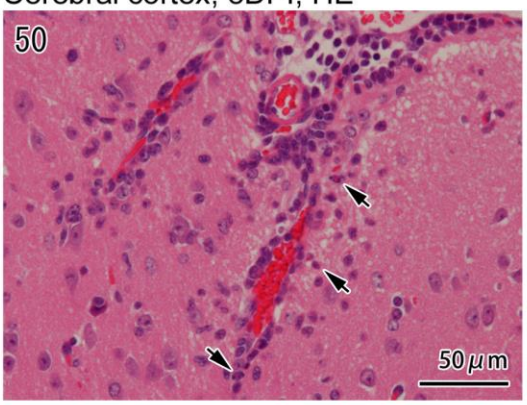

Cerebral cortex, 8DPI, TUNEL

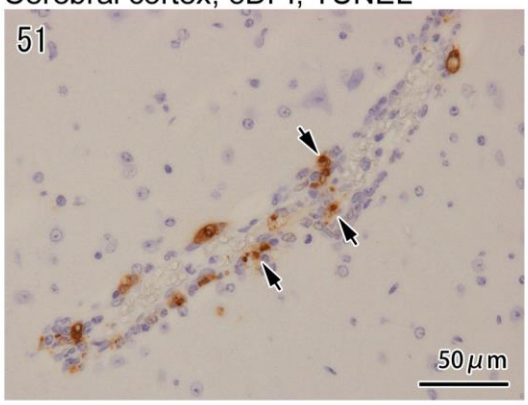

Figs. 52-53: Cerebral cortex

Cerebral cortex, 11DPI, TUNEL

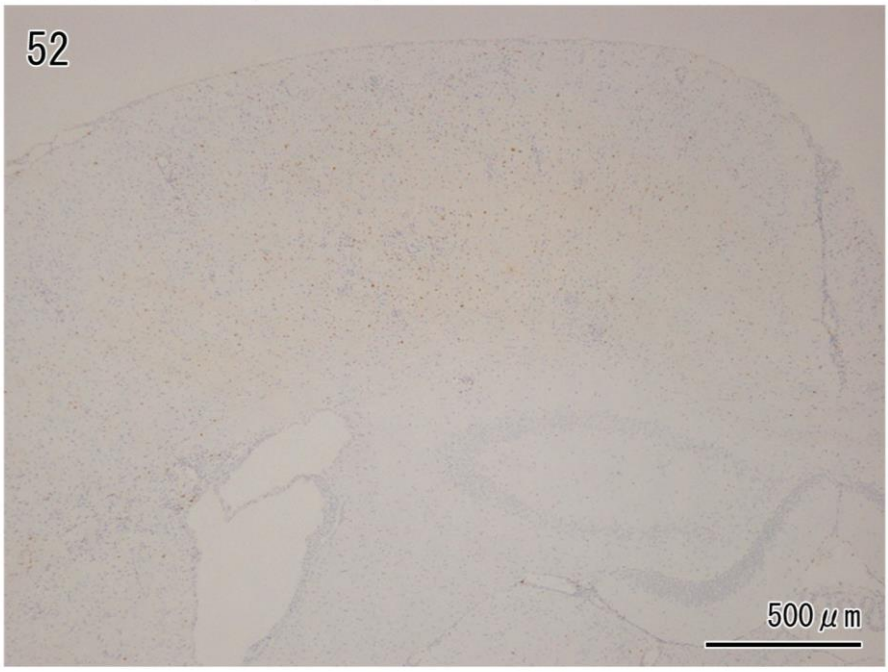

Cerebral cortex, 11DPI, TUNEL

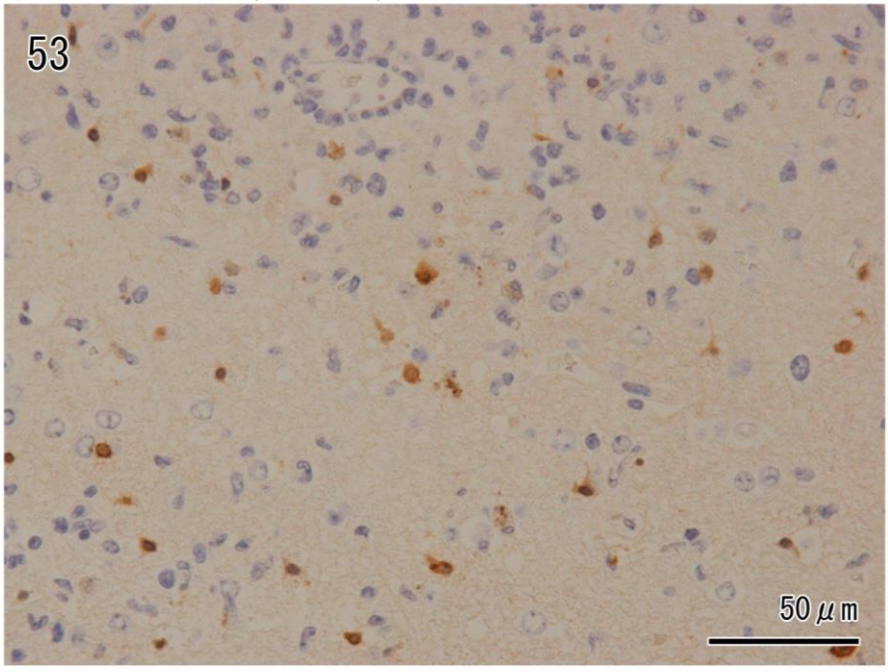

Figs. 54-59: Dorsal root ganglion

Dorsal root ganglion, 11DPI, NF

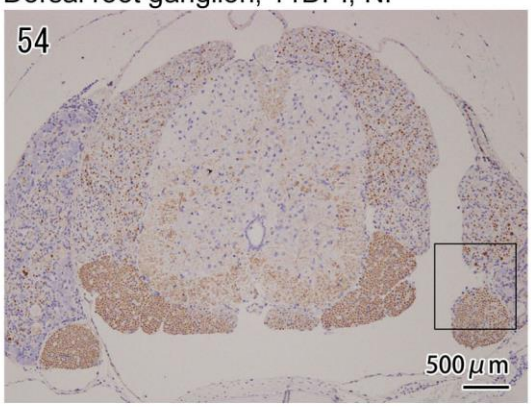

Dorsal root ganglion, sacrum, 11DPI, NF

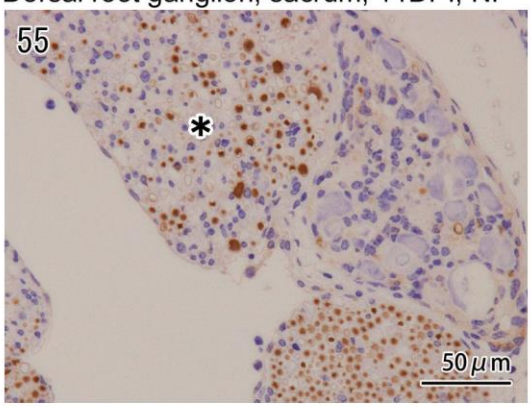

Dorsal root ganglion, sacrum, 11DPI, LFB

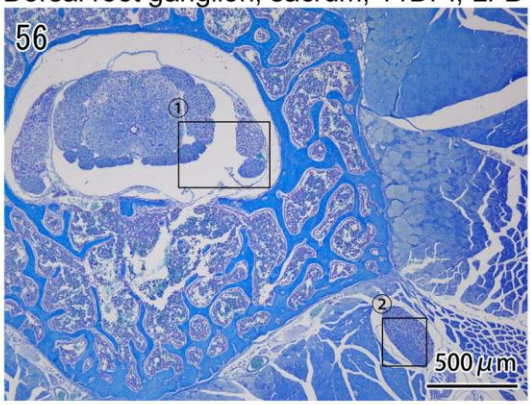

Dorsal root ganglion, sacrum, 11DPI, LFB

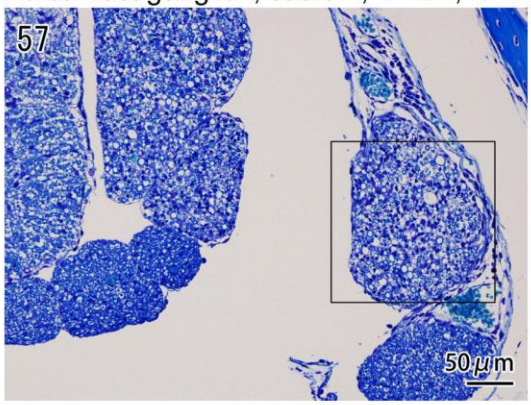

Dorsal root ganglion, sacrum, 11DPI, LFB

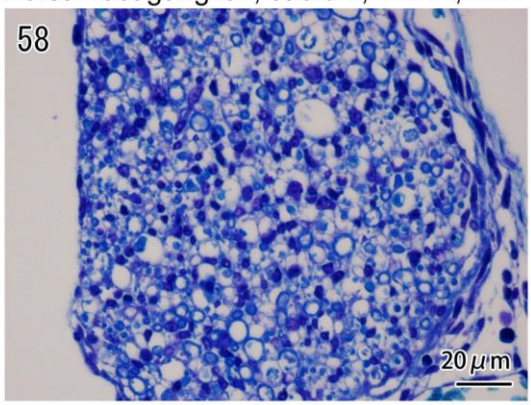

Spinal nerve, sacrum, 11DPI, LFB

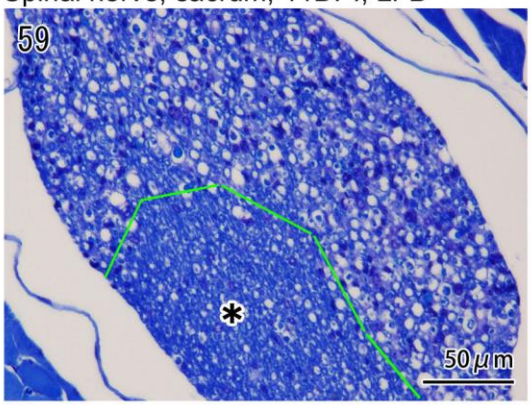

Acknowledgements

Any significant milestone in one's life is made successful by the contributions of many others along the way. The successful completion of this research is a significant milestone for me. I would like to commit that while writing this section I went through all the memories with sweats, tears, late nights, early mornings as well as the sweet memories full with words of appreciations, encouragements, achievements, success and happiness. I find it very difficult, rather lack words to express my feelings to the people who have provided me their immense help and support during my Ph.D. work. I would like to convey my special and heartiest thanks to some very important people without whom the journey of achieving my Ph.D. would have been impossible.

It is a privilege to express my sincere gratitude and deep appreciation to my major supervisor Associate Professor Dr. Chun-Ho Park, Laboratory of Veterinary Pathology, School of Veterinary Medicine, Kitasato University, Japan, for his valuable advices, helpful, guidance, encouragement, suggestions and intensive review. Dr. Park stimulated my interest in the field of pathology of rabies virus infection and improved my ability in writing. Furthermore, he was always my greatest role model for a pathologist, teacher, researcher and mentor. My dissertation would not have been possible without his constant guidance, assistance and support. I owe a lot of gratitude to him for always being there for me and I feel privileged to be associated with a person like him during my life.

I would like to express my sincere gratitude to Professor Dr. Toshifumi Oyamada and Assistant Professor Dr. Hitoshi Hatai, Laboratory of Veterinary Pathology, School of

Veterinary Medicine, Kitasato University, Japan, for their valuable advice, kindness, and helpfulness.

I would also like to acknowledge the invaluable help of Dr. Daria Llenaresas Manalo and the staff members of the Research Institute for Tropical Medicine, Department of Health, Philippines, for tissue collection of dogs and the permission to use these sample for my Ph.D. work.

I would also like to express my deepest appreciation to Mahanakorn University of Technology, Thailand, for providing me a scholarship throughout my doctoral program, especially, Associate Professor Dr. Jatuporn Kajaysri, Dean of Faculty of Veterinary Medicine, Mahanakorn University of Technology, Thailand, for giving me a great opportunity to study abroad in Japan. I would not have been here without his guidance and support.

I would also like to express my sincere gratitude to Assistant Professor Dr. Thanongsak Mamom, Associate Dean for Academic Affairs of Faculty of Veterinary Medicine, and Head of the Division of Veterinary Pathology, Mahanakorn University of Technology, Thailand, for his motivation, valuable suggestions and guidance throughout my times as both an undergraduate student and work life.

I would also like to express my sincere thanks to my Japanese teacher, Mr. Kunio Negishi for his attention to us, the students from abroad, and for his kindness and give me a precious help he has provided throughout my academic life in Japan.

I would also like to thank Dr. Titaree Laoharatchatathanin and Dr. Duangjai Rieanrakwong for their suggestion, kindness, and helpfulness.

I am also thankful to my colleagues, Mr. Kazunori Kimitsuki (Ph.D. student) and all the other members of the Laboratory of Veterinary Pathology, for their friendship, friendly atmosphere, and great help to me through my academic studies.

Special thanks are extended to Dr. Varat Vorabannarat and Dr. Pinkarn Chantawong for their everlasting encouragement and cheerfulness whenever I needed.

I am also indebted to all my experimental animals for their silent sacrifice, which bring me to succeed in my study.

Finally, I would like to acknowledge the people who mean world to me, my family. My family has always been a source of inspiration and encouragement. I wish to thank my parents, Mr. Siri and Mrs. Supattra Boonsriroj, whose love, teaching, foresight and values paved the way for a privileged education and support have brought me this far. I bow my head to my father for his generous support, invaluable blessings, and selfless but untold sacrifices for my better and bright future. I don't imagine a life without their love and blessings. Thank you Dad and Mom, for showing faith in me and giving me liberty to choose what I desired. My gratitude is extended to my uncle, aunt, sister (Dr. Tidarat Tripipitsiriwat), brother-in-law (Dr. Kanin Tripipitsiriwat), and nephew for their affection, patience and understanding me in all my pursuits. I consider myself the luckiest in the world to have such a supportive family, standing behind with their love and support. I appreciate and love you all dearly.

Hassadin Boonsriroj

1 January 2016